Quantifying chromophore concentration in tissue simulating phantoms using an optical detection system based on an integrating sphere

QUANTIFYING CHROMOPHORE CONCENTRATION IN TISSUE SIMULATING PHANTOMS USING AN OPTICAL DETECTION SYSTEM BASED ON AN INTEGRATING SPHERE

BY

DIANA F. MOSCU, B.Sc., M.Sc.

A THESIS

SUBMITTED TO THE DEPARTMENT OF MEDICAL PHYSICS

AND THE SCHOOL OF GRADUATE STUDIES

OF MCMASTER UNIVERSITY

IN PARTIAL FULFILMENT OF THE REQUIREMENTS

FOR THE DEGREE OF

DOCTOR OF PHILOSOPHY

Doctor of Philosophy (2009) McMaster University

(Medical Physics) Hamilton, Ontario, Canada

TITLE: Quantifying chromophore concentration in tissue simulating phantoms using an optical detection system based on an integrating sphere

AUTHOR: Diana F. Moscu

B.Sc. (Honours), M.Sc., Medical & Health Physics

McMaster University, Hamilton ON, Canada

SUPERVISOR: Dr. Joseph E. Hayward

NUMBER OF PAGES: xv, 153

for my family

Abstract

An integrating sphere system has been developed to study the optical properties of biological tissues non-invasively, over a broad spectral range with the ultimate goal of quantifying erythema resulting from external beam radiotherapy. An empirical model was defined to calculate the absorption coefficient, μ_a, from the normalized integrating sphere signal, R*, and the reduced scattering coefficient, μ_s'. As erythema is associated with an increase in the apparent concentration of oxygenated haemoglobin in the skin, the potential of the technique in quantifying erythema was assessed using measurements made in homogenous tissue simulating phantoms containing whole horse blood. After system validation in this simple model, a two-layer model was investigated. Whole blood from a horse was added to the bottom layer, while the top layer was fixed at an optical thickness simulating the epidermis. Reflectance measurements were made through the top layer while the bottom layer was deoxygenated using yeast. The retrieved concentrations of oxy- and deoxygenated haemoglobin were used to calculate the total haemoglobin concentration and the haemoglobin oxygen saturation. Errors in estimating the total haemoglobin concentration ranged from 3-12%; decreasing as a broadband absorber was added to the top layer. Preliminary *in vivo* measurements were also

performed on areas of erythema induced by a topical anesthetic. For regions of erythema there was an increase in the apparent haemoglobin oxygenation which correlates to values of the erythema index calculated from the definition established by Dawson *et al.* These results demonstrate that the apparent haemoglobin oxygenation has the potential to be used as a surrogate in quantifying erythema.

Acknowledgements

On this journey many have walked with me. Their company has been appreciated.

I would like to thank my supervisor, Dr. Joe Hayward. Twelve years ago I was excited to peek over your shoulder at the work you were doing. It has been a great pleasure to work with you. I doubt I would be in this position if it hadn't been for you, and I mean that as a good thing. Your patience will not be forgotten.

I would like to thank Dr. Michael Patterson and Dr. Tom Farrell for scaring me just enough to want to learn everything I could to avoid looking ridiculous during committee meetings, even though I'm certain that wasn't their intention. Thank you for your insight, direction, and continued support.

Finally, I would like to thank my family and friends. Mom and Dad, after too many years of asking when I would be finished school, I am happy to say that I am nearly there. Thank you all.

Contents

List of Figures

Chapter 1

Introduction

1.1 Motivation

In treating cancer with external beam radiotherapy, radiation doses are prescribed to the tumour and to a volume of tissue immediately surrounding it. A treatment plan is developed to ensure that radiation doses are delivered as prescribed while minimizing the radiation dose incurred by normal tissues. However, it is not always possible to spare all normal tissue. Some tissues, such as the skin, may receive radiation doses sufficient to cause a variety of adverse effects. Radiation doses to the skin can cause it to become irritated and damaged. This first appears as a reddening of the skin called erythema. Through the course of treatment, the amount of erythema is currently assessed qualitatively through physical observation. Such subjective observations can provide only rough estimates of skin damage and hence, it is difficult to predict the possible onset of more severe dermatological complications. A method to quantify erythema in its early stages may provide

an opportunity for intervention prior to its progression to more serious conditions such as desquamation or necrosis (Hopewell, 1990). Although it is unlikely that the course of radiation therapy will be interrupted based on the appearance of such adverse effects, quantifying erythema so measurements can be compared over time may dramatically improve a clinician's ability to predict the integrity of the skin throughout treatment (Pearse *et al.*, 1990).

The appearance of skin colour is ultimately determined by physical characteristics — the way light is scattered and absorbed — and changes in the appearance of tissue are due to changes in these optical properties (Kienle *et al.*, 1996b). As scattering of light in a particular tissue generally remains nearly constant, monitoring erythema becomes a problem of monitoring the changes in optical absorption, arising from changes in the concentration of haemoglobin, the chromophore responsible for the redness.

A region of erythema is likely to have an increased apparent concentration of oxygenated haemoglobin, as compared to deoxygenated haemoglobin, as capillaries dilate and oxygen-rich blood is delivered to the areas of injury to promote healing (Stamatas and Kollias, 2007). The absorption spectrum of oxygenated haemoglobin is different than that of deoxygenated haemoglobin; oxyhaemoglobin has two characteristic absorption peaks, one at 540 nm and another at 576 nm, while deoxyhaemoglobin has a single absorption peak at 555 nm (shown in Figure 1.1). These unique absorption characteristics allow for the quantification of erythema through monitoring changes in concentration of either oxyhaemoglobin or deoxyhaemoglobin as determined from measurements of tissue absorption and knowledge of both absorption spectra.

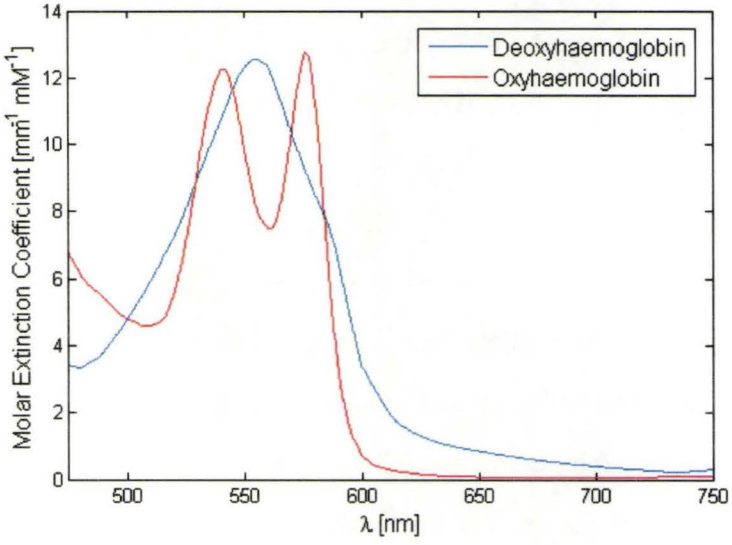

Figure 1.1: The molar extinction coefficients of oxyhaemoglobin and deoxyhaemoglobin (Prahl, 1998).

1.2 Light propagation models

Changes in optical properties can be assessed by probing the tissue with visible light. Visible light penetrates into tissue and, at low intensity, has no adverse biological effects. Measurements can be performed rapidly and non-invasively. However, understanding light propagation in tissue is essential to its use as a diagnostic tool. Photons incident on a surface may be reflected specularly, in a mirror-like reflection, or diffusely, after undergoing several interactions below the surface. The amount of specular reflection depends on the relative index of refraction of the material and the surrounding environment, and yields little information about the optical properties of the underlying medium. However, diffuse reflectance is determined by the amount of scattering and absorption that occurs within the material. Measuring this diffuse reflectance reveals information about these optical properties.

Diffuse reflectance has been measured using several techniques: integrating sphere (Taylor (1920), Jacquez (1955), Pickering *et al.* (1992)), spatially-resolved steady-state (Farrell *et al.* (1992), Kienle *et al.* (1996a), Doornbos *et al.* (1999)), time-domain (Chance *et al.* (1988b), Delpy *et al.* (1988), Patterson *et al.* (1989)), and frequency-domain (Patterson *et al.* (1991a), Pogue and Patterson (1994)). Integrating sphere and steady-state methods often use continuous-wave light sources and measurements of diffuse reflectance over a broad area, or with some degree of spatial resolution. The technological requirements of these techniques are minimal, giving integrating sphere and steady-state methods the advantage of having affordable and accessible components that are relatively simple to use and maintain. The absence of spatial information makes integrating sphere methods unable to accurately separate the individual effects of scattering and absorption without prior knowledge of the scattering spectrum (Hull *et al.*, 1998). Many combinations of scattering and absorption can result in the same diffuse reflectance spectrum. Meanwhile, the relatively few measurement points used in spatially-resolved methods means that derived optical properties are sensitive to local variations (Kienle *et al.*, 1996a). Time-domain diffuse reflectance techniques use a pulsed light source and measure the reflectance over time, at specific source-detector separations. A short pulse of light is incident on the medium. As the photons travel within the medium, scattering interactions broaden the pulse and absorption events attenuate the pulse. The advantage of time-domain techniques is that both scattering and absorption coefficients can be retrieved from a single measure of diffuse reflectance over time (Patterson *et al.*, 1989). However the main disadvantage of time-domain

measurements is that the required equipment is typically complex and thus expensive. Frequency-domain diffuse reflectance systems use an intensity modulated light source and measure changes in phase and amplitude at a single point, or at multiple source-detector separations. The advantages of the frequency-domain method include a reduced sensitivity to noise and a simpler, more reliable data analysis process when compared to time-domain methods. While the use of time-domain and frequency-domain methods in measuring tissue optical properties have been extensively reported, only integrating sphere and spatially-resolved steady-state techniques will be addressed further.

The dependence of diffuse reflectance on optical properties is expressed by light transport models. Used to analyze the measurements, each model defines how light from the source reaches the detector after traveling through the tissue. Several light transport models have been described in the literature. However, only two of these will be considered in this work: Diffusion theory (Patterson *et al.* (1991b), Farrell *et al.* (1992)), and Monte Carlo techniques (Wilson and Adam (1983), Flock *et al.* (1989)).

1.2.1 Diffusion theory

Transport of light in tissue can be described mathematically by the neutral particle transport equation (Star *et al.* (1988), Cheong *et al.* (1990), Patterson *et al.* (1991b)). This accounts for the light scattered into and out of an infinitesimal volume, the light that is absorbed, and any sources of light. While it is difficult to solve the neutral particle transport equation, the general properties of tissue allow for a number of assumptions which can simplify the problem through the diffusion

approximation. Diffusion theory describes the tendency of the radiance, within a highly scattering medium, to become isotropic even when scattering interactions are highly forward-directed (Farrell *et al.*, 1992). When scattering interactions are much more likely than absorption interactions, a narrow collimated beam of light normally incident on the surface of a the medium can be approximated as an isotropic point source at a depth determined by the scattering and absorption properties of the medium (Farrell *et al.*, 1992). However, when the source and detector are close together, or when absorption and scattering are comparable, the diffusion approximation cannot be used; there is not enough scattering to ensure the formation of an isotropic source. When diffusion theory is valid, applying this approximation to the radiative transfer equation yields the diffusion equation

$$\nabla^2\Psi(r) - \frac{\mu_a}{D}\Psi(r) = -\frac{S_0(r)}{D} + 3\nabla \cdot S_1(r) \tag{1.1}$$

where $\Psi(r)$ is the fluence rate at a distance r from the source, $S_0(r)$ and $S_1(r)$ are source terms, and D is the diffusion constant

$$D = \frac{1}{3[\mu_a + (1-g)\mu_s]} \tag{1.2}$$

(Farrell *et al.*, 1992). The scattering coefficient, μ_s, and the absorption coefficient, μ_a, describe the probability per unit pathlength that either a scattering or an absorption interaction occurs, in the limit of infinitesimal pathlengths. Scattering interactions may be directional and the phase function is used to characterize the angular dependence of these interactions; the phase function is a probability density function which specifies the probability associated with scattering through

each angle θ. The anisotropy parameter, g, is the mean cosine of the scattering angle, taking values ranging from g=1 for total forward scattering, g=0 for isotropic scattering, to g=-1 for total backward scattering. Because different combinations of μ_s and g will result in comparable distributions of light, the two parameters are often combined, designating the reduced scattering coefficient, $\mu_s^{'}$, such that $\mu_s^{'} = (1-g)\mu_s$.

The diffusion equation is a differential equation for the energy fluence rate and can occasionally be solved analytically using appropriate boundary conditions. Characterization of these boundary conditions has been the subject of much attention (Haskell *et al.* (1994), Kienle and Patterson (1997b)). For tissue, there is often an index of refraction mismatch between the tissue surface and the incident medium, and the internal reflections at the boundary must be considered. Although there have been several boundary conditions described in the literature — zero boundary condition (Patterson *et al.*, 1989), the extrapolated boundary condition (Farrell *et al.*, 1992), and the partial current boundary condition (Haskell *et al.*, 1994) — in this work only the extrapolated boundary condition was used to assess the spatially-resolved diffuse reflectance measurements. The extrapolated boundary condition has been shown to yield more accurate and consistent optical properties from diffuse reflectance measurements (Kienle and Patterson (1996), Comsa *et al.* (2006)).

1.2.2 Monte Carlo techniques

Monte Carlo techniques model physical processes through computer simulation. First proposed in 1949 by Metropolis and Ulam as a method to investigate neutron

pathlengths through shielding materials, the use of Monte Carlo techniques to simulate the transport of light in tissue was initially described by Wilson and Adam in 1983 (Metropolis and Ulam (1949), Wilson and Adam (1983)). Simulating the path of photons in a medium that both scatters and absorbs, these computational techniques allow for the forward calculation of the diffuse reflectance expected when a material with a given set of optical properties is illuminated under specific conditions.

The Monte Carlo method is the most general technique for modeling light transport based on particle-like photon interactions. Provided the physical conditions are properly defined within the code, the Monte Carlo method can simulate even complex systems where the diffusion approximation fails. However, simulations are computationally expensive, particularly when many millions of photon histories are required for precise results. Recording individual photon histories is time consuming as a photon may scatter many times before being absorbed and lost within the medium. To improve efficiency, simulations make use of photon packets where several photons are launched *en masse*. As the packet moves along a particular path, an absorption interaction no longer implies the loss of an entire photon but rather the adjustment of the packet weight, indicating that some fraction of the packet has been lost to a given interaction. This is a common variance reduction technique to reduce the number of photons necessary to achieve the desired accuracy for a given simulation.

Simulation begins by launching a photon packet into the tissue. Once inside, direction vectors are generated to move the packet through the tissue; the direction vectors are dependent on the scattering phase function and a series of random

numbers. A check is performed after each change in position to determine whether the packet has moved out of the medium. Packets remaining within the tissue are propagated further, changing direction and losing weight at each interaction. If the packet is found to have left the tissue, its weight is scored according to its position (typically given by ρ, the radial distance from the source) and, after many photon histories are recorded, a spatially-resolved diffuse reflectance spectrum is formed. These results can be used to estimate optical properties from spatially-resolved diffuse reflectance measurements, $R(\rho)$, though minimization of the differences between the forward calculated expected results and the observed reflectance.

1.3 Steady-state measurements - Continuous-wave spatially-resolved diffuse reflectance

The technique of determining optical properties from measurements of diffuse reflectance was first presented in 1983 by Groenhuis *et al.*, who illuminated a small area of the upper surface of a material and then measured diffuse reflectance as a function of radial distance from the illumination spot (Groenhuis *et al.*, 1983). In the absence of specular reflection—when the refractive indices match—light incident upon the surface of a material will enter, and undergo several interactions. Photons may be scattered, changing directions after each interaction according to the phase function, without any loss of energy until they are transported through the material or remitted from the upper surface where they originated. Photons may also be absorbed and the energy of the photon is lost within the material. Both scattering and absorption interactions will affect the amount of light that is diffusely reflected

from the surface of the material, and the distance that a given photon travels. The total interaction coefficient, defined as the probability that either a scattering or an absorption interaction occurs, in the limit of infinitesimal pathlengths, is given by $\mu_t' = \mu_a + \mu_s'$. Based on μ_t', the transport mean free pathlength (mfp') is given by $mfp' = 1/\mu_t'$, and defines the average pathlength between interactions. When the total interaction coefficient is low, the mfp' is large, photons will likely travel greater distances between interactions and will be diffusely reflected at greater distances as shown schematically in Figure 1.2. However, when μ_t' is high, the mfp' is low, photons are more likely to interact within a smaller volume and are therefore diffusely reflected at shorter distances as shown in Figure 1.3.

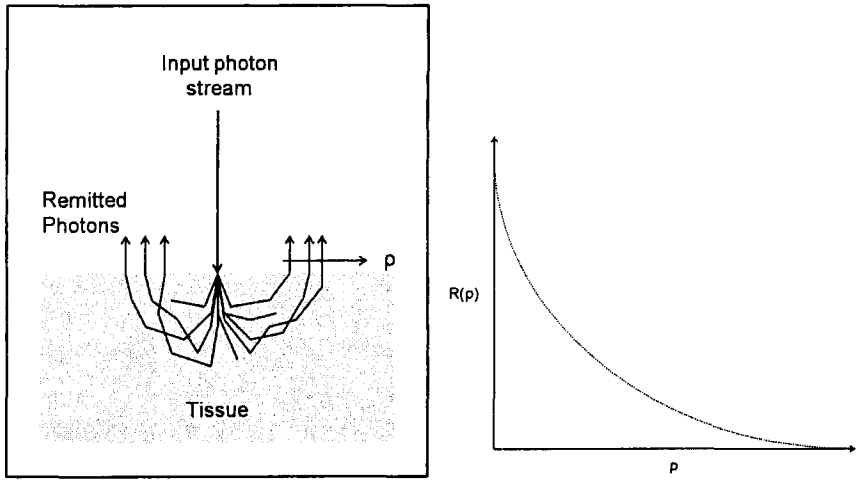

Figure 1.2: Diffuse reflectance for cases where the total interaction coefficient is low. The transport mean free path is large signifying that photons travel a greater distance between interactions. This increases the number of photons diffusely reflected at greater distances as seen on the R(ρ) versus ρ curve presented.

It is evident that the optical properties of the material define the radial dependence of the diffuse reflectance measurement, R(ρ). Therefore, using an appropriate

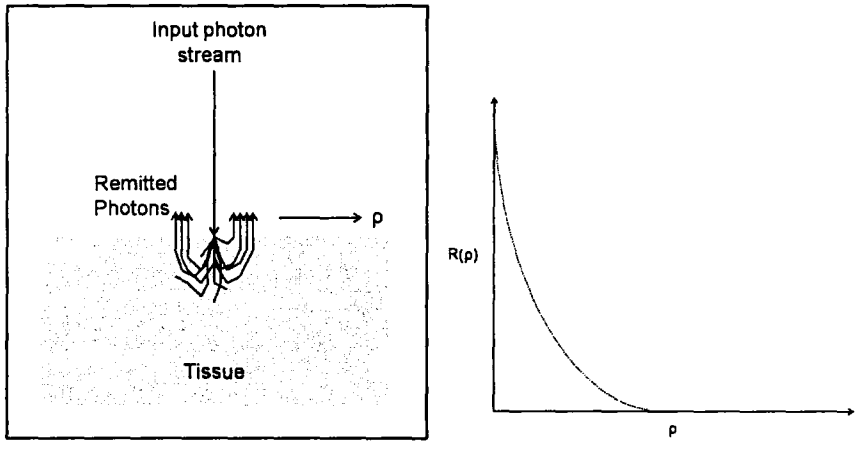

Figure 1.3: Diffuse reflectance for cases where the total interaction coefficient is high. The transport mean free path is low indicating that photons travel a shorter distance between interactions. This decreases the number of photons diffusely reflected at greater distances, and increases the number of photons detected close to the illumination source as seen on the R(ρ) versus ρ curve presented.

light transport model, it is possible to determine μ_a and μ_s' from R(ρ). In this thesis, both diffusion theory models and Monte Carlo techniques were applied to experimental measurements to estimate optical properties from spatially-resolved diffuse reflectance measurements.

Spatially-resolved diffuse reflectance measurements can be made with a monochromatic light source, as originally described by Groenhuis *et al.*, determining optical properties at a given wavelength. However, as tissue optical properties vary with wavelength, the use of a broadband continuous-wave light source together with a spectrometer and "imaging detector" allows simultaneous measurements of reflectance at several wavelengths and several radial distances, in order to estimate tissue optical properties accurately over a wide spectral range (Mourant *et al.* (1997), Nichols *et al.* (1997), Doornbos *et al.* (1999)). This approach has also been

used to quantify the concentration of exogenous chromophores in tissue, such as photosensitizers used in photodynamic therapy (Weersink *et al.*, 1997), and endogenous chromophores in tissue, such as oxygenated and deoxygenated haemoglobin, and melanin (Chance *et al.* (1988a), Cope and Delpy (1988)).

1.4 Steady-state measurements - Integrating sphere diffuse reflectance

The integrating sphere is a simple, optical device. Initially proposed in the early 20th century as a tool to quantify the total output of a light source, integrating spheres are typically used to collect the light remitted from a material, or transmitted through it, by spatially integrating radiant flux. However, applications of the integrating sphere are not limited to detection. With an inner wall made of a highly reflective material, photons incident on the walls of the sphere are scattered multiple times within the cavity prior to their exit through the exit port, whereupon the light source has a uniform radiance within a solid angle, or a uniform irradiance as measured across the port or at larger distances from the opening (Labsphere® (1998), Ducharme *et al.* (1997)). A typical integrating sphere is shown in Figure 1.4.

The surface of an ideal sphere is considered to be Lambertian, appearing to have a constant radiance independent of viewing angle. Materials that display nearly Lambertian reflectance have been developed for use in integrating sphere applications. Labsphere® (North Sutton, NH), a maker of integrating spheres, provides integrating spheres for use as diffuse illumination sources that exhibit

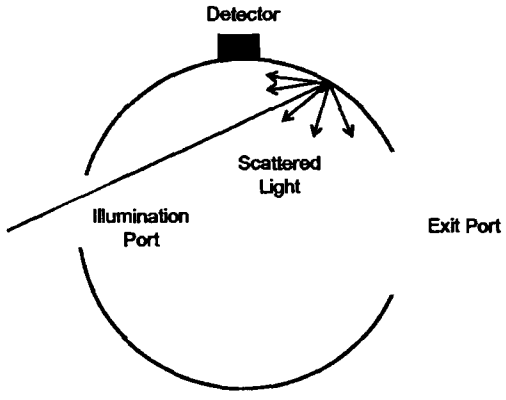

Figure 1.4: Schematic diagram of a simple integrating sphere used as a diffuse illumination source.

greater than 97% radiance uniformity across the opening of the port (Labsphere®, 1998). When used as a detector, photons may enter the cavity of the integrating sphere over a wide range of incident angles. Upon interaction with the sphere walls, photons are scattered multiple times within the cavity until they are collected by an optical fibre, or other detector coupled to the device.

The use of integrating spheres for the determination of optical properties, through the measurements of diffuse reflectance, is an established technique (Taylor (1920), Jacquez (1955), Pickering *et al.* (1993)). Measurements are generally made using two spheres: one sphere serving to measure diffuse reflectance, a second sphere used to determine the amount of light transmitted through a thin slab of the material. The coupled measurement of reflectance and transmittance allows for the estimation of tissue optical properties, both μ_a and $\mu_s^{'}$, with relative ease (Pickering *et al.*, 1993). However, transmittance measurements require samples to be of a finite thickness (where thickness typically ranges from 15 μm to 1 mm), which makes *in vivo* measurements of transmittance difficult (Beek *et al.*, 1997). Figure

1.5 shows a common configuration of a two integrating sphere measurement system used in measuring the optical properties of tissue simulating phantoms.

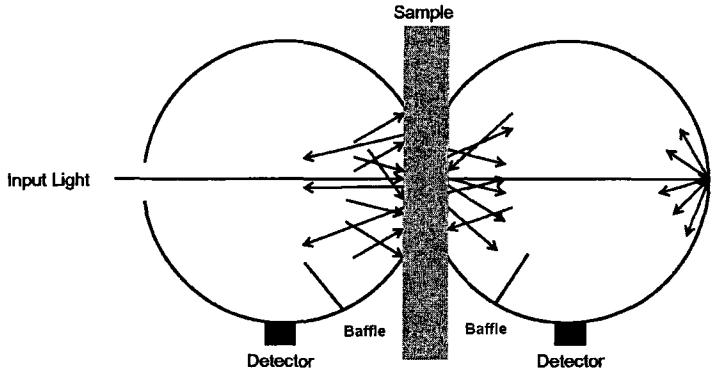

Figure 1.5: A schematic of a typical integrating sphere system using two spheres. In this case, the sample is illuminated with a collimated beam. The integrating sphere on the left side of the sample measures diffuse reflectance while the other measures diffuse transmittance. Typically the detectors are shielded using a baffle, a physical barrier, to prevent the detection of specularly reflected light (Pickering *et al.*, 1993).

The single integrating sphere can be used to illuminate the material under investigation directly, or diffusely; the light is diffused through repeated scattering within the sphere before illuminating the sample. Light remitted from the material re-enters the sphere where it is detected using an optical fibre leading to a spectrometer. Typically, the detector connection is positioned such that there is no direct view of the material. As a result, the reflectance is measured indirectly, after the light scatters within the sphere. However, without a transmittance measurement, or information about the spatial distribution of diffuse reflectance, μ_a and μ_s' can not be determined individually from a diffuse reflectance measurement made with a single integrating sphere. Nevertheless, using estimates of the reduced scattering coefficient, diffuse reflectance measurements made with a single integrating sphere

can be used to determine the absorption coefficient of the material under investigation (Stratonnikov and Loschenov, 2001). Figure 1.6 shows the configuration of a single integrating sphere used for diffuse reflectance measurements using diffuse illumination. Single-sphere measurements of reflectance can thus be performed on thick samples (Bargo *et al.*, 2005).

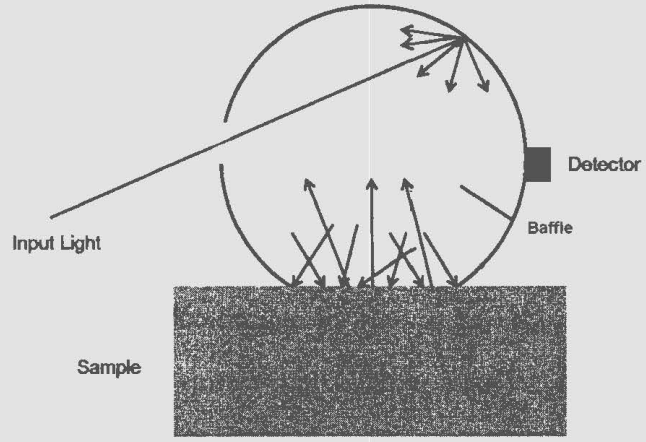

Figure 1.6: Schematic diagram of a simple integrating sphere used in diffuse reflectance measurements. The sample is illuminated with diffuse light. Photons are remitted into the sphere cavity and detected using a coupled optical fibre or detector.

It should be noted that fibre-based spatially-resolved diffuse reflectance systems are limited by a finite number of measurement positions, making them sensitive to local inhomogeneities. The effect of these local variations can be minimized by increasing the area over which the remitted light is measured. The total diffuse reflectance, R_d, is the integral of all the light remitted from a material. Measurements of the total diffuse reflectance would require a detector capable of sampling the entire surface. However, measurements of diffuse reflectance made over a large area are related to the total diffuse reflectance. Using an integrating sphere, such

measures of diffuse reflectance—where the radius of the port opening is large compared to the photon mean free path—can be obtained with relative ease. Unfortunately, the estimation of the optical properties of a semi-infinite medium, using measurements of reflectance made with an integrating sphere, is difficult. A single measurement of diffuse reflectance, in the absence of spatial information, can not yield the two independent values, $\mu_s^{'}$ and μ_a. Characterization of the measurement system determines its sensitivity to changes in the optical properties. Calibration is required to determine the relationship between changes in optical properties and eventual estimates of scattering and absorption. Once well characterized and calibrated, estimates of absolute chromophore concentrations can be made from values of μ_a calculated using integrating sphere measurements of diffuse reflectance and an *a priori* knowledge of $\mu_s^{'}$. There are several techniques which may be used to address the requirement of an *a priori* knowledge of $\mu_s^{'}$. First, published values for $\mu_s^{'}$ exist for many tissues. These estimates can be used in place of individual measured quantities, as scattering varies less between individuals than between tissue types. Second, several measurements, such as haemoglobin oxygen saturation, are relative quantities and therefore do not require an absolute determination of chromophore concentration, or μ_a. Lastly, scattering is presumed to remain constant over time, provided that the original tissue structure remain intact. A single spatially-resolved diffuse reflectance measurement can be used to determine $\mu_s^{'}$ for a given individual and this value can be used in all subsequent integrating sphere measurements.

1.5 Steady-state measurements - Other skin colourimetry measurement techniques

Reflectance spectrometry has been used for the objective assessment of skin colour for more than 50 years. However, many of the spatially-resolved diffuse reflectance measurement systems are considered expensive and too complicated for use in clinical settings (Taylor *et al.*, 2006). Tristimulus reflectance colourimetry has been used as an alternative to traditional reflectance techniques. One of the most common tristimulus colourimeters is the Minolta CR 300 (Elsner, 1995). The light from a xenon flash lamp is separated into two beams: one beam going to a set of colour sensors to control for variations in illumination, the second beam going to illuminating the material under investigation. The remitted light is detected at 450 nm, 550 nm, and 610 nm by three photodiodes. The sensitivity of each of the photodiodes simulates the response of one set of photoreceptors of the human eye. The photodiodes measure the remitted light as an electrical signal expressed in the Commission International d'Eclairage (CIELab) Lab system. The CIELab system describes colours in terms of their lightness (L*), the amount of red or green (a*), and the amount of yellow or blue (b*) (Elsner, 1995). Colours defined in the CIELab colour space are easily compared between measurements, and between measurement devices. However, this ease of use and simplicity comes with several drawbacks. First, colourimeters typically have a small measurement area (≈ 0.5 cm^2) making these measurements sensitive to local variations. Second, colour measurements made in the CIELab colour space do not necessarily quantify physiological changes. Colourimeters use CIELab colour space values to quantify relative changes in the

absorption spectrum at specific wavelengths without assessing these changes as an effect associated with the change in concentration of specific chromophores.

The use of digital photography in quantifying skin colour has also been investigated (Setaro and Sparavigna, 2002). Digital images, acquired as still photographs or video images, can be analyzed using a computer to assess skin colour over the area of the image. A colour reference marker is placed on the skin and images are acquired. Using the reference marker, the contribution of red, blue, and green signals to the skin image is determined (Setaro and Sparavigna, 2002). If the reference marker has known CIELab colour space values, the image can be converted to the CIELab colour space (Yang *et al.*, 2003). These values are used to quantify changes in skin colour due to erythema or increases in pigmentation. The assessment of skin colour using digital photography is highly sensitive to illumination conditions. Without an accurate method to correct for illumination conditions, it is very difficult to compare measurements of skin colour over time. While the quantification of skin colour using digital images is relatively simple and cost-effective it does not provide information on the change in chromophore concentrations resulting in changes in skin colour. Like tristimulus reflectance, digital images provide little information about the physiological changes, e.g., haemoglobin oxygen saturation, causing the apparent changes in colour.

1.6 Clinical applications of diffuse reflectance

Quantification of erythema has been the focus of many investigations and continues to be an area of research in biomedical optics (Dawson *et al.* (1980), Diffey

et al. (1984), Pearse *et al.* (1990), Nyström *et al.* (2004)). Whether induced by external beam radiotherapy, ultraviolet (UV) light exposure, or other irritants, diffuse reflectance spectroscopy has been the primary technique for monitoring changes in skin colour. While useful for assessing the protective ability of sunscreens, or the effect of other topical agents, quantitatively determining the concentration of haemoglobin in the skin is also relevant to studies of tissue oxygenation.

Monitoring tissue oxygenation has been useful in several clinical scenarios. For patients with weakened circulatory systems, or conditions which adversely affect vascular structures, such as heart disease and diabetes, tissue oxygenation is an indication of tissue perfusion. How well a tissue is supplied with blood is an indication of vascular performance, and may allow for clinical intervention to preserve tissue function (Shoemaker *et al.* (1988), Ballard *et al.* (1995)).

A device that can quantitatively determine the concentration of hemoglobin in tissue may be applied to the *in vivo* assessment of other chromophores. For instance, the accumulation of photosensitizer in tissue is of primary interest in photodynamic therapy. The systemic administration of certain photosensitizers for photodynamic therapy (e.g., Photofrin®) has an adverse effect of photosensitizer accumulation in the skin, which may take several weeks to clear. While the concentration of photosensitizer in the skin remains elevated, a patient is light-sensitive and is restricted from exposure to sunlight and other intense light sources. A method to quantify the remaining photosensitizer would likely improve patient quality of life, as the time they are required to protect themselves from light can be determined for each individual.

There is clinical interest in assessing the age of bruises using diffuse reflectance

measurements as the age of a bruise is often an important consideration in forensic investigations (Hughes *et al.* (2004), Randeberg *et al.* (2006)). Soft tissue trauma causes localized vessel damage, allowing blood to pool in the subcutaneous tissues. As haemoglobin is transported into the dermis, a characteristic blue-purple bruise colour is established. Over time the haemoglobin is degraded, first to biliverdin causing a green tint, then rapidly to bilirubin giving the yellow colour associated with older injuries. Assessing the age of the injury for forensic applications can be attempted through estimates of the relative concentration of haemoglobin and its degradation products, biliverdin and bilirubin.

There are many other applications where the *in vivo*, non-invasive, quantification of a particular chromophore would be advantageous. A technically simple, portable device, like an integrating sphere probe, would be a useful tool for these studies.

1.7 Thesis proposal

An integrating sphere system has been developed at the Juravinski Cancer Centre in Hamilton, Ontario, to study the optical properties of biological tissues non-invasively, over a broad spectral range. Constructed of Spectralon®, a highly reflective material, the integrating sphere served as both a diffuse illumination source and a diffuse reflectance detector. It is a technically simple measurement apparatus with numerous advantages; the integrating sphere system is portable, easy-to-use and samples the remitted light over a larger area than traditional fibre-based systems therefore minimizing the effect of local inhomogeneities. The aim of the thesis

was to use the integrating sphere based system and to identify the applicability of the system as a method to quantify the concentration of haemoglobin in the skin.

Simple, preliminary investigations had demonstrated that the system was capable of monitoring changes in the reflectance spectrum of tissue. When the uncharacterized probe was placed on the skin surface, oxygenated haemoglobin absorption peaks were observed in the reflectance spectrum. As the the flow of blood was restricted using a tourniquet, the reflectance spectrum changed; the oxygenated haemoglobin absorption peaks were gradually replaced by the absorption peak of deoxygenated haemoglobin. However, without thorough characterization it was unclear how these observable changes related to the change in optical properties.

Characterization experiments were performed in tissue simulating liquid phantoms. Using these phantoms to simulate a wide range of physiologically-relevant optical properties, a relationship was determined between the measured signal R*, and the optical properties $\mu_s^{'}$ and μ_a. With this relationship established, experiments in single-layer homogeneous phantoms demonstrated that the integrating sphere system could be used to determine the concentration of an added absorber. Haemoglobin deoxygenation experiments were carried out in a homogenous geometry to ensure that the haemoglobin concentration of a simple phantom could be assessed.

The successful performance of the integrating sphere system in the homogenous geometry led to two-layer experiments. A two-layer geometry was chosen for its relative simplicity, allowing for the use of homogeneous liquid phantoms representing each of the distinct layers, and for its approximation of human skin. The bottom of the two-layer phantom contained varied concentrations of an absorber. By varying

the thickness of the top-layer, the response of the integrating sphere system was determined for various top layer thicknesses. It was demonstrated that the system could measure changes in haemoglobin oxygen saturation, and therefore changes in erythema, in a layered, skin-like geometry. Finally erythema, induced by the application of a topical anesthetic cream, was measured *in vivo* for a human volunteer and quantified according to a defined erythema index and apparent haemoglobin oxygen saturation. These results demonstrated that the integrating sphere system was a viable tool for quantifying changes in tissue optical properties which could be used to monitor erythema in a clinical setting.

Chapter 2

Theory and Data Analysis

2.1 Introduction

Measurements made with the integrating sphere system were verified by measurements using a fibre-based continuous-wave spatially-resolved system. Data from each system were analyzed independently: integrating sphere measurements were analyzed using an empirically defined model and spatially-resolved measurements were analyzed using both a diffusion model and Monte Carlo simulations. Using the estimated absorption coefficient from the integrating sphere measurements, the concentration of a particular absorber was calculated and compared with the "gold standard" values determined from the spatially-resolved system and from a determination of expected concentration based on volumetric analysis. In deoxygenation experiments, haemoglobin deoxygenation was accomplished through the addition of dry-active yeast to the phantom volume. However, the use of yeast made it impossible to calculate the expected concentration of oxy- and deoxyhaemoglobin from

volumetric analysis due to the continuous consumption of oxygen by the yeast. At any point in the deoxygenation, it was not possible to assess the expected concentration of oxygenated or deoxygenated haemoglobin as the rate of oxygen consumption of yeast was not known. Therefore the absorption coefficients retrieved from integrating sphere measurements were compared only with the values determined from the spatially-resolved system. A singular value decomposition algorithm was used to determine the concentrations of oxy- and deoxyhaemoglobin from the absorption coefficient obtained using the integrating sphere. These concentrations were used to calculate the oxygen saturation of haemoglobin. Measurements of oxygen saturation were found to correlate well with the erythema index as defined by Dawson *et al.* (Dawson *et al.*, 1980). A modified erythema index, which may be used to assess changes in skin colour, was derived based on the Dawson erythema index, using measurements of tissue oxygen saturation. This modified erythema index was then used to monitor changes in skin redness in an *in vivo* application.

2.2 Integrating sphere measurements

The "signal" detected at the output port of an integrating sphere is a function of several parameters: the surface area of the sphere, the area of any openings, the reflectance of the material composing the sphere, and the reflectance of the sample under investigation. Theoretical models have been developed to describe this interrelationship for specific integrating sphere measurement geometries (Pickering *et al.* (1992), Pickering *et al.* (1993)). These geometries are shown in Figure 2.1.

However, this theory does not extend to the measurement geometry of the integrating sphere probe being assessed in this study, where light is detected directly by a downward-looking optical fibre (Figure 2.2). As a result, generalized integrating sphere theory cannot be applied and an alternate model must be derived. This geometry was selected in part, for its similarity to commercially available tristimulus reflectance colourimeters and for its simplicity and ease of construction. Experimental measurements on tissue-simulating phantoms were used to define an empirical light transport model specific to this particular probe and measurement geometry. Other factors, such as the effect of using a transparent cellophane wrapping to prevent the liquid from tissue-simulating phantoms from entering the probe cavity or the possible contribution of specularly reflected photons, were incorporated into the model. While this provides a robust empirical model, it also implies that any changes to the integrating sphere probe, or detection system, requires both a new characterization and empirical model. Measurements using the integrating sphere probe were assessed using the empirically-derived model in order to determine the absorption coefficient of the material under investigation.

2.2.1 Using reflectance standards

Calibrated reflectance standards are commonly used to normalize measured reflectance spectra. Normalization is required to account for a number of variations including temporal changes in lamp intensity, probe configuration, optical fibre replacement, and equipment set-up. Typically, the calibrated reflectance standards are composed of Spectralon®, a highly reflective material. The reflectance of a particular reflectance standard can be lowered by doping the Spectralon® with a

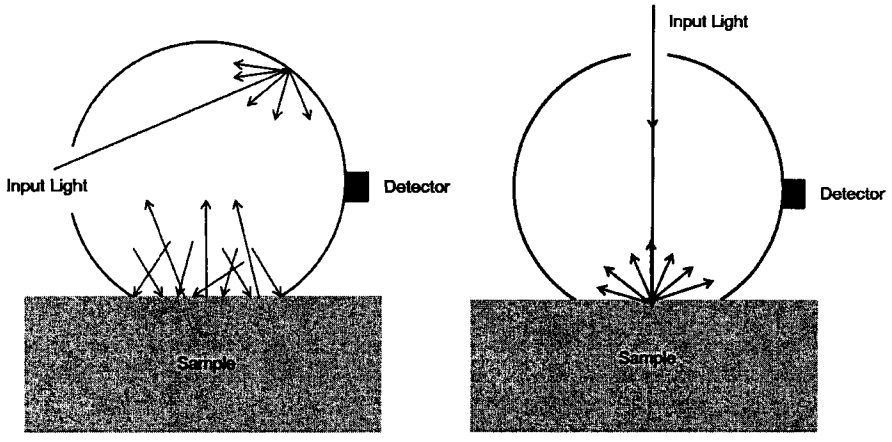

Figure 2.1: A schematic of two typical integrating sphere systems using a single sphere. The figure on the left shows the case where a sample is diffusely illuminated. The figure on the right shows the case where the sample is illuminated with a collimated beam. In both geometries remitted photons are detected only after scattering within the sphere cavity (Pickering *et al.*, 1993).

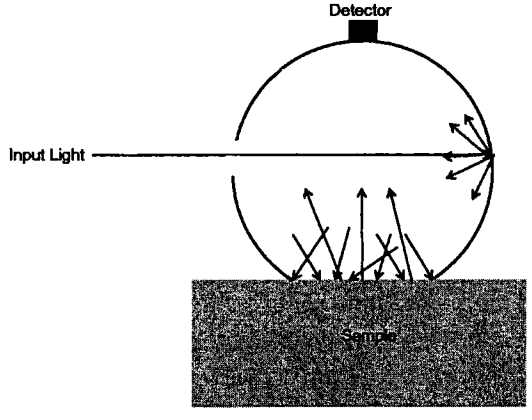

Figure 2.2: A schematic of integrating sphere system used in the current study. Light is first incident on the sphere walls resulting in a diffuse illumination source. Remitted photons are detected by a downward-looking optical fibre.

pigment to increase the amount of absorption. Spectralon® however, has an extremely high scattering coefficient ($\mu_s' = 50$ mm^{-1} at 660 nm) as compared to tissue (Caucasian skin has $\mu_s' = 2.3 \pm 0.5$ mm^{-1} at 650 nm) (Tseng *et al.*, 2008).

The integrating sphere system measures the light collected at the detection fibre port with signal intensity being measured in a unitless value called "counts", where the number of counts is proportional to the number of photons collected (Ocean Optics, 2000). Measurements of calibrated reflectance standards were used to assess the system response, mapping measured signal intensity to reflectance values. The high scattering of Spectralon® introduced a significant challenge when used with the integrating sphere probe. The finite port opening of the integrating sphere probe should measure only a fraction of the total diffuse reflectance, as R_d is the integral of radially-dependent diffuse reflectance across the entire surface (Farrell *et al.*, 1992). However, light entering the Spectralon® standards was remitted after traveling short distances; the high reduced scattering coefficient implies very short photon pathlengths such that very few photons scatter beyond the port opening of the sphere, minimizing lateral losses.

For tissue or tissue-simulating phantoms there is a lower value of reduced scatter coefficient such that photons may travel deeper into the material and farther from their original entrance position. As photons penetrate more deeply there is a greater chance that they will be scattered away from the port opening of the sphere. This lowered the detected signal intensity and, when compared to the response curve generated using the reflectance standards, corresponded to a lower reflectance value than expected for the optical properties of these materials. Thus, normalizing reflectance measurements made on tissue or tissue-simulating phantoms to the reflectance measured on the reflectance standards yielded values lower than expected. Rather than using the instrument response curve generated from

measurements of the reflectance standards a different approach was used. Integrating sphere measurements were normalized to a single standard (99% reflectance) to account for any day-to-day variations due to changes in lamp intensity or probe set-up and an empirical model was defined using measurement on tissue simulating phantoms to describe the instrument response.

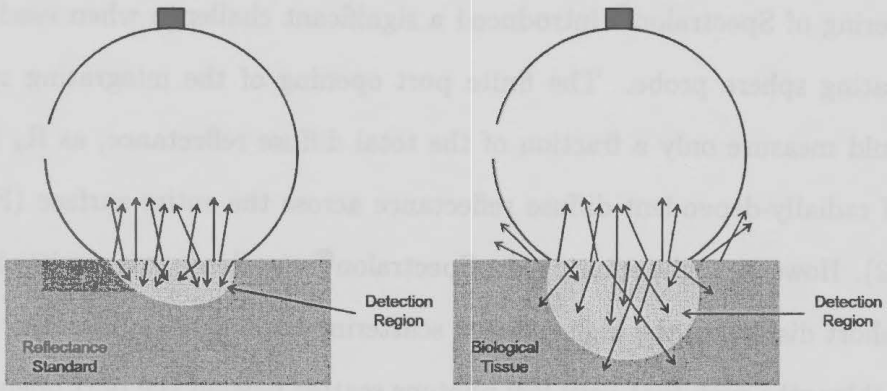

Figure 2.3: Comparison of measurements made on Spectralon® and biological tissue. The short photon pathlength within the Spectralon® standard increases the likelihood that these photons will be detected when they are remitted. In the case of biological tissue, photon pathlengths are longer and photons can move beyond the port opening decreasing the probability that they will be detected when these photons are remitted.

2.2.2 Empirical model

Homogeneous, tissue-simulating phantoms were used to determine the relationship between the integrating sphere system response and various optical properties. The port opening on the bottom of the probe was sealed with an adhesive transparent dressing (Tegaderm™, 3M®, St. Paul, MN) and the probe was wrapped in a cellophane film to prevent the liquid phantom material from entering the sphere.

A series of liquid phantoms simulating a wide range of physiologically-relevant tissue optical properties was prepared, and these optical properties were verified using measurements made with the continuous-wave, spatially-resolved measurement system.

Measurements of liquid phantoms were normalized using a measurement of the 99% reflectance standard, to correct for any day-to-day variations. The normalized reflectance values determined by the integrating sphere were given by R* and a relationship between R*, μ_s', and μ_a was determined.

2.2.3 Concentration of added absorbers

Experiments in single-layer homogeneous phantoms with added absorbers used the empirical model to determine values of μ_a from integrating sphere measurements of R* and a value of μ_s' determined from the spatially-resolved diffuse reflectance system. A singular value decomposition fitting algorithm was used to resolve the measured absorption spectrum into the concentration of each absorber using its corresponding extinction coefficient. The extinction coefficient is an optical property which measures the absorption per unit concentration. The singular value decomposition algorithm was used to solve a set of linear equations, $Ax = b$, where A is a matrix formed from the extinction coefficients of the chromophores present, x is the concentration matrix and b is the measured absorption spectrum, through a least squares minimization technique.

The ability of the integrating sphere system to determine absorber concentration as a function of top layer thickness was characterized using experiments performed in a two-layer geometry. The reflectance spectrum was measured through

a top-layer phantom material of various thicknesses. These data were analyzed as though the two layer geometry were homogenous; no modifications were made to the method of analysis to differentiate measurements made in two-layers from those made in homogeneous phantoms.

2.2.4 Haemoglobin oxygen saturation

The concentration of oxygenated and deoxygenated haemoglobin can be used to determine haemoglobin oxygen saturation, SO_2 as

$$SO_2 = \frac{[HbO_2]}{[Hb] + [HbO_2]} \tag{2.1}$$

where $[HbO_2]$ is the concentration of oxyhaemoglobin and $[Hb]$ is the concentration of deoxyhaemoglobin. The total haemoglobin concentration, $[tHb]$, can be calculated such that $[tHb] = [Hb] + [HbO_2]$. The concentration of oxy- and deoxyhaemoglobin can be determined through measurements of the absorption coefficient

$$\mu_a(\lambda) = [HbO_2]\epsilon(\lambda)_{HbO_2} + [Hb]\epsilon(\lambda)_{Hb} + \mu_a(\lambda)_{background} \tag{2.2}$$

where $\mu_a(\lambda)$ is the absorption coefficient measured at wavelength λ, $\epsilon(\lambda)$ are the extinction coefficients for each absorber at wavelength λ, and $\mu_a(\lambda)_{background}$ is the background absorption associated with other absorbers (Hull *et al.*, 1998).

For tissue-simulating liquid phantoms, the concentration of oxy- and deoxyhaemoglobin was determined by applying a singular value decomposition algorithm to the measured absorption spectrum using the known extinction coefficients of

both absorbers. The absorption spectra were verified using spatially-resolved diffuse reflectance measurements, while the retrieved total haemoglobin concentration was compared to the expected value as assessed through the volumetric addition of whole blood. The estimated concentrations were then used to determine the haemoglobin saturation using Equation 2.1.

Dry-active yeast was added to deoxygenate the phantom. It was impossible to determine the concentration of oxy- or deoxyhaemoglobin volumetrically due to the continuous consumption of oxygen by the yeast. The retrieved concentrations of each product were verified with an alternative method. The haemoglobin oxygen dissociation curve (Figure 2.4) has a characteristic sigmoidal shape that can be described mathematically as

$$SO_2 = \frac{pO_2^n}{p_{50}^n + pO_2^n} \tag{2.3}$$

where pO_2 is the oxygen partial pressure, p_{50} is the oxygen partial pressure at which haemoglobin is 50% saturated, and n is a dimensionless parameter known as the Hill coefficient (Zwart *et al.*, 1984). The oxygen partial pressures of the tissue-simulating phantom were measured using a Clark-type oxygen electrode. Calculating SO_2 from the retrieved concentration of oxygenated and total haemoglobin, the values for p_{50} and for n were determined, for a given set of experimental conditions, and compared with published values thus assessing the haemoglobin oxygen saturation estimates determined using the integrating sphere.

The values for the Hill coefficient n and for p_{50} describe the shape of the oxygen dissociation curve. The Hill coefficient measures the degree of cooperativity in

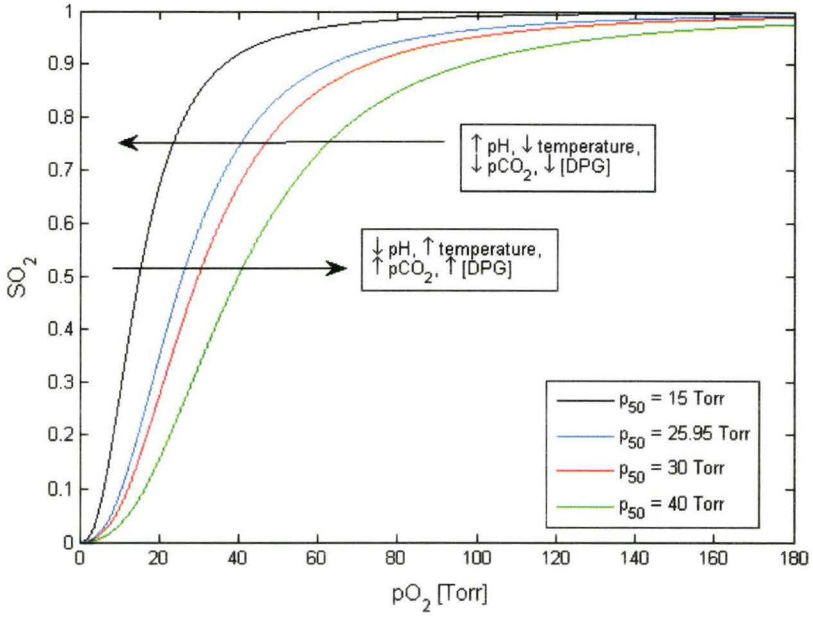

Figure 2.4: The haemoglobin-oxygen dissociation curve as described by Equation 2.3 for values of a constant value of n and a range of p_{50} values, where n = 2.46±0.05 (pH ≈ 7 at 37 °C).

oxygen binding, increasing with the degree of cooperativity. There are four oxygen binding sites associated with each haemoglobin molecule. As oxygen is bound to one site, there is a conformational change in the haemoglobin molecule that facilitates oxygen binding at the remaining sites (Stryer, 1988). The cooperative binding of oxygen by haemoglobin enhances the ability of the haemoglobin molecule to deliver oxygen under typical physiological conditions as compared to independent oxygen binding (Stryer, 1988). There are several factors which affect haemoglobin oxygen affinity, and therefore the shape of the haemoglobin oxygen dissociation curve: pH, the partial pressure of carbon dioxide, temperature, and the concentration of 2,3-di-phosphoglycerate (DPG) (Tortora, 2000).

Decreases in pH decrease haemoglobin oxygen affinity. The increased acidity shifts the haemoglobin oxygen dissociation curve to the right such that the haemoglobin molecule is less saturated at a given pO_2. This increases the value of p_{50} while having no effect on the cooperativity (for pH between 7 and 9) (Tsuneshige *et al.*, 2002). The partial pressure of carbon dioxide, pCO_2, also affects oxygen affinity. When carbon dioxide enters the blood much of it is converted to carbonic acid (H_2CO_3) thus lowering the pH and shifting the haemoglobin oxygen dissociation curve to the right. Even without an associated decrease in pH, increasing concentrations of carbon dioxide lower the oxygen affinity to promote the release of oxygen into metabolically active tissues; carbon dioxide is a product of metabolic reactions (Tortora, 2000). Increasing temperature also shifts the haemoglobin oxygen dissociation curve to the right. Heat is also by-product of metabolic reactions. DPG is produced in cells during the metabolism of glucose. When DPG combines with haemoglobin, oxygen affinity is lowered to allow for greater oxygen unloading from the haemoglobin molecule. Changes in the way oxygen is bound and then released from the haemoglobin molecule are reflected in the values of p_{50} and n. Hull *et al.* described a method to verify the concentration of oxygenated and deoxygenated haemoglobin retrieved using an optical system by comparing the calculated values of p_{50} and n to values published in the literature. However, calculating the value of p_{50} for three different human samples, Zwart *et al.* found that p_{50} varied with intra-erythrocytic concentration of DPG such that a 10% increase in intra-erythrocytic DPG concentration resulted in a roughly 8% increase in p_{50} (Zwart *et al.*, 1982). Additionally, Zwart *et al.* found that p_{50} varied with temperature where p_{50} increased from 10.43 ± 0.90 Torr at 22 °C to 32.33 ± 1.35 Torr at 42

°C. Thus, the value of p_{50} depends on the physiological conditions of measurement and it is therefore necessary to replicate the physiological conditions under which p_{50} was measured when comparing results to published values. This is particularly true for tissue-simulating phantoms where the range of pH, pCO_2, and temperature of the phantoms can extend well beyond the values typically observed *in vivo*. As such, variations in calculated p_{50} may not necessarily indicate invalid measurements of haemoglobin oxygen saturation, as it is dependent on many parameters which may not be measured directly, or are difficult to control (e.g., pCO_2). However, the Hill coefficient, n, is relatively insensitive to small changes in pH, pCO_2, temperature, and concentration of DPG (Bunn and Guidotti (1972), Zwart *et al.* (1982), Zwart *et al.* (1984)). Therefore it is more suited to be used as an indicator of the accuracy of retrieved optical properties, as the Hill coefficient generally remains constant over a wide range of physiological conditions. Typically, the Hill coefficient, $n = 2.46 \pm 0.05$ determined at physiological conditions, at $pH = 7.4$ and temperature of 37°C (Zwart *et al.*, 1984).

2.2.5 Modified erythema index

The apparent colour of is skin is primarily determined by melanin and haemoglobin. Increasing concentrations of melanin make the skin appear dark, while haemoglobin adds a red hue. Attempts to quantify skin colour have resulted in the definition of a variety of indices. The erythema index was first introduced by Dawson *et al.* who defined the use of the logarithm of the inverse of the reflectance (LIR) curve to be analogous to absorbance. Dawson *et al.* defined the erythema index to be proportional to the area under the LIR curve, above a determined

baseline level, for wavelengths between 510 nm and 610 nm (Dawson *et al.*, 1980). The erythema index quantifies changes in the LIR spectrum associated with an increased concentration of haemoglobin in the skin. It remains the most commonly used index in quantifying skin redness. However, several other parameters, such as the pigmentation index (Dolotov *et al.*, 2004), the hemoglobin index (Feather *et al.*, 1989), the oxygenation index (Feather *et al.*, 1989), and the melanin index (Dawson *et al.*, 1980) have also been derived. Each of these factors is intended to quantify the complex colour changes associated with measured reflectance spectra using a single numerical value. Characterization of each index results in an ability to discern colour changes barely visible through visual observation, but correlated to a change in the concentration of the chromophore associated with it. While these parameters should reflect physiological changes, they do not reflect these changes explicitly. For instance, the melanin index does not quantify changes in the absolute concentration of melanin in the skin; the melanin index is used to quantify changes in the absorption spectrum which can be attributed to an increase in skin pigmentation. The value of the melanin index thus reflects a physiological change (increased pigmentation of the skin) without explicitly determining the increased concentration of melanin present.

Since erythema is associated with an increase in the apparent concentration of oxygenated haemoglobin, measures of apparent SO_2 were found to be correlated with the erythema index derived by Dawson *et al.* (Kollias *et al.*, 1995). This is particularly true for irritant-induced erythema for which the apparent concentration of oxygenated haemoglobin (Kollias *et al.*, 1995) can be used to quantify skin redness. For erythema induced by exposure to ultraviolet (UV) light there is

an increase in the apparent concentration of oxygenated haemoglobin accompanied by a slight increase in the apparent concentration of deoxygenated haemoglobin. However, the increase in the apparent concentration of oxygenated haemoglobin dominates this effect (Kollias N, 1988). As such, a modified erythema index was defined to be equal to the apparent haemoglobin oxygen saturation of a region of tissue. The haemoglobin oxygen saturation in a tissue-simulating phantom, where haemoglobin is in a homogenous mixture, is calculated from the measured concentration of oxy- and deoxyhaemoglobin. However, when measuring tissue *in vivo* the haemoglobin is not uniformly distributed and the calculated haemoglobin oxygen saturation is reduced. Although haemoglobin within the artery is still more that 95% saturated, the measured concentration of oxy- and deoxyhaemoglobin is measured over the bulk of the tissue. To indicate this variation, the term apparent haemoglobin oxygen saturation will be used to denote haemoglobin oxygen saturation measurements made across the bulk of the tissue. The comparison of apparent haemoglobin oxygen saturation to the Dawson erythema index are shown for the two-layer experiments in Section 6.3.1.

2.3 Continuous-wave, spatially-resolved measurements

The optical properties of each material under investigation were verified using the continuous-wave method of optical fibre-based spatially-resolved diffuse reflectance measurements. Using physical models of light propagation, the dependence of the measured reflectance on the distance from the source was used

to determine optical properties. The data were fitted with both a semi-infinite diffusion model, and a Monte Carlo based non-linear regression model.

2.3.1 Application of the diffusion model to experimental measurement

Light propagation in tissue can be modeled using the neutral particle transport equation. Farrell *et al.* developed a diffusion theory model to solve the neutral particle transport equation whereby the optical properties of a material could be determined from the shape of the radially-dependent diffuse reflectance curve. The reflectance due to an external pencil beam was considered equivalent to that produced by an isotropic point source embedded in the material at a depth of one transport mean free path. Several assumptions must be made in order to produce analytic solutions using the diffusion equation; the source is assumed to be isotropic, the resulting radiance is assumed to be nearly isotropic while the tissue is presumed to be homogeneous and semi-infinite. Although these assumptions introduce limitations in the diffusion model, provided several conditions are met it is possible to produce valid analytical solutions for spatially-resolved steady-state reflectance due to a point-source. However, there are several conditions for which diffusion theory solutions are invalid. First, when the source-detector distances are small, i.e., $\mu_s'\rho \leq 1$, the source is not considered to have become isotropic before being detected (Farrell *et al.*, 1992). Second, diffusion theory solutions are invalid when absorption and scattering coefficients are similar. For tissue, which is highly forward scattering, absorption is typically much smaller than scattering, satisfying the relationship $\mu_a < 0.1\mu_s'$ (Farrell *et al.*, 1992). The design of the probe used in

the spatially-resolved measurements, and the optical properties of the phantoms, ensures that diffusion theory solutions are valid for these measurements.

Much attention has been devoted to the selection of appropriate boundary conditions in solving the diffusion equation; the improper application of boundary conditions yields incorrect optical properties. Diffuse reflectance measurements made by the continuous-wave, spatially-resolved system were fitted using the diffusion model and the extrapolated boundary condition described by Haskell *et al.* and Kienle and Patterson (Haskell *et al.* (1994), Kienle and Patterson (1997b)).

Deriving an expression for the radially-dependent diffuse reflectance involves solving the diffusion equation (Equation 1.1) with a source term due to a normally incident pencil beam source at the boundary. The extrapolated boundary condition is applied and requires that the fluence rate tends to zero at an extrapolated boundary a distance z_b beyond the surface (Farrell *et al.* (1992), Haskell *et al.* (1994), Kienle and Patterson (1997a)). The solution for the fluence, $\Psi(\rho)$, is

$$\Psi(\rho) = \frac{1}{4\pi D}\left[\frac{exp(-\mu_{eff}\cdot r_1)}{r_1} - \frac{exp(-\mu_{eff}\cdot r_2)}{r_2}\right] \tag{2.4}$$

where ρ is the radial distance from the source, D is the diffusion constant defined in Equation 1.2, $r_1 = [d^2+\rho^2]^{1/2}$, $r_2 = [(d+2z_b)^2+\rho^2+]^{1/2}$, where d = $1/\mu_s^{'}$ and z_b is the position of the extrapolated boundary on which the fluence rate equals zero such that $z_b = \frac{1+R_{eff}}{1-R_{eff}}\cdot 2D$, and R_{eff} is the fraction of photons internally reflected at the boundary (Farrell *et al.*, 1992).

The radially-dependent diffuse reflectance is thus given by

$$R(\rho) = T_\Phi \cdot \Psi(\rho, z=0) + T_j \cdot \frac{\partial\Psi(\rho, z=0)}{\partial z} \tag{2.5}$$

where for a refractive index of n=1.33, assumed for the liquid phantoms under investigation, the Fresnel transmission coefficients are $T_\Phi = 0.132$ and $T_j = 0.336$ and $\frac{\partial \Psi(\rho, z=0)}{\partial z}$ is the partial derivative of Equation 2.4 with respect to z.

Using a non-linear least squares fitting routine, the measured reflectance data were fitted using the expression for $R(\rho)$ in Equation 2.5, iteratively optimizing the values of $\mu_s^{'}$ and μ_a. The retrieved values of the reduced scattering and absorption coefficient were compared to those retrieved using Monte Carlo methods and to the expected values of $\mu_s^{'}$ and μ_a calculated from the estimated optical properties of each phantom component and their volumetric proportion in the final phantom.

2.3.2 Application of Monte Carlo methods to experimental measurement

Monte Carlo methods were also used to determine optical properties from measurements of spatially-resolved, diffuse reflectance. Measured reflectance data were fitted using Monte Carlo simulations generated using different optical properties and a non-linear least squares fitting routine. However, generating a complete set of Monte Carlo simulations for the entire range of expected optical properties bears an enormous computational expense. To overcome this challenge, Kienle and Patterson introduced a modified approach to the Monte Carlo technique in which the optical properties of turbid media could be determined from a single Monte Carlo simulation when both the relative refractive index, n_{rel}, and the anisotropy parameter are known (Kienle and Patterson, 1996).

The probability of absorption, at some exit distance ρ (see Figures 1.2 and 1.3), can be determined from knowledge of both the mean free path between scattering

events and the total number of such events. The distance between the scattering events can be scaled to account for various scattering coefficients as the mean free path (mfp) between events is defined as the inverse of the scattering coefficient.

Rather than assign fixed values of μ_s, μ_a, n_{rel}, and g at the beginning of each simulation (tantamount to launching photons into a medium of uniquely specified optical properties and scoring millions of photon histories) only n_{rel}, and g are fixed. The scoring routine was modified; photons exiting the material were scored in radial bins measured in units of mean free paths, as compared to the scoring scenario for a standard Monte Carlo approach, in which radial bins are defined according to their physical distance from the source. In addition to scoring photon weight as described in Section 1.2.2, the number of scatters a given photon packet experienced were also scored. With this added information, the reflectance data were scaled for any combination of $\mu_s^{'}$ and μ_a producing a spatially-resolved reflectance curve that was used to fit experimental data by repeatedly adjusting μ_s and μ_a, minimizing χ^2, until the fit converged.

In previous studies, an extensive mega Monte Carlo look-up table was produced for determining optical properties from spatially-resolved diffuse reflectance measurements. A computer algorithm was added to the software used for data analysis and using values of n_{rel} and g as inputs, a non-linear least squares fitting routine determined μ_s and μ_a from measured reflectance. The resultant optical properties were compared to those retrieved using the diffusion model fit and a mean of the retrieved $\mu_s^{'}$ and μ_a was taken; the values returned from fitting with the diffusion model and those from fitting with Monte Carlo simulations agreed within fitting uncertainties.

Chapter 3

Experimental Methods

3.1 Introduction

The aim of this study was to characterize the integrating sphere system and ultimately assess its performance in quantifying the concentration of chromophores in the skin, with the goal of quantifying erythema. This chapter describes the integrating sphere system used throughout this thesis, its components and their use, as well as the preparation of the probe and typical calibration measurements. It also describes the continuous-wave, spatially-resolved system used to verify the optical properties measured by the integrating sphere system. The preparation of liquid phantoms and the properties of added absorbers are also discussed as the majority of measurements were made using liquid phantoms.

3.2 Integrating sphere system

The integrating sphere system (IS) was comprised of several components: the integrating sphere probe, a broadband white light source, a spectrometer, and a computer. The organization of the instrumentation is shown in Figure 3.1.

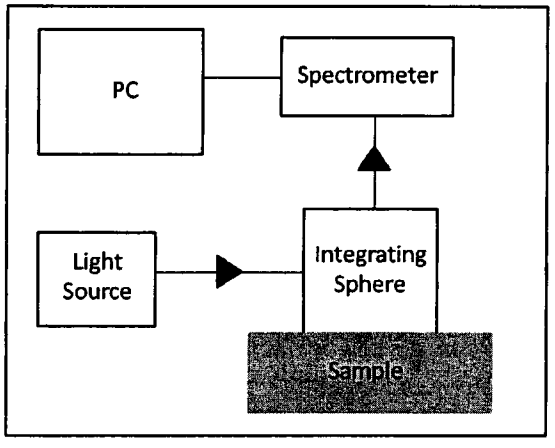

Figure 3.1: Schematic diagram of the integrating sphere measurement system.

The integrating sphere was constructed from Spectralon® (Labsphere®, North Sutton NH), a highly reflective material with 99% reflectance from 400 nm to 1500 nm (Labsphere® Optical-Grade Spectralon® Datasheet). At the Juravinski Cancer Centre, a solid Spectralon® block measuring 5.1 cm wide, 5.1 cm deep and 3.9 cm high, was cut into two slabs to allow a void to be machined inside. The slabs were rejoined forming a hollow sphere, having a diameter of 3.18 cm, within the block. Optical fibre connectors were positioned to provide access for optical fibres used for illumination and detection. An opening was then machined in the bottom of the probe. The port opening, having a diameter of 1.47 cm, allowed light to leave the sphere and enter the material under investigation; light remitted from the

material re-enters the sphere through the same port. Figures 3.2 and 3.3 show the dimensions of the integrating sphere probe and the positions of the optical fibre connectors.

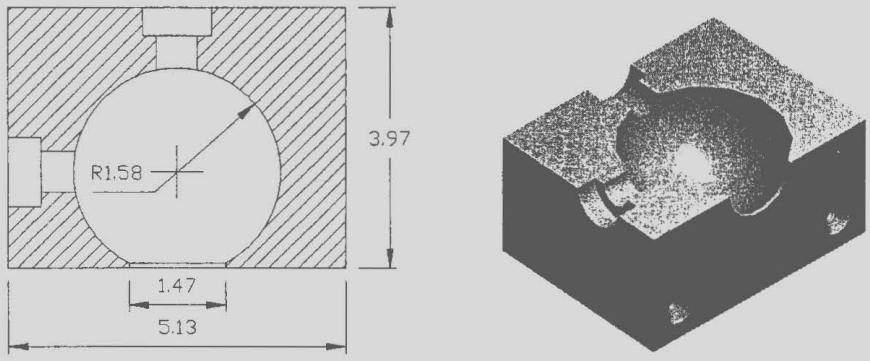

Figure 3.2: The figure on the left is a side view of the integrating sphere. The dimensions are in units of centimetres. The optical fibre connectors can be seen at the top of the sphere (opposite the port opening) and on the left side of the sphere (90° to the port opening). The figure on the right is a three dimensional cross-section of thc integrating sphere probe. The cylindrical grooves denote the position of the optical fibre connectors.

As shown in Figures 3.2 and 3.3, connectors for attaching optical fibres are placed at 90° to the port opening (light from an optical fibre connected in this position is incident directly on a sphere wall) and directly above the port opening (a detection fibre connected in this position has a direct view of the material surface). Placing fibres in the reverse configuration, with an illumination fibre above the port opening, provided direct illumination of the sample. However, connecting the illumination fibre so that light is incident on a sphere wall ensured that light leaving the sphere was diffuse. There was a small difference in the detected reflectance signal based on the illumination scheme (Figure 3.4). Light incident on the material directly will penetrate deeper into the material, before becoming isotropic at

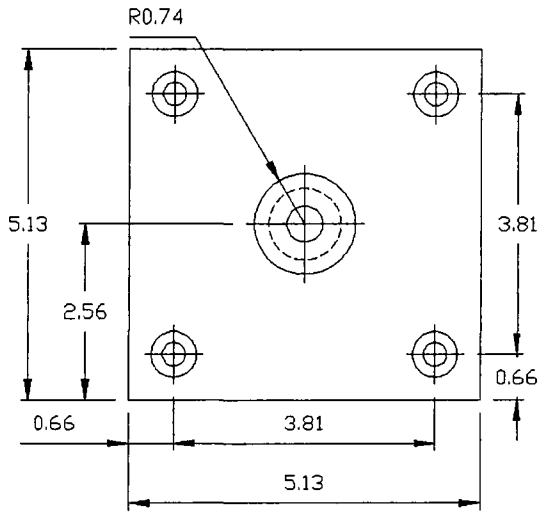

Figure 3.3: A view of the integrating sphere across the bottom surface showing the size and position of the port opening. An optical fibre connector can be seen through the port opening. The dimensions are in units of centimetres.

a depth of one transport mean free path. When using a reflectance standard, the difference in detected reflectance signals was small as the high reduced scattering coefficient associated with the Spectralon® corresponded to a lower value for the transport mean free pathlength. Illuminating with diffuse light reduces the penetration depth of the photons, so comparatively fewer photons traveled distances beyond the port opening. Using a tissue-simulating phantom, the difference in the detected reflectance signals was greater. The lower reduced scattering coefficient corresponded to a greater transport mean free pathlength, so under direct illumination a greater number of photons traveled beyond the port opening, resulting in a lower detected reflectance signal.

The final configuration, indirect illumination with direct detection shown in Figure 3.5, is common among commercially available colourimeters (Elsner, 1995).

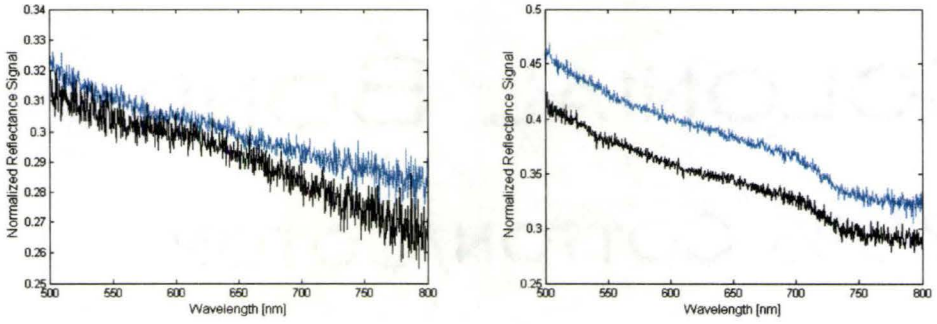

Figure 3.4: The detected reflectance signals from the two illumination schemes possible using the integration sphere. The figure on the left shows measurements of the 50% reflectance standard made under diffuse (blue line) and direct (black line) illumination. The figure on the right shows measurements of a tissue-simulating phantom under diffuse (blue line) and direct (black line) illumination. All measurements were normalized using the 99% reflectance standard illuminated under similar conditions.

It was selected to provide diffuse light for illumination minimizing the number of photons traveling beyond the port opening, as photons did not penetrate as deeply. The diffusing effect of the integrating sphere also provided a uniform light source across the port opening of the sphere.

Light was provided by a radiometric fibre optic source (Oriel® Radiometric Fibre Optic Source Model 77501, Newport® Corporation, Irvine CA). It consisted of a broadband quartz-tungsten-halogen (QTH) lamp which was coupled to the integrating sphere with a 200 μm core optical fibre (NA=0.22). The source intensity was varied to maximize the reflectance signal by adjusting the voltage applied to the bulb. Light to the integrating sphere could be cut off completely using a physical shutter. This was required when making measurements using the continuous-wave, spatially-resolved system without removing the integrating sphere probe from the phantom. It ensured that light from the integrating sphere did not contribute

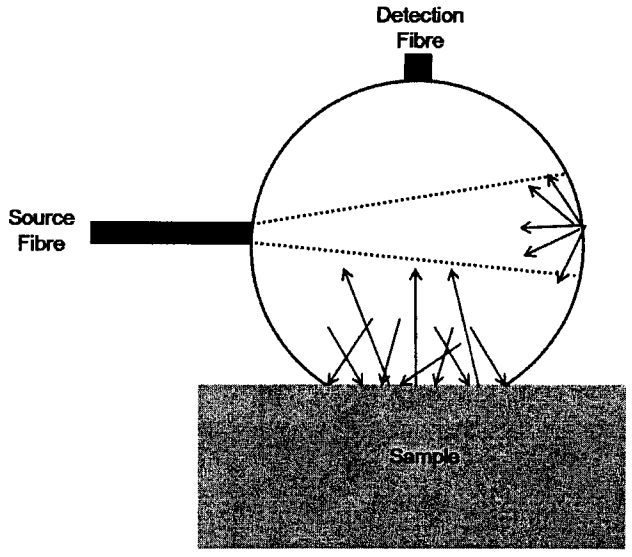

Figure 3.5: The final configuration of the integrating sphere and connected optical fibres. The illumination fibre is connected 90° to the port opening such that light is incident on a sphere wall. The incident light is diffused as it scatters around the interior of the sphere. A detection fibre is positioned directly above the port opening.

to the diffuse reflectance measured by the spatially-resolved system, which would adversely affect the calculation of phantom optical properties. The QTH lamp spectrum is shown in Figure 3.6.It was measured on the 99% reflectance standard using the integrating sphere system and thus includes the effects of the integrating sphere system response.

A fibre optic spectrometer (SD2000 Miniature Fiber Optic Spectrometer, Ocean Optics®, Dunedin, FL) accepted light transmitted through a 400 μm core optical fiber (NA=0.22) and dispersed it using a fixed grating onto a 2048-element linear charge-coupled device (CCD) array. The spectrometer was connected to a portable computer with a serial cable. The spectrometer resolution is approximately 0.3

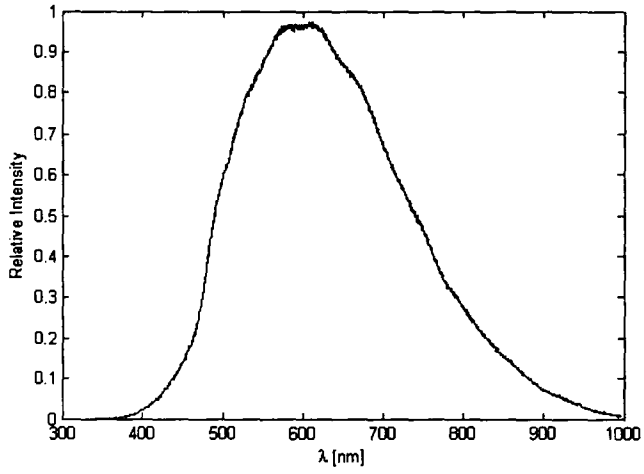

Figure 3.6: The QTH lamp spectrum, measured on the 99% reflectance standard using the integrating sphere system.

nm per pixel with a detectable range from 340 nm to 996 nm (Ocean Optics, 2000). A wavelength calibration was performed using a mercury-argon light source. Software installed on the portable computer controlled the spectrometer integration time (typical integration times ranged from 25 ms for the highly reflective 99% Spectralon® standards to 100 ms for liquid phantoms) and allowed for spectral information to be saved for subsequent analysis.

3.2.1 Probe preparation and reflectance standard measurements

Due to the open-bottom of the integrating sphere probe, measurements on liquid phantoms required the use of a transparent dressing (Tegaderm™, 3M®, St. Paul, MN) and further wrapping using transparent cellophane film, to prevent liquid

from entering the sphere. While the use of a transparent dressing prevented cross-contamination of the probe surface when making clinical measurement on tissue, the dressing did not sufficiently protect the probe from the liquid phantom material, and additional wrapping was necessary. It was difficult to use the transparent cellophane without the underlying transparent dressing as it did not adhere to the probe surface, allowing wrinkles and bulges to form in the wrapping. The cellophane must be stretched tightly across the opening to ensure consistency in its contribution to the reflectance measurement. First, the adhesive transparent dressing was stretched over the bottom of the probe and fixed in place. Then the probe was placed on a large piece of transparent cellophane film and, due to the slight adhesion between the two wrapping materials, was pulled tightly across the bottom of the probe before being secured to the side of the probe using adhesive tape.

When the probe was illuminated there was specular reflectance from the surface of these layers. To correct for this, a background measurement was made with an illuminated probe directed into a darkened room, and this measurement was subtracted from subsequent measurements. This was presumed to be a measure of 0% reflectance.

To correct for temporal variations in lamp intensity, or other component variation such as equipment set-up or variations in probe wrapping, measurements of a calibrated 99% reflectance standard (Labsphere®, North Sutton NH) were made immediately before and after all experiments. All experimental measurements were normalized for integration time and further normalized to the reflectance signal remitted from the 99% reflectance standard following background subtraction such

that,

$$R^* = \frac{S_0 - S_{background}}{S_{99} - S_{background}} \tag{3.1}$$

where R* is the background-corrected, normalized signal, S_0 is the measured signal, S_{99} is the signal measured on the 99% reflectance standard, and $S_{background}$ is the light-on background signal.

3.3 Continuous-wave, spatially-resolved measurement system

A continuous-wave, spatially resolved measurement system (SR) was used to verify the optical properties of phantoms, rather than relying on the published optical properties of each phantom component. The SR system has proven effective in the measurement of optical properties and a detailed description of the SR system can be found in Bruulsema *et al.* (1997). Figure 3.7 shows the basic arrangement of these components and Figure 3.8 shows a schematic of the probe face. Briefly, the SR system consisted of a broadband QTH light source (Oriel® Instruments Model 71445, Newport® Corporation, Irvine CA) which delivered light to the sample through a fibre optic probe.

The probe was composed of a source fibre with a 200 μm core diameter and 23 detector fibres, each with 200 μm core diameters, located at distances from 1 to 9.5 mm from the source. Each detector fibre was connected to a variable optical attenuator (Oz Optics, Ottawa, ON). This was required to balance the higher signals from light remitted close to the source with the lower signals from light remitted at

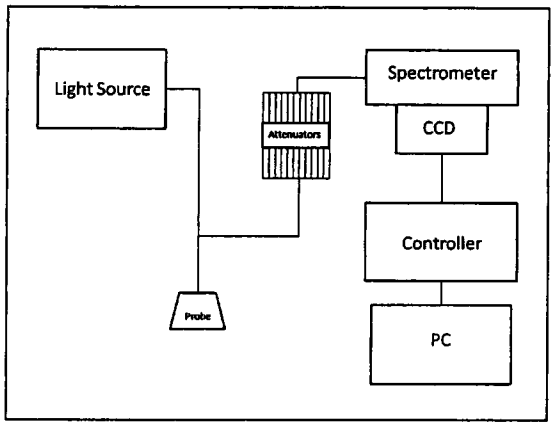

Figure 3.7: Schematic diagram of the continuous-wave, spatially-resolved measurement system.

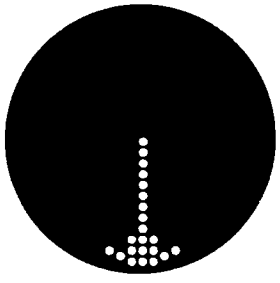

Figure 3.8: A representation of the SR system probe. Optical fibres were embedded in a black epoxy probe at specific radial distances from the source fibre. At increasing distances, several fibres are used to measure reflectance at a single radial distance, improving signal to noise in the region where a reduced signal is expected.

greater distances. This increased the signal-to-noise ratio for more distant detector fibres without detector saturation for detector fibres close to the source. Correction for this attenuation was provided through normalization using a measurement made at the exit port of a large integrating sphere. A spectrometer (Kaiser Optical Systems, Ann Arbor, MI) dispersed the collected light, imaging each fibre onto a two-dimensional thermoelectrically cooled CCD (Princeton Instruments, Trenton, NJ). Both spectral and spatial information were gathered simultaneously by a PC,

and Windows-based spectroscopy software was used to save the raw CCD images. The spectral range was approximately 520 nm to 950 nm. A wavelength calibration was performed using a mercury-argon light source. Figure 3.9 shows a typical raw image acquired by the CCD.

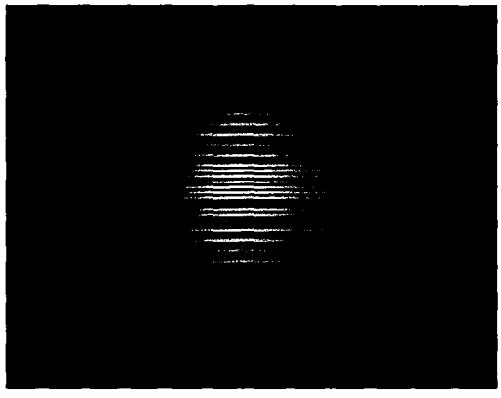

Figure 3.9: A raw image acquired by the CCD of the SR system. The pixels along the horizontal direction denote wavelength, with lower wavelengths beginning at the left and increasing towards the right. The bands in the vertical direction are the images of the optical fibres in the detection probe, each at a specific radial distance from the light source.

Raw images required further processing. First, the background signal was subtracted from each data set. The wavelength calibration was applied to define wavelengths for pixel values across the image and the image was binned according to the distance of the detector fibres from the source fibre. A cross-talk correction was also applied to minimize the effect of spurious signals detected in the region between two detector fibres. A reflectance measurement was made at the exit port of a large integrating sphere and the images from phantom measurements were normalized using the measurement made with the large integrating sphere. This corrected variations

in transmission through individual detector fibres and the effect of the variable optical attenuators. The resulting spatially-resolved diffuse reflectance spectra were fitted with a diffusion theory model or Monte Carlo simulations to determine optical properties as described in Section 2.3.

3.4 Phantom preparation - Single layer

Although skin has a layered structure, the response of the integrating sphere was initially characterized using homogeneous liquid phantoms simulating human skin. A range of optical properties were chosen to span the values published in the literature for the absorption and reduced scattering of skin. Dilute solutions of Intralipid®, an intravenous lipid supplement whose use in optical phantoms has been described in the literature, formed the base of each phantom (van Staveren *et al.* (1991), Martelli and Zaccanti (2007)). A 1% Intralipid® phantom has a reduced scattering coefficient of approximately 1.0 mm^{-1} at 650 nm. The reduced scattering coefficient is wavelength dependent and increases proportionally with the Intralipid® concentration such that $\mu_s' \propto$ concentration $\times (\lambda^{-1.4} + \lambda^{-2.4})$ (van Staveren *et al.*, 1991). The contribution of Intralipid® as an absorber is expected to be negligible as $\mu_a \approx 1.5 \times 10^{-5}$ mm^{-1} (10% Intralipid® at 630 nm) (van Staveren *et al.*, 1991). When required, a broadband absorber (India Ink) was added to the phantom. Its extinction coefficient was determined by optical transmission measurements using a 10 mm pathlength cuvette. Using known concentrations of ink in cuvettes, an extinction coefficient was determined using Beer's law such that

$$T(\lambda) = ke^{-\mu_a(\lambda)\bar{x}} \tag{3.2}$$

where $\mu_a(\lambda) = [concentration] \times \epsilon(\lambda)$ and $\epsilon(\lambda)$ is the extinction coefficient at wavelength λ and [concentration] is the absorber concentration, $T(\lambda)$ is the transmission at wavelength λ, $\bar{x}$ is the effective pathlength and k is a constant dependent on the experimental setup. The product of the concentration of ink added to a liquid phantom and the extinction coefficient were used to determine the value of μ_a. The contribution of ink to the total scattering of the liquid phantom was negligible. Figure 3.10 depicts the typical range of optical properties for Intralipid® and ink. A wide range of optical properties was used to mimic skin using numerous concentrations of Intralipid® as a scatterer, and range of concentrations of ink as an absorber. Although the optical properties of each phantom were calculated from the optical properties of its individual components and a volumetric analysis, the optical properties of the phantom as a whole were also verified by measurements on the SR system and compared to the integrating sphere measurements.

3.4.1 Alternate absorbers - Green food colour

Following the characterization of the IS system in a semi-infinite geometry using simple phantoms of Intralipid® and ink, experiments were performed using absorbers with spectral characteristics of interest. Green food colour (Club House™ Food Colour Preparation, Lot #8176AH) was selected for having a single absorption peak in the wavelength range of interest for this work, its solubility in Intralipid®, and for its inert nature with respect to other phantom components. Like the ink, the green food colour was characterized through a series of optical transmission measurements. An extinction coefficient was determined and is depicted in Figure 3.11.

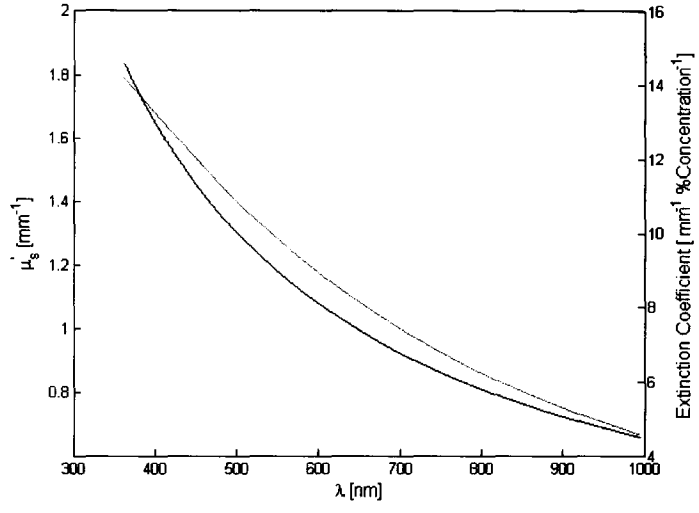

Figure 3.10: The typical optical properties for Intralipid® and ink used in tissue simulating phantoms. The reduced scattering coefficient for 1% Intralipid® is shown in blue while the extinction coefficient for the India Ink is shown in black.

3.4.2 Alternate absorbers - Haemoglobin

Red blood cells were also used as absorbers. Initial work used whole blood from a rat. Blood was drawn from rats immediately following sacrifice, and an anti-coagulant was added to the sample to prevent clotting. Later, a supplier was found (Hemostat Laboratories, Davis, CA) which provided whole horse blood and data regarding the packed cell volume of the blood samples. The total concentration of haemoglobin added to the liquid phantom was calculated from the packed cell volume of the original blood sample used to produce the added aliquots. The packed cell volume and hematocrit are considered equivalent quantities; the hematocrit is related to the total haemoglobin concentration through the rule of three (Riedinger

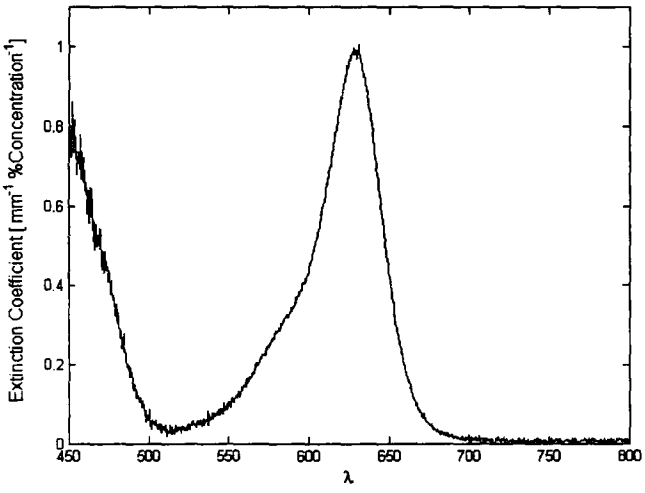

Figure 3.11: The extinction coefficient of green food colour. The units of the extinction coefficient are given as the value of the absorption coefficient per percent green food colour where percent green food colour is determined by the volume fraction of green food colour compared to the total phantom volume.

and Rodak, 1998). Roughly,

$$\text{Total haemoglobin concentration (g/L)} \pm 10\% = \frac{\text{Hematocrit (\%)}}{3} \times 10. \quad (3.3)$$

A more complete relationship between hematocrit and total haemoglobin concentration requires the mean corpuscular haemoglobin concentration (MCHC) such that

$$\text{Total haemoglobin concentration (g/L)} = \frac{\text{Hematocrit (\%)}}{100} \times \text{MCHC (g/L)} \quad (3.4)$$

where the mean corpuscular haemoglobin concentration has a value of 340 ± 30 g/L (Turgeon, 1999). Using the molar mass of haemoglobin, 64 500 g/mol, the molar

concentration can be calculated as follows:

$$\text{Molar concentration of haemoglobin (M)} = \frac{\text{Total haemoglobin concentration (g/L)}}{64500 \text{ g/mol}}. \quad (3.5)$$

The optical properties of both rat and horse haemoglobin were assumed to be identical to those of human haemoglobin (Zijlstra *et al.* (1994)). As a result, the molar extinction coefficient was not measured but taken from compiled data by Prahl who used data from W. B. Gratzer (Med. Res. Council Labs, Holly Hill, London) and N. Kollias (Wellman Laboratories, Harvard Medical School, Boston) (Prahl, 1998). Figure 1.1 shows the molar extinction coefficients of both oxygenated and deoxygenated haemoglobin used through this study.

Oxygen electrode

While the continuous-wave, spatially resolved measurement system was used to verify the measured optical properties, the oxygen partial pressure (pO_2) in the phantom was used together with the measured haemoglobin oxygen saturation (SO_2) to determine values for the Hill coefficient n and p_{50}. A Clark-type oxygen electrode (Diamond General Model 730, Ann Arbor, MI) was used to determine the partial pressure of oxygen in the liquid phantoms. These electrodes are technically simple devices which measure oxygen as molecular oxygen diffuses across a thin polyethylene membrane to the electrode. The polyethylene membrane is used to trap a small volume of an electrolytic solution, typically potassium chloride, around the tip of the electrode. The molecular oxygen interacts with the solution generating a measurable current (Nei and Compton, 1996). The main advantage

of Clark-type oxygen electrodes is their simplicity and ease of use. However, this simplicity is accompanied by several disadvantages. First, the polyethylene membrane is sensitive to contact and can be easily punctured. The device must remain submersed in liquid to prevent the evaporation of the electrolytic solution. Additionally, the measured current is often unstable and fluctuates dramatically making it difficult to record an accurate value.

Before each haemoglobin deoxygenation experiment, the oxygen electrode was calibrated to determine the linear relationship between the electrode current and oxygen partial pressure. A measurement was made on a well-oxygenated sample of water, having a known pO_2 of 158.84 Torr, calculated from an atmospheric pressure of 760 Torr and an 20.9% oxygen content in air. Uncertainty in this value, which results from variation in the atmospheric pressure or the composition of oxygen in air, is not expected to be more than 3%. Second, a measurement was made of a sample of water completely deoxygenated using $Na_2S_2O_4$ and assumed to have a pO_2 of 0 Torr (Hunter, 2001). These values were used to determine the linear relationship between the oxygen electrode signal and the oxygen partial pressure. The linearity of Clark-type oxygen electrodes is described in the literature (LeFevre, 1969). There have been difficulties reported with the use of the oxygen electrode in experimental measurements (Hunter, 2001). In spite of minor issues with stability and drift described by Hunter, measurements were used to determine the pO_2 for every measurement point throughout the experiment as the relatively short duration of deoxygenation experiments (complete deoxygenation occurring in less than 20 minutes) was assumed to minimize the effects of instability and drift; instability and drift had been observed only over several hours. Experimentally, the electrode

was placed in the phantom container below the surface of the liquid in a location where it did not interfere with reflectance measurements.

3.5 Measurement geometry - Single layer phantoms

The phantoms used in the IS system characterization were primarily composed of water. However, in phantoms where blood was added as an absorber, water was replaced with a 0.9% saline solution (pH $\approx$ 5.5) or with a 1% phosphate-buffered saline solution (pH $\approx$ 7.4). This ensured that the solution was isotonic, preventing the red blood cells from rupturing. In all cases the liquid phantom was poured into a black polyethylene container. The container was large enough to allow access to the liquid phantom for measurements using both the integrating sphere probe and the spatially-resolved system without removing each probe, while ensuring that neither probe was close to the container wall. The integrating sphere probe was typically positioned several millimetres below the surface of the liquid phantom using a clamp. The probe from the SR system was also clamped in a similar fashion, alongside the IS probe. To maintain a homogeneous solution the phantom was stirred, using a magnetic stir-bar, throughout the measurement. A schematic diagram of the single-layer, homogeneous phantom measurement set-up is shown in Figure 3.12.

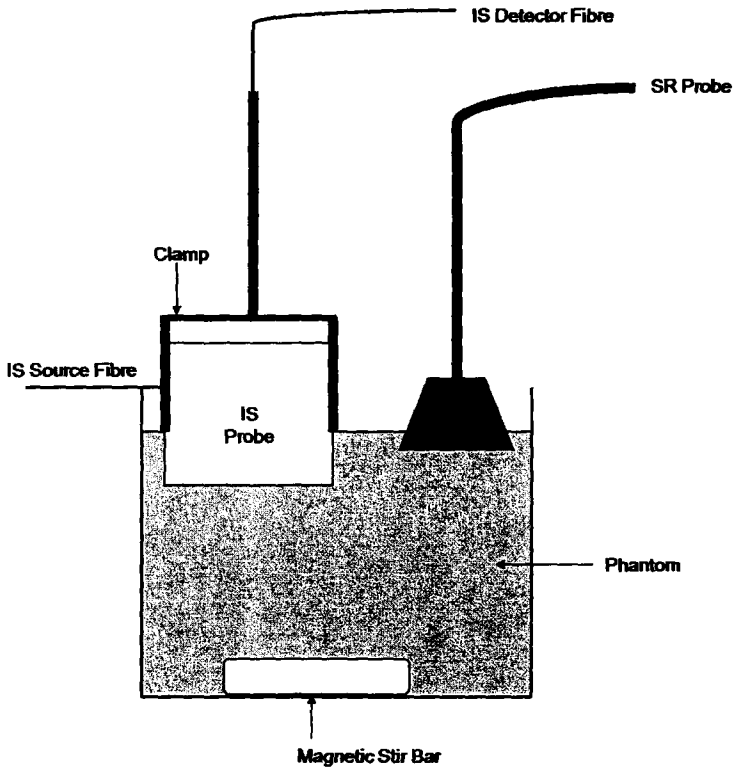

Figure 3.12: Experimental set-up of the single-layer tissue-simulating phantom used in characterization of the integrating sphere probe. Both the integrating sphere probe and the SR probe measure reflectance in the phantom material.

3.6 Measurement geometry - Two layer phantoms

To simulate the layered structure of tissue, experiments were performed using two-layered, liquid phantoms. The black polyethylene container used in the single-layer experiments was modified to include a stand, for a smaller second container, which held the top layer of liquid. The bottom of the small container, also composed of polyethylene, was cut out to form an opening slightly smaller than the bottom

surface of the integrating sphere probe. A piece of transparent cellophane film was used to seal the opening, and was sealed using silicone. The configuration of the top layer container can be seen in Figure 3.13.

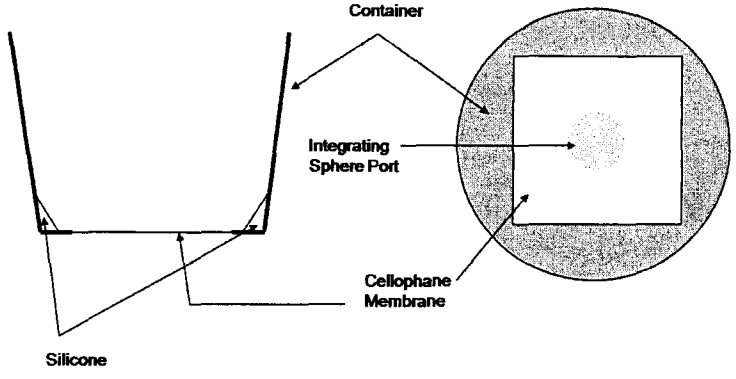

Figure 3.13: A cross-section and bottom view of the top layer container. Transparent cellophane was stretched across a square opening cut into the bottom of a polyethylene container. The membrane was sealed, making it liquid-tight, using clear silicone.

The clamp used to hold the integrating sphere probe was modified to include a translation micrometer. This allowed the integrating sphere probe to be moved to precise distances from the cellophane membrane, representing the interface between the layers.

Figure 3.14 shows the arrangement of the phantom container, and the positions of both the integrating sphere probe and the SR system probe in the two-layer configuration.

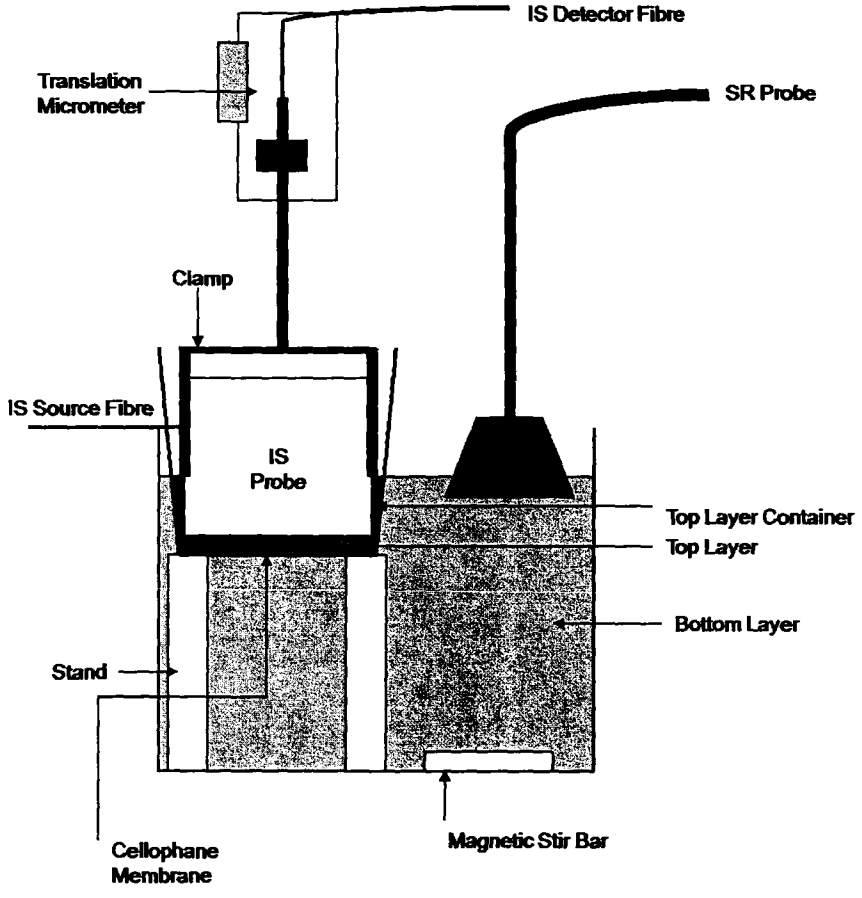

Figure 3.14: Experimental set-up of the two-layer Intralipid® phantoms. The integrating sphere probe is clamped and mounted onto a translation micrometer. This allowed precise positioning of the integrating sphere probe at distances from the cellophane membrane. The integrating sphere probe measured the reflectance of the two layer system. The SR system probe was clamped to directly measure the reflectance of the bottom layer.

Chapter 4

Measurements in homogeneous phantoms

4.1 Introduction

The response of the integrating sphere system was characterized in simple homogeneous media. Experiments were first conducted with Intralipid® phantoms in concentrations from 1% to 3% with μ_s' ranging from 1.08 ± 0.05 mm^{-1} to 3.25 ± 0.16 mm^{-1}, at 650 nm, as measured by the SR system. India ink was added in increasing amounts to simulate the range of absorption coefficients typically observed in skin over the wavelength range of interest. The absorption coefficient μ_a ranged from 0.005 mm^{-1} to 0.3 mm^{-1}, at 650 nm, as determined by optical transmission measurements. The optical properties of each phantom were verified by comparing the expected optical properties, determined from volumetric analysis and values

reported in the literature, with measurements using the continuous-wave, spatially-resolved measurement system. An empirical mathematical relationship was derived linking the normalized integrating sphere measurement, R*, the reduced scattering coefficient, μ_s', and the absorption coefficient, μ_a.

With this relationship established, further experiments were conducted using absorbers with defined spectral characteristics. Integrating sphere measurements were used together with knowledge of the reduced scattering coefficient, as determined by the SR system, to calculate the absorption coefficient from the empirical relationship. The absorption coefficient was subsequently verified using the SR system. In addition, the concentration of the absorber in the phantom was determined from its extinction coefficient and the calculated μ_a, and the retrieved concentration was compared to the concentration known from the volumetric addition of the absorber.

Once the system was characterized and it was determined that the integrating sphere system could adequately determine the concentration of an added absorber, deoxygenation experiments were performed. The phantom oxygenation, measured as the partial pressure of oxygen in the phantom, was verified using the oxygen electrode, while the retrieved absorption coefficient was verified using the SR system. For a series of deoxygenation experiments, the physiological parameters, n and p_{50}, were determined from calculations of SO_2 and the measured pO_2, and compared to published values to assess the accuracy of extracted haemoglobin concentrations.

4.2 Definition of the empirical model

To assess the response of the integrating sphere system, measurements were made on Intralipid® phantoms ranging in concentration from 1% to 3%, simulating a range of reduced scattering coefficients from 1.08 ± 0.05 mm^{-1} to 3.25 ± 0.16 mm^{-1} at 650 nm as determined by the SR system. India ink was added to the phantom volume such that the total ink concentration ranged from 0.02% to 0.31%, simulating a range of absorption coefficients of 0.015 ± 0.001 mm^{-1} to 0.229 ± 0.016 mm^{-1} at 650 nm as determined by optical transmission measurements. Complete descriptions of the optical properties of these phantoms can be found in Appendix A. An initial reflectance measurement was made using both the integrating sphere system and the SR system on a phantom of a particular Intralipid® concentration. An aliquot of ink was added to the phantom volume and mixed throughout the material to ensure that the phantom was homogeneous. A second set of reflectance measurements were acquired and this procedure was repeated until the desired set of ink concentrations was measured.

The integrating sphere measurements were normalized to the 99% reflectance standard to determine a value for R* (Equation 3.1). Measurements made with the SR system were used to determine the reduced scattering coefficient, $\mu_s'(SR)$, and the absorption coefficient, $\mu_a(SR)$. Estimates of the optical properties, $\mu_s'(V)$ and $\mu_a(V)$ were also determined through a volumetric analysis that used the known optical properties of each phantom component, and the total volume added, to estimate the optical properties of the phantom. The values of $\mu_s'(SR)$ and $\mu_a(SR)$ were compared to $\mu_s'(V)$ and $\mu_a(V)$ to assess the optical properties retrieved from the SR system; these values were found to agree to within 10%.

Initially, values of $\mu_a(SR)$ were plotted against R* (Figure 4.1), for constant values of reduced scattering coefficients, and a simple exponential relationship was observed.

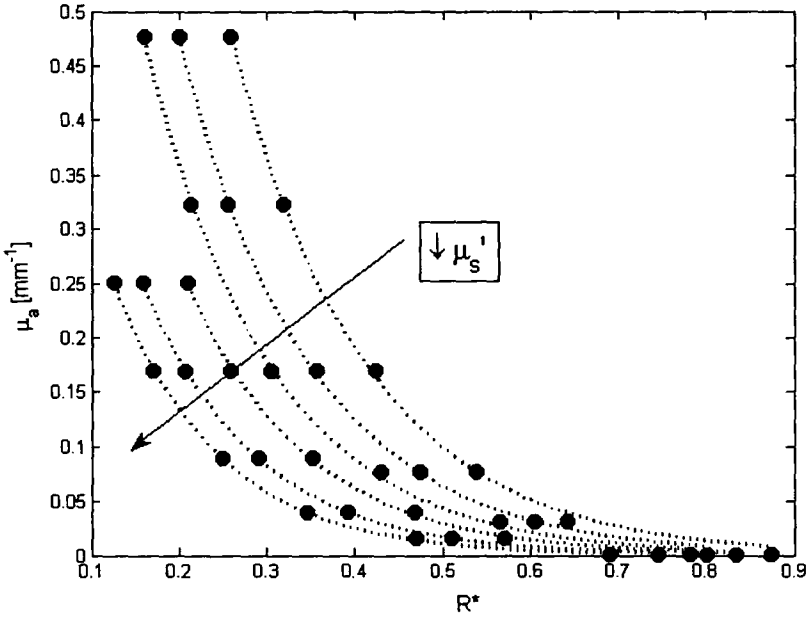

Figure 4.1: The results of an initial attempt to use the integrating sphere system to measure μ_a. The absorption coefficient measured using the spatially-resolved diffuse reflectance system was plotted against normalized reflectance values, R*. The value of μ_s' ranged from 3.5 mm^{-1} to 0.9 mm^{-1}.

These data were fitted using a simple exponential function, $\mu_a = a \times e^{-(b \times R^*)}$. The fitted paraments a and b were found to depend on μ_s'. Figures 4.2 and 4.3 show the values of the fitted parameters for several values of reduced scattering coefficient. The a parameter was found to have a proportional relationship with μ_s', $a = f \times \mu_s'$ and the b parameter was found to vary inversely with μ_s', $b = g + 1/\mu_s'$.

Values of R* were plotted against the known optical properties $\mu_s'(SR)$ and

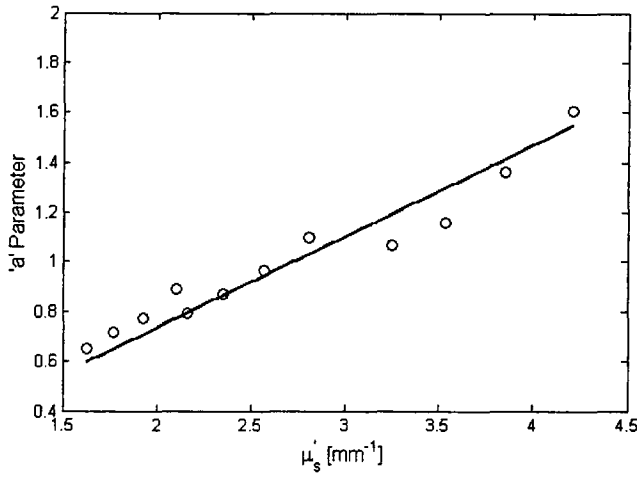

Figure 4.2: A representation of the values of the fitting parameter a as a function of the reduced scattering coefficient. There is a linear relationship between μ_s' and a.

$\mu_a(SR)$. Because estimates of the absorption coefficient are the desired end product, these data were fitted to determine an expression for μ_a in terms of μ_s' and R* such that

$$\mu_a = f \cdot \mu_s' \cdot e^{-[g+\frac{1}{\mu_s'}]R^*} \tag{4.1}$$

where f and g are parameters determined by the fit, μ_s' is the reduced scattering coefficient as measured by spatially-resolved diffuse reflectance, and R* is the value resulting from the normalization of integrating sphere measurements. The scattering dependence of the fitted parameters was folded into a simple exponential equation. Values of f and g were found such that $f = 0.431 \pm 0.005$ and $g = 8.002 \pm 0.279$ where

$$\mu_a = 0.431 \cdot \mu_s' \cdot e^{-[8.002+\frac{1}{\mu_s'}]R^*}. \tag{4.2}$$

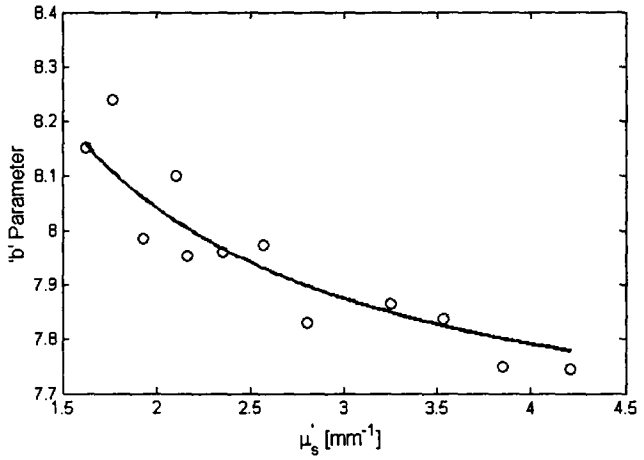

Figure 4.3: A representation of the values of the fitting parameter b as a function of the reduced scattering coefficient. There is an inverse relationship between μ_s' and b.

Figure 4.4 shows the empirical relationship as a contour plot where the absorption coefficient is calculated for a range of values of R* and μ_s'. Figure 4.5 shows a comparison of the absorption coefficient calculated using Equation 4.2 and the absorption coefficient measured using the spatially-resolved diffuse reflectance system.

The empirical model was used to map the normalized integrating sphere measurement for a phantom to a value of μ_a, using μ_s' as measured using the SR system, for the remaining investigations. In general, as SR measurements were required to determine μ_s' for use with the empirical model, the values of μ_a from the SR measurements were used to verify the absorption coefficient determined by the model.

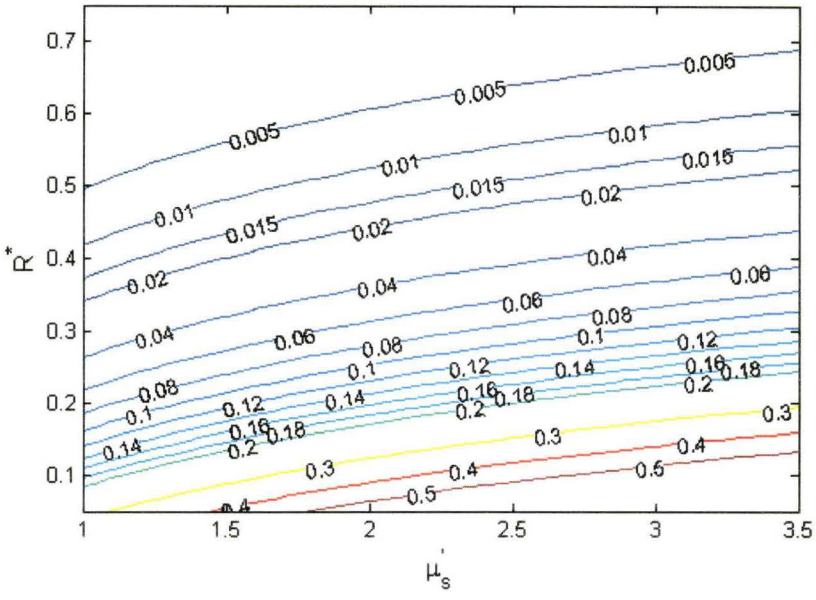

Figure 4.4: A contour plot of the empirical relationship. Lines of equal μ_a are shown for values of R* and μ_s'.

4.3 Concentration of added absorbers - green food colour

Green food colour was used as an absorber. It was selected for its spectral characteristics (having a single absorption peak at approximately 630 nm), its solubility in Intralipid®, and for its inert nature with respect to other phantom components. Its extinction coefficient was determined and is shown in Figure 3.11. Integrating sphere and SR system measurements were made on homogenous phantoms of 1.5% Intralipid® ($\mu_s' = 1.679 \pm 0.084$ at 630 nm, the wavelength of the absorption peak of green food colour, measured by the SR system) and green food colour added to total concentrations ranging from 0.01% to 0.15% in approximately 0.01% steps.

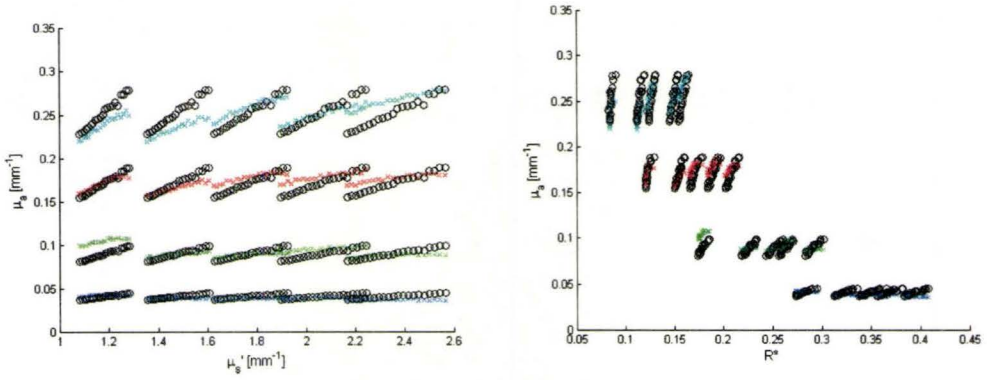

Figure 4.5: The fitting of the empirical relationship. The black circles are the results of applying the empirical relationship to measurements made using the integrating sphere. The coloured marks are the values of μ_a retrieved from the SR system. The results are plotted in two dimensions for clarity.

This range of concentrations was chosen as it resulted in a wide range of absorption coefficients from $\mu_a = 0.010 \pm 0.001$ mm^{-1} to $\mu_a = 0.148 \pm 0.010$ mm^{-1} (at 630 nm), which included the range of μ_a values expected for several chromophores under physiological conditions over the wavelength range of interest. The expected optical properties associated with these phantoms can be found in Appendix A. The values of μ_a retrieved by the integrating sphere system using the empirical relationship showed agreement to within experimental uncertainties with values of μ_a determined by the SR system, where $\mu_s^{'} = 1.679 \pm 0.084$ at 630 nm. These values of μ_a were then used to calculate absorber concentration using a singular value decomposition algorithm to fit the absorption spectrum to the extinction coefficient for green food colour.

Figure 4.6 shows a representative experiment where the absorption coefficient retrieved using integrating sphere measurements and the empirical model are compared to μ_a as determined by the SR system. The concentration of green food

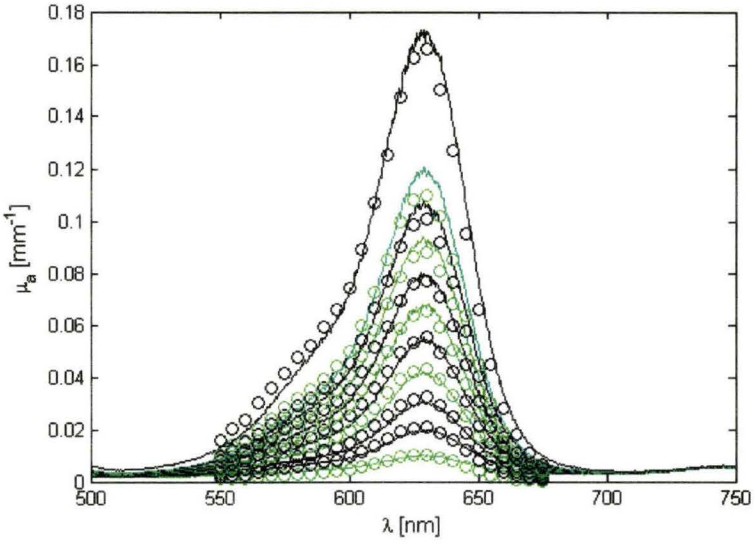

Figure 4.6: A comparison of the μ_a retrieved from measurements using the integrating sphere (solid lines) and verified by the spatially-resolved diffuse reflectance measurement system (open circles). There is overlap between measurements and the values agree to within experimental uncertainties. Uncertainties in the extracted μ_a have been left off the plot for clarity, but are typically less than 10%.

colour was determined for three independent measurements of green food colour in 1.5% Intralipid®. Figure 4.7 shows the retrieved concentration of green food colour (open circles) as the mean of triplicate measurements. The error bars were determined from the uncertainty in μ_a, calculated through propagation of uncertainties in R* and μ_s' through the empirical model, and shows the mean of the errors of the retrieved concentration. The rms error in the retrieved concentration is 10%. The expected concentration was determined from the volumetric addition of food colour and the straight line is the line of equality.

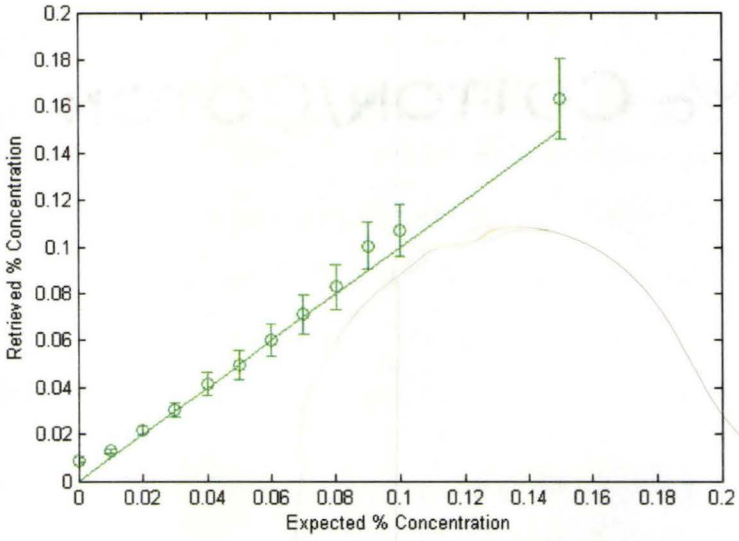

Figure 4.7: A comparison of retrieved concentration with expected concentration of green food colour. The expected concentration is determined from the volume of green food colour added to the total phantom volume. A line of unity is also shown for comparison. The uncertainties in the retrieved concentration are due to the uncertainties in the calculated μ_a.

4.4 Concentration of added absorbers - whole rat blood

The homogeneous single-layer phantom measurements were repeated using whole rat blood to assess the empirical model with an absorber having a more complex absorption spectrum. Whole blood was added in known volumes to a 1.5% Intralipid® in a 0.9% saline solution base phantom with $\mu_s' = 1.925 \pm 0.096$ mm^{-1} at 550 nm. Saline solution was used as an isotonic base, in place of water, to prevent rupture of the red blood cells. Measurements were made with both the SR system and the

integrating sphere probe. Subsequent calculations yielded μ_a values from both systems for inter-comparison. Figure 4.8 is a representative example of the comparison between retrieved values of μ_a for three volumes of rat blood: 400 μL, 800 μL, and 1750 μL. In this figure, the solid dark lines represents the absorption coefficient as determined by the integrating sphere using the empirical model. The dotted lines above and below the solid lines are the upper and lower estimates of uncertainty in the integrating sphere measurement, while the open circles reflect the absorption coefficient as recovered by the spatially-resolved diffuse reflectance system.

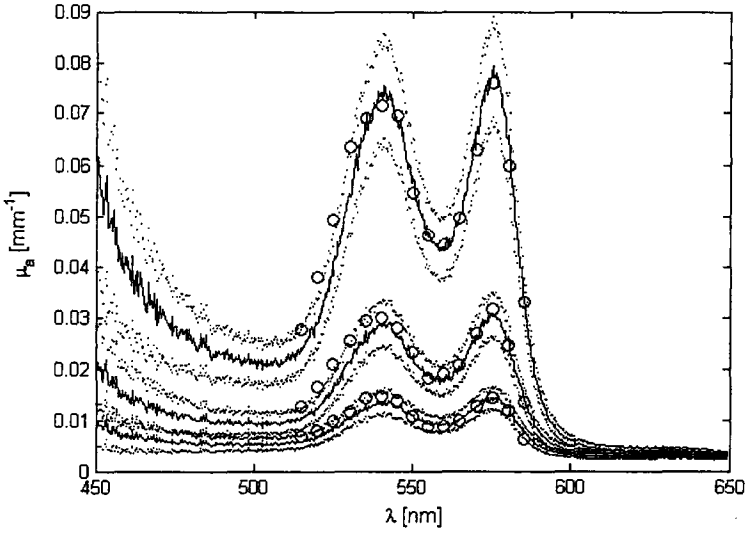

Figure 4.8: A comparison of retrieved absorption coefficient for 400 μL, 800 μL, and 1750 μL of rat whole blood added to a 1.5% Intralipid® ($\mu_s' = 1.925 \pm 0.096$ mm^{-1} at 550 nm) phantom, using a 0.9% saline base. The solid lines show the absorption coefficient determined from integrating sphere measurements and use of the empirical model while the open circles show the absorption coefficient retrieved from measurements made using the SR system.

Rat whole blood absorption measurements were performed in triplicate and a comparison of the absorption coefficient retrieved from the integrating sphere

measurements using the empirical model and the SR system is shown in Figure 4.9. These points compare values of μ_a at wavelengths across both absorption peaks associated with oxygenated haemoglobin. Agreement between the optical properties retrieved using the empirical model and those determined by the SR system suggest that the empirical model is valid even for absorbers with complex absorption spectra.

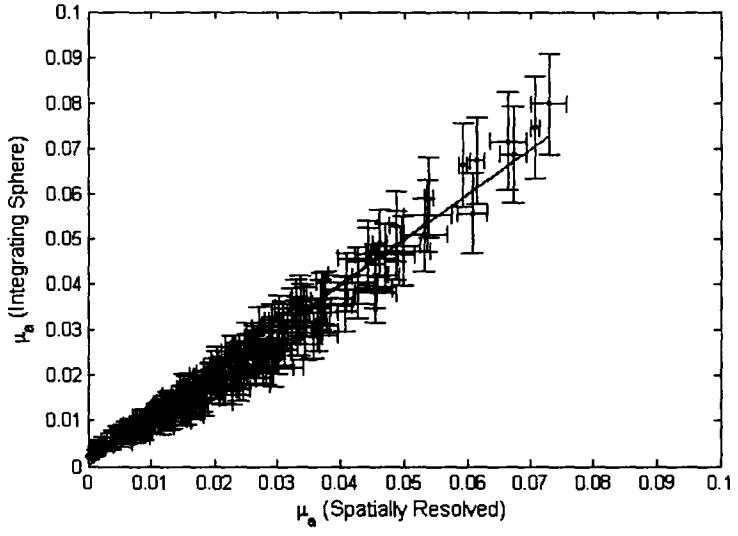

Figure 4.9: A comparison of retrieved absorption coefficient for the addition of rat whole blood added to a 1.5% Intralipid® ($\mu_s' = 1.925 \pm 0.096$ mm^{-1} at 550 nm) phantom, using a 0.9% saline base. Volumes of whole blood from a rat were added to the phantom to a maximum of 1750 μL. The horizontal error bars show the error of the retrieved values of μ_a as determined by the spatially-resolved diffuse reflectance system while the vertical error bars show the error in the absorption coefficient as determined by the integrating sphere system. A line of equality is also shown.

The rat whole blood was drawn from rats immediately after sacrifice. No haematological analysis was performed so there was no knowledge of the concentration of red blood cells in the sample, or even knowledge of the initial volume of blood

prior to the addition of heparin. As a result, it was not possible to assess the haemoglobin concentration explicitly for each phantom as there was no estimate of concentration for comparison.

4.5 Concentration of added absorbers - whole horse blood

The experiments previously performed with rat blood were repeated using whole horse blood. The supplier (Hemostat Laboratories, Davis CA) provided an estimate of the packed cell volume of a specific blood sample. Using this value, an estimate of the total haemoglobin concentration could be determined for the volume of blood added to the phantom. Additionally, horse blood was chosen for its safety with regard to potential cross-species infection and ease of import.

Horse blood was added in 200 μL aliquots to a 1.5% Intralipid® ($\mu_s' = 1.925 \pm 0.096$ mm^{-1} at 550 nm) in 0.9% saline phantom while being constantly stirred to ensure a homogeneous suspension of blood cells. Measurements were made using both the integrating sphere and the SR system, and pO_2 was monitored using the oxygen electrode. Following the final addition of horse blood, an amount of yeast was added to the phantom and measurements were made as the oxygen in the phantom was consumed.

The optical properties were calculated using both measurement systems and comparisons of the calculated values for μ_a for three concentrations of red blood cells are shown in Figure 4.10; 0.03% whole blood ($400\mu L$), 0.08% whole blood ($800\mu L$), and 0.1% whole blood ($1400\mu L$). These three concentrations were selected

as representative of a wide range of absorption coefficients. The retrieved absorption coefficients were confirmed by measurements using the SR system at several wavelengths across the absorptions peaks. Having confirmed the absorption coefficients retrieved from measurements with the integrating sphere in the oxygenated homogeneous horse blood phantom, the empirical model was used to determine the absorption coefficient for integrating sphere measurements made throughout the deoxygenation of the phantom. The concentration of both oxy- and deoxyhaemoglobin was determined from the calculated values of μ_a and the appropriate molar extinction coefficients using a singular value decomposition algorithm. Figure 4.11 shows two examples of the decomposition of an absorption spectrum, measured at a single time point in the deoxygenation experiment, into the separate contributions of oxygenated and deoxygenated haemoglobin.

The calculated concentrations of oxyhaemoglobin, deoxyhaemoglobin, total haemoglobin, and expected total haemoglobin were plotted against phantom pO_2. An example of the retrieved concentrations plotted against oxygen partial pressure is shown in Figure 4.12.

As expected, the concentration of deoxyhaemoglobin is seen to rise as the pO_2 decreases while the concentration of oxyhaemoglobin is seen to decrease as the pO_2 decreases. As shown, there is agreement between the calculated and expected total haemoglobin concentration to within 9%.

The calculated concentration of oxy- and deoxyhaemoglobin can be used to calculate the haemoglobin oxygen saturation via Equation 2.1. As described in Hull *et al.* there is a relationship between the haemoglobin oxygen saturation and the oxygen partial pressure. This relationship was used to verify the measurements

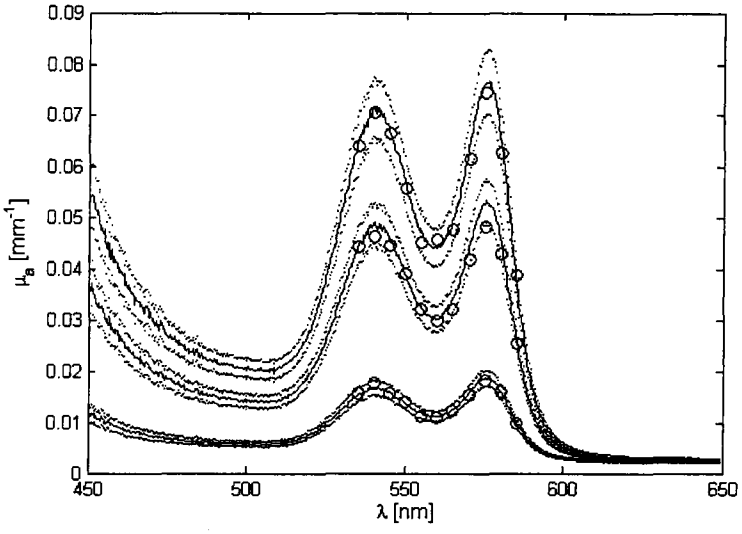

Figure 4.10: A comparison of retrieved absorption coefficient for 400 μL, 800 μL, and 1400 μL of whole horse blood added to a 1.5% Intralipid® ($\mu_s' = 1.925 \pm 0.096$ mm^{-1} at 550 nm) phantom, using a 0.9% saline base. The solid lines show the absorption coefficient determined from integrating sphere measurements and use of the empirical model while the open circles show the absorption coefficient retrieved from measurements made using the SR system.

of the optical system by determining SO_2 from the calculated concentration of oxygenated and total haemoglobin. The resulting values for p_{50} and for the Hill coefficient n, were calculated and compared with published values validating the oxygen saturation estimates determined using the integrating sphere.

The p_{50} of haemoglobin under non-physiological conditions can be estimated using an empirically derived mathematical model where, for standard values of pCO_2 and concentration of DPH,

$$p_{50} = 26.8 - 21.279(pH_{rbc} - 7.24) + 8.872(pH_{rbc} - 7.24)^2$$
$$+ 1.4945(T - 37) + 0.04335(T - 37)^2 + 0.0007(T - 37)^3$$

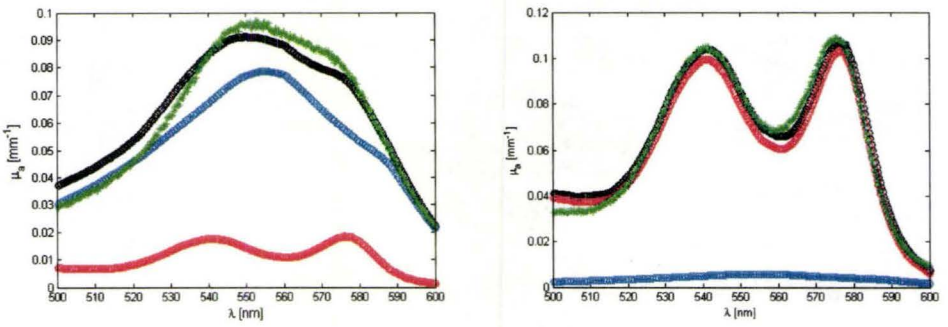

Figure 4.11: Decomposition of the measured absorption coefficient (green stars) into the contributions of oxygenated (red circles) and deoxygenated (blue circle) and summed for the total μ_a (black circles) for a tissue simulating phantom with $\mu_s^{'} = 1.925 \pm 0.096$ mm^{-1} at 550 nm. Error bars have been left off the plot for clarity, but are typically less than 10%. The figure on the left shows the decomposition of the absorption coefficient for a phantom at the end of the deoxygenation ($pO_2 \approx 20$ Torr) while the figure on the right is from a phantom at the start of deoxygenation ($pO_2 \approx 120$ Torr).

where pH_{rbc} is the pH of the red blood cells and T is temperature (Dash and Bassingthwaighte, 2004). For the measurement conditions, the p_{50} value was calculated to be approximately 35 Torr. From Figure 4.13 showing the calculated haemoglobin oxygen saturation over a range of oxygen partial pressures, p_{50} was found to be approximately 30 Torr. The value of n was found to be 2.29 ± 0.22, which while lower than the expected value (at 22 °C) of 2.52 ± 0.04 (Zwart *et al.*, 1984), still shows agreement with the published value.

Further measurements were made under conditions closer to those found in human physiology, so as to compare the values of n and of p_{50} with results reported in the literature. Experiments were also performed using different Intralipid® concentrations with $\mu_s^{'}$ of 1.283 ± 0.064 mm^{-1}, 1.925 ± 0.096 mm^{-1}, and 2.57 ± 0.13 mm^{-1} at 550 nm. The concentrations of oxy- and deoxyhaemoglobin were determined

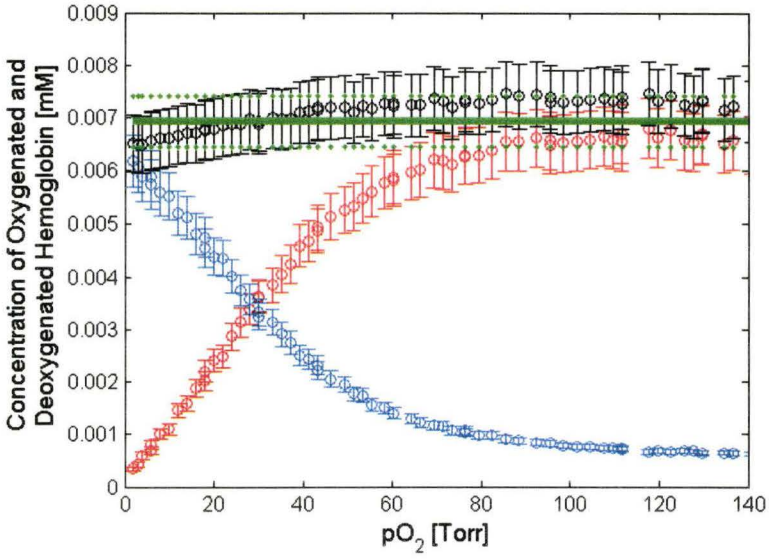

Figure 4.12: The retrieved concentration of total haemoglobin (black circles), oxygenated haemoglobin (red circles), and deoxygenated haemoglobin (blue circles) as a function of the oxygen partial pressure measured with the oxygen electrode in a 1.5% Intralipid® ($\mu_s^{'} = 1.925 \pm 0.096$ mm^{-1} at 550 nm) phantom, using a 0.9% saline base. The expected concentration of total haemoglobin is also shown (green squares).

from values of μ_a and the extinction coefficient for oxy- and deoxyhaemoglobin, and the total haemoglobin concentration was compared with the expected values as calculated from the total volume of blood added to the phantom and the packed cell volume provided by the supplier. Figure 4.14 shows these results for a phantom with $\mu_s^{'} = 1.925 \pm 0.096$ mm^{-1} as a representative example.

The oxygen saturation of the phantom was calculated from the total haemoglobin concentration, the oxygenated haemoglobin concentration and Equation 2.1. Figure 4.15 shows these data plotted as a function of of oxygen partial pressure for $\mu_s^{'} = 1.925 \pm 0.096$ mm^{-1} at 550 nm. These values are used to determine the values

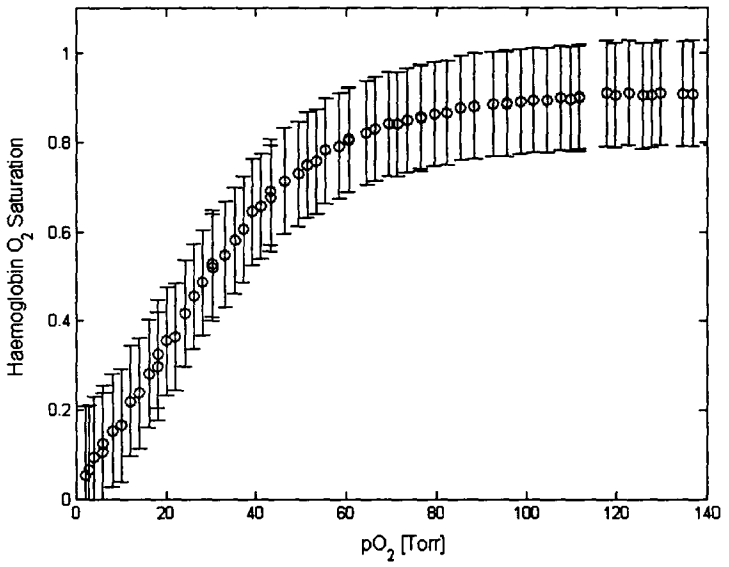

Figure 4.13: The haemoglobin oxygen saturation (SO_2) for a tissue simulating phantom at temperature $\approx 20 \pm 2°$ C and pH ≈ 6.0.

of the Hill coefficient and p_{50}. From this $p_{50} = 18 \pm 3$ Torr.

The Hill coefficient was determined from the slope of the plot of $\log_{10}[SO_2/(1 - SO_2)]$ with SO_2 given as a decimal fraction versus $\log_{10}(pO_2)$ for oxygen saturation values ranging from 0.2 to 0.8 (20% to 80%) is shown in Figure 4.16. The slope of a line through these data yielded the Hill coefficient.

These experiments were also repeated with a constant scattering coefficient ($\mu_s' = 1.283 \pm 0.064$ mm^{-1} at 550 nm) and with ink added to simulate melanin absorption. An added $\mu_a = 0.025 \pm 0.002$ mm^{-1} was used to simulate a fair skin type (Tuchin, 2007) while an added $\mu_a = 0.15 \pm 0.01$ mm^{-1} was used to simulate a darker skin type (Tuchin, 2007). The concentrations of ink, oxy- and deoxy-haemoglobin were determined and the total haemoglobin concentration was found to agree with the expected value to within experimental uncertainties. Table 4.1

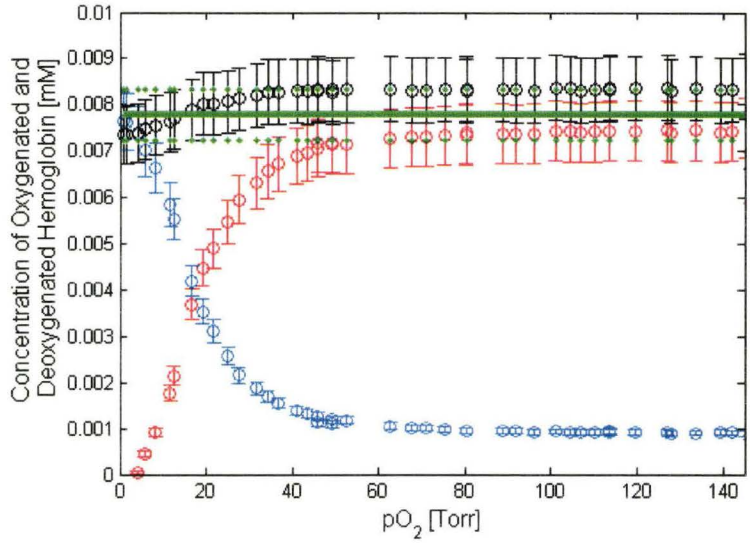

Figure 4.14: Retrieved concentration of total (black circles), oxy- (red circles), and deoxyhaemoglobin (blue circles) at temperature = $36 \pm 1°$ C and pH ≈ 7.4. There is agreement between the retrieved concentration of total haemoglobin and the expected concentration (green squares) to within 6% for a tissue-simulating phantom ($\mu_s^{'} = 1.925 \pm 0.096$ mm^{-1} at 550 nm)

$\mu_s^{'}$ [mm^{-1}] (at 550 nm)	μ_a [mm^{-1}] (added ink)	rms error in [tHb]	n	p_{50} [Torr]
1.283 ± 0.064	0	12 %	2.63 ± 0.21	18 ± 3
1.925 ± 0.096	0	8 %	2.39 ± 0.23	18 ± 3
2.57 ± 0.13	0	7 %	2.41 ± 0.22	24 ± 3
1.283 ± 0.064	0.025 ± 0.002	7 %	2.39 ± 0.23	21 ± 3
1.283 ± 0.064	0.15 ± 0.01	7 %	2.45 ± 0.21	23 ± 3
Mean			2.45 ± 0.22	21 ± 3

Table 4.1: Summary of results for haemoglobin deoxygenation experiments.

summarizes the results for each phantom.

Typical published values for the Hill coefficient are 2.46 ± 0.05 (Zwart *et al.*, 1984) and 2.42 ± 0.05 (Hull *et al.*, 1998). The p_{50} value is shown in the literature

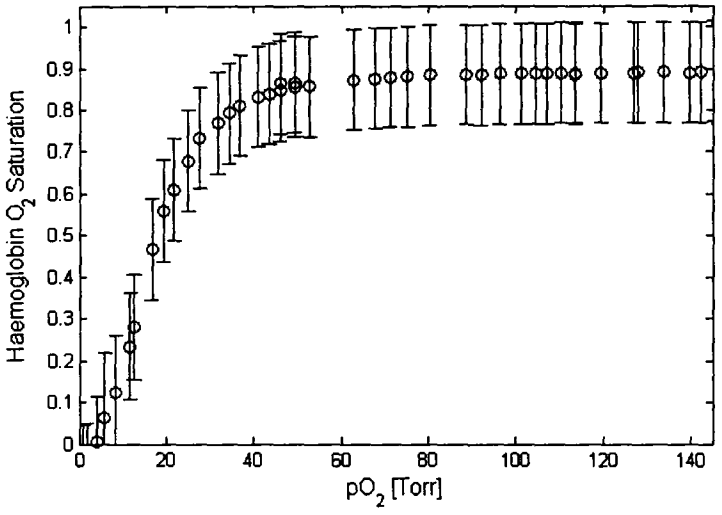

Figure 4.15: Calculated haemoglobin oxygen saturation (SO_2) as a function of oxygen partial pressure pO_2 for $\mu_s' \approx 1.925 \pm 0.096$ mm^{-1} at 550nm.

to be sensitive to several physiological parameters. For the temperature and pH described, assuming normal values of other parameters such as pCO_2 and intra-erythrocytic concentration of DPG, p_{50} takes values of 21.8 ± 0.9 Torr (Hull *et al.*, 1998) and 25.95 ± 1.43 Torr (Zwart *et al.*, 1984). The calculated mean vales for each parameter agree with the published values.

4.6 Discussion - Measurements in homogeneous phantoms

The use of the empirical relationship, described in Section 4.2, to determine the absorption coefficient is dependent on the *a priori* knowledge of the reduced scattering coefficient. The accuracy of the reduced scattering coefficient, whether

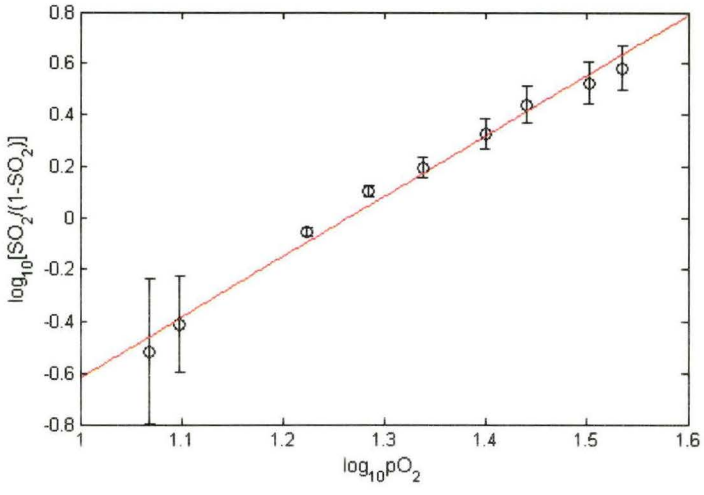

Figure 4.16: A plot of $\log_{10}(SO_2/(1-SO_2))$ versus $\log_{10}(pO_2)$ for oxygen saturation values ranging from 20% to 80%. The slope of a straight line (black line) fit through these data is the Hill coefficient.

determined through measurement or published estimates, ultimately affects the accuracy of the value of μ_a measured with the IS system. The sensitivity of μ_a to the input value of μ_s' was explored by assessing the results of measurements included in Section 4.3 with small deviations in the value of μ_s'. The values of μ_a and the estimated concentration of added absorber were subsequently compared to those calculated using the original value of μ_s'.

In Section 4.3, integrating sphere and SR measurements were made on homogenous phantoms of 1.5% Intralipid® and green food colour, to total concentrations ranging from 0.01% to 0.15%. The reduced scattering coefficient was measured, using the SR system, as 1.63 $\pm$ 0.08 mm^{-1} at 650 nm. Using this value, the corresponding R* and the empirical relationship, the absorption coefficient and subsequently the concentration of green food colour, was determined for each of the phantom mixtures. As shown in Figure 4.7, the retrieved concentration agreed

with the expected concentration to within 10%.

Presume that μ_s' could not be measured, but was estimated from values published in the literature. Considering skin in bulk, published ranges of $\mu_s' = 1.8$ to 2.8 mm^{-1} (Tseng *et al.*, 2008) are not uncommon. For example, an overestimate of 15% yields $\mu_s' = 1.87 \pm 0.09$ mm^{-1}. Propagating this value through the empirical relationship (and not changing R*) returns values for μ_a which are also overestimated as shown in Figure 4.17.

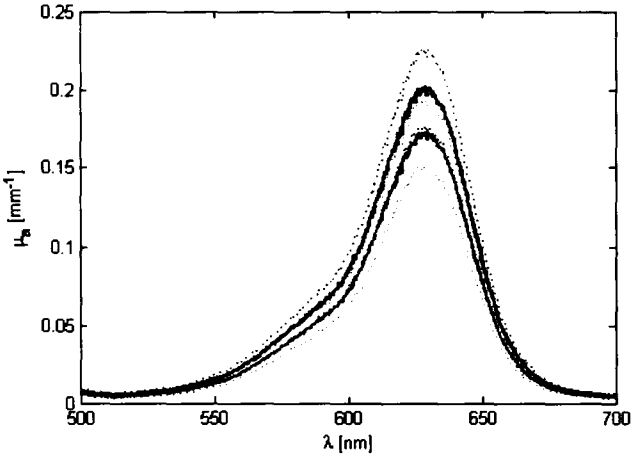

Figure 4.17: A comparison of the μ_a retrieved using the value of $\mu_s' = 1.63 \pm 0.08$ mm^{-1} as determined by measurement using the SR system (green solid line) and a 15% overestimate (black solid line) of $\mu_s' = 1.87 \pm 0.09$ mm^{-1}. The uncertainties in μ_a are shown by the dotted lines.

The rms error in μ_a calculated using the overestimate in μ_s' as compared to the original value is 19%. Using the recalculated μ_a to determine the concentration of added absorber leads to an overestimate of 19%. Similarly, an underestimate in μ_s' of 15% results in a rms error in the recalculated μ_a of 19% while the rms error in the retrieved concentration is 19%.

Figure 4.18 shows the results of these analyses plotted as the rms error in μ_a, as a function of the over- and underestimates of reduced scattering given as a percentage of the measured μ_s'. The uncertainty in μ_s' propagates through the empirical model, affecting the calculation of μ_a and the concentration of added absorbers.

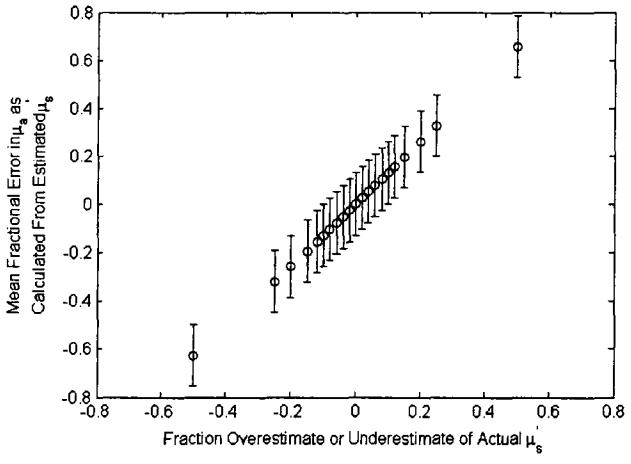

Figure 4.18: The rms error in retrieved μ_a calculated for several overestimates and underestimates of a single μ_s'. There is a linear relationship between these values; rms error in $\mu_a \approx 1.29\times$ the percent over- or underestimate in μ_s'.

The empirical model requires estimates of μ_s' to determine values of μ_a which can be used in subsequent calculations to yield the concentration of an added absorber. Uncertainties in the estimate of μ_s' are propagated through the empirical model, affecting the accuracy of the retrieved quantities. When determining the absolute concentration of an added absorber, or chromophore, accurate knowledge of the reduced scattering coefficient is thus important. However a relative measurement, i.e., determining the change in concentration of a chromophore, may be sufficient to quantify physiological conditions such as erythema or a decrease in the concentration of a photodynamic therapy drug in the skin. In these cases, the

absolute concentration of the chromophore may be less important than the time evolution of the chromophore concentration. The effect of overestimates and underestimates of the reduced scattering coefficients on the relative concentration of an added absorber is negligible.

There are several measurements, and applications, which can be made using relative quantities. For example, the haemoglobin oxygen saturation, SO_2, is a relative measurement of the concentration of oxygenated haemoglobin and the total haemoglobin concentration as shown by Equation 2.1. Historically, measurements of the erythema index are typically relative measurements. The reflectance signal measured in the erythematic regions under investigation are normalized using reflectance signals associated with normal control areas (Dawson *et al.*, 1980).

4.7 Summary

An empirical model was defined to relate the normalized integrating sphere signal R*, to the reduced scattering coefficient μ_s', and the absorption coefficient, μ_a. Using this model and estimates of μ_s' measured using a fibre-based spatially-resolved diffuse reflectance (SR) measurement system, values of μ_a were determined for tissue simulating phantoms doped with an added absorber. The retrieved values of μ_a were verified by measurements with the SR system. The concentration of the added chromophore was determined from the retrieved values of μ_a together with the known absorption spectrum of the chromophore. Experiments using green food colour showed that the integrating sphere system could determine the concentration of an added absorber in a homogenous tissue-simulating liquid phantom to within

10%.

Through a series of deoxygenation experiments the integrating sphere system was able to determine the concentration of haemoglobin added to homogeneous phantoms to within 12% of the expected values for $\mu_s' = 1.283 \pm 0.064$ mm^{-1} at 550nm with no broadband absorber added. For optical properties in the range of those measured for human skin ($\mu_s' = 1.283 \pm 0.064$ mm^{-1} to $\mu_s' = 2.57 \pm 0.13$ mm^{-1} at 550nm, and $\mu_a = 0.025 \pm 0.002$mm^{-1} to $\mu_a = 0.15 \pm 0.01$mm^{-1} at 550 nm) the accuracy in retrieving the concentration of haemoglobin improves to within 7%.

Provided the reduced scattering coefficient is well known, μ_a and the absolute absorber concentration can be retrieved to within 10%. To ensure that the relative uncertainties in μ_a and the retrieved concentration remain below 15%, μ_s' should be be known to within 10%. However, in the absence of accurate knowledge of the reduced scattering coefficient, relative measurements of absorber concentration can be made using any estimate of μ_s'. For a relative measurement the effect of the uncertainty in μ_s' is removed through the comparison of values. As such the change in the relative absorber concentration can be retrieved to with 10% regardless of the over- or underestimate in the value of μ_s' used.

Chapter 5

Measurements in layered phantoms

5.1 Introduction

The integrating sphere system was able to determine the concentration of haemoglobin added to homogeneous phantoms to within 12% of the expected values with no broadband absorber added. For optical properties in the range of those measured for human skin ($\mu_s' = 1.283 \pm 0.064$ mm^{-1} to $\mu_s' = 2.57 \pm 0.13$ mm^{-1} at 550nm, and $\mu_a = 0.025 \pm 0.002$mm^{-1} to $\mu_a = 0.15 \pm 0.01$mm^{-1} at 550 nm) the accuracy in retrieving the concentration of haemoglobin improves to within 7%. However, biological tissues are not simple, homogeneous media. Skin, in particular, possesses a layered structure, with various chromophores found in specific layers. Therefore, it is logical to characterize the response of the integrating sphere system in a more

complex, layered geometry. A two-layer geometry was chosen for its relative simplicity, allowing for the use of homogenous liquid phantoms representing each of the distinct layers, and for its approximation of human skin.

Two-layered liquid phantoms were made according to the description in Section 3.6. The effects of top layer thickness and changes in top layer optical properties, on the measurement of the absorption coefficient for a chromophore in the bottom layer, were determined using different chromophores in the top and bottom layers. The retrieved absorption coefficients at each top layer thickness were used to establish a relationship between top layer thickness, top layer optical properties and the accuracy with which the concentration of absorber added to the bottom layer could be retrieved.

This relationship, together with estimates of optical properties for human skin, were used to devise a two-layer geometry for haemoglobin deoxygenation experiments. Similar to those experiments performed in homogeneous phantoms, deoxygenation experiments were performed in two-layers with several top-layer configurations simulating a range of skin optical properties. These measurements showed that the integrating sphere system could determine the concentration of haemoglobin in the bottom layer of two-layer phantoms to within 11 % when no broadband absorber was present in the top layer and improved to 8% when a broadband absorber was present. Additionally, for the range of reduced scattering coefficients and top layer thicknesses (such that $\mu_s^{'}\times$ top layer thickness < 2), the absorption coefficient retrieved for an absorber in the bottom layer of a two-layered geometry is similar to that for the homogeneous case.

5.2 Derivation of the top layer thickness response model

Dilute solutions of Intralipid® were prepared in three concentrations with resulting scattering properties: $\mu_s' = 1.119 \pm 0.056$ mm^{-1}, $\mu_s' = 1.679 \pm 0.084$ mm^{-1}, and $\mu_s' = 2.224 \pm 0.112$ mm^{-1} at 630 nm. A fraction of each solution was used in the bottom layer of the phantom and the remainder was used in the top layer of the phantom. Green food colour was added to the bottom layer phantom material to achieve several concentrations: 0.01%, 0.05% and 0.1% such that $\mu_a = 0.010 \pm 0.001$ mm^{-1}, $\mu_a = 0.049 \pm 0.003$ mm^{-1}, and $\mu_a = 0.098 \pm 0.007$ mm^{-1} at 630 nm. Measurements of each concentration of green food colour in the bottom layer were made through two different top layer configurations: 0.04% and 0.08% red food colour such that $\mu_a = 0.082 \pm 0.006$ mm^{-1} and $\mu_a = 0.219 \pm 0.015$ mm^{-1} at 525 nm (the wavelength associated with the absorption peak of red food colour). These concentrations were chosen for their representation of the range of optical properties expected in skin tissue. The reduced scattering coefficient of the base phantom ranged from $\mu_s' = 1.119 \pm 0.056$ mm^{-1} to $\mu_s' = 2.224 \pm 0.112$ mm^{-1} at 630 nm (the wavelength associated with the absorption peak of green food colour). Using the translation micrometer, measurements were made at numerous top layer thicknesses ranging from 0 mm to a maximum of 7 mm since beyond 7 mm the absorption characteristics of the bottom layer were no longer visible through the top layer.

Green food colour was added to produce an initial absorption value of $\mu_a =$

0.010 ± 0.001 mm^{-1}. Reflectance measurements were made using both the integrating sphere system and the SR system prior to the addition of the top layer. The top layer container was installed, ensuring that no air bubbles were trapped between the liquid phantom material and the cellophane membrane, and was fixed into position. The integrating sphere probe was placed inside the top layer container in contact with the cellophane membrane. A clamp, attached to a translation micrometer, was lowered toward the probe and the translation micrometer was zeroed. The integrating sphere probe was clamped in position while still in contact with the cellophane membrane between the layers. Measurements were started at a maximum displacement from the cellophane membrane as it was noticed that the cellophane wrapping the integrating sphere probe and the cellophane comprising the membrane separating the layers often remained stuck together. Two top layer phantoms were prepared, composed of a volume of the same Intralipid® solution as the bottom layer but with red food colour added to $\mu_a = 0.082 \pm 0.006$ mm^{-1} or $\mu_a = 0.219 \pm 0.015$ mm^{-1} at 525 nm, measured using the SR system. With the integrating sphere probe 7 mm from the membrane, one of the top layer solutions was added to the small container such that the bottom of the integrating sphere probe was submerged in liquid. The levels of liquid in the bottom and top layers were kept equal to ensure that the pressure on the cellophane membrane did not cause it to deflect. Reflectance measurements were made at this initial position and the integrating sphere was incrementally moved towards the dividing membrane with measurements made at each distance. A small pipet was used to remove quantities of phantom from the top layer to maintain equal levels in both containers as the descending probe displaced more and more liquid in the top layer.

After the measurement at 0 mm, the integrating sphere probe was withdrawn. The top layer phantom material was replaced and the SR system probe was positioned in the top layer container and a reflectance measurement was made using the SR system. This measurement was used to verify the optical properties of the top layer phantom. The top layer phantom liquid was removed,the integrating sphere probe was repositioned, and the top layer liquid phantom material with different μ_a was added to the container. The measurements were then repeated allowing a single configuration of bottom layer optical properties to be measured through two top layer liquid phantoms with differing optical properties.

This measurement scheme was repeated with increasing amounts of green food colour added to the bottom layer for each of the three Intralipid® concentrations. Each set of measurements was performed in triplicate to demonstrate reproducibility. The concentration of added absorbers in the top and bottom layers retrieved with the IS system was plotted against top layer thickness in millimeters as in Figure 5.1. The expected concentration of green food colour was 0.1% and the expected concentration of red food colour was 0.08% for a scattering solution of $\mu_s^{'} = 1.119 \pm 0.056$ mm^{-1} at 630 nm.

There are several features of Figure 5.1 which are of interest. First, the concentration of green food colour in the bottom layer was retrieved to within experimental uncertainties for top layer thicknesses ranging from 0 mm to approximately 1.2 mm. Beyond this, as the thickness of the top layer increased, there was an underestimate in the retrieved concentration for green food colour in the bottom layer. Second, the retrieved concentration of red food colour in the top layer increased until at a top layer thickness greater than 3.5 mm the concentration of red food colour

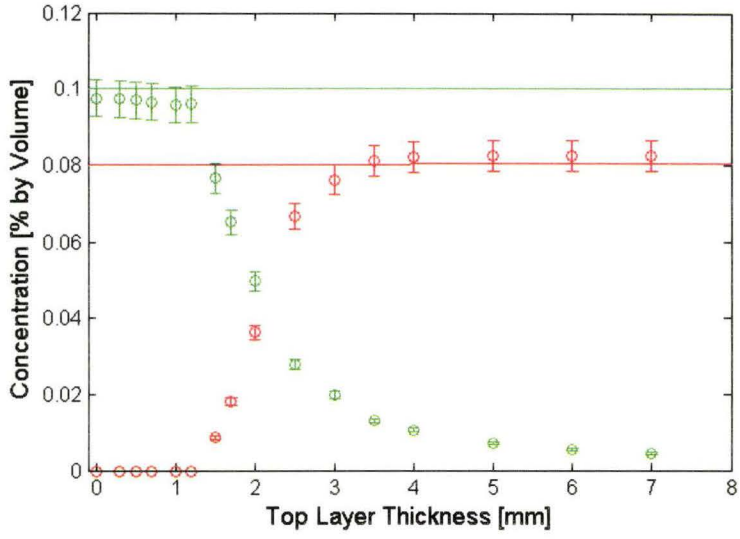

Figure 5.1: The concentration of green food colour (green circles) in the bottom layer is retrieved accurately over top layer thicknesses ranging from 0 mm to 1.2 mm, as compared to an expected concentration of 0.1% (green line) where $\mu_s' = 1.119 \pm 0.056$ mm^{-1} at 630 nm. The concentration of red food colour (red circles) is retrieved accurately for top layer thicknesses greater than 3.5 mm with the expected value shown by the red line.

was correctly determined to within experimental uncertainties. Third, there was a range of top layer thicknesses which were optically invisible to the integrating sphere system. As the thickness of the top layer increased, the integrating sphere probe sampled a greater volume of the top layer phantom material and a decreasing volume of the bottom layer phantom material until the chromophore in the bottom layer was not detectable through the top layer. Figure 5.2 shows the results for a two-layer phantom with the same μ_s' but with different concentrations of each chromophore.

Performing similar experiments with phantoms having different scattering properties, it was evident that the physical thickness of the top layer material through

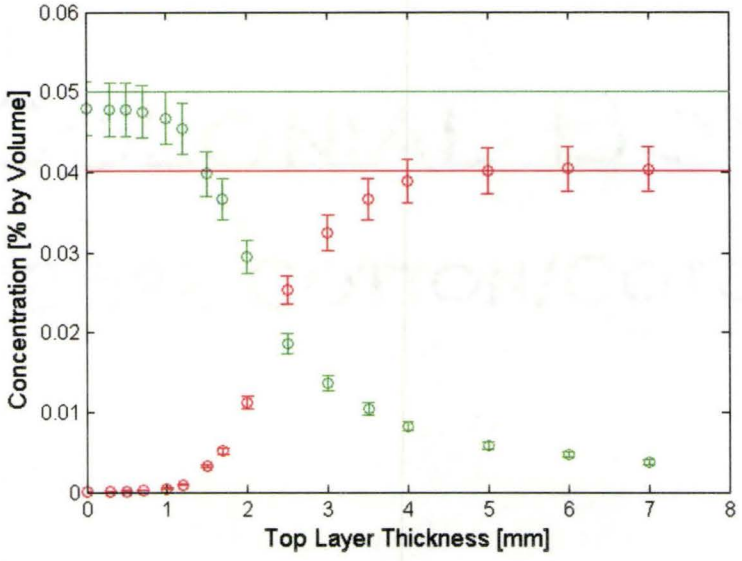

Figure 5.2: The concentration of green food colour (green circles) as compared to an expected concentration of 0.05% (green line) where $\mu_s^{'} = 1.119 \pm 0.056$ mm^{-1} at 630 nm. The concentration of red food colour (red circles) as compared to the expected concentration of 0.04% (red line).

which the integrating sphere system could accurately detect the concentration of a chromophore in the bottom layer was also affected by the amount of scattering in the top layer. Figure 5.3 shows the results from two-layer phantoms with different reduced scattering coefficients ($\mu_s^{'} = 2.224 \pm 0.112$ mm^{-1} at 630 nm).

Compiling these data, this relationship is shown graphically in Figure 5.4. Included in this figure are the results of 0.01%, 0.05%, and 0.1% green food colour in the bottom layer of 1%, 1.5% and 2% Intralipid® phantoms, with 0.04% and 0.08% red food colour in the top layer. A dimensionless parameter was used to compare the results from different reduced scattering coefficients in order to determine a relationship between the accuracy of the retrieved absorber concentration in the bottom layer for a variety of top layer optical thicknesses. The optical thickness of

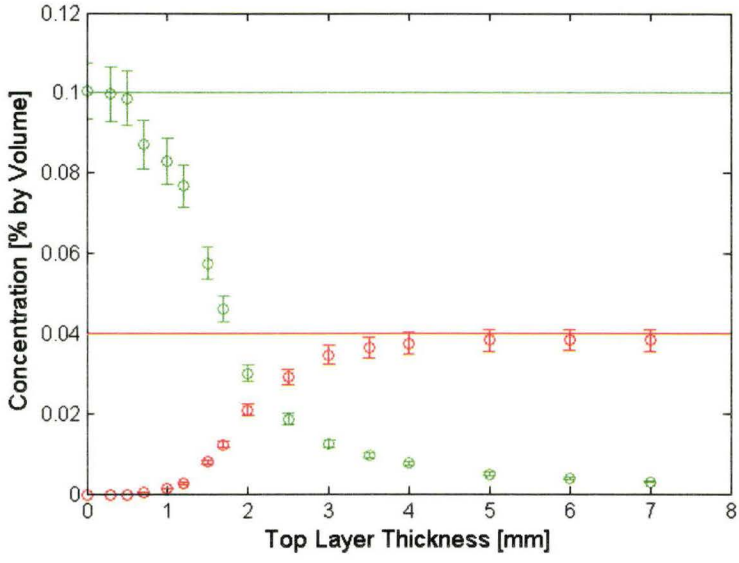

Figure 5.3: The concentration of green food colour (green circles) in the bottom layer is retrieved accurately over top layer thicknesses ranging from 0 mm to approximately 0.7 mm, as compared to an expected concentration of 0.1% (green line) where $\mu_s' = 2.224 \pm 0.112$ mm^{-1} at 630 nm. The concentration of red food colour (red circles) is retrieved accurately for top layer thicknesses greater than 4 mm with the expected value (0.04%) shown by the red line.

the top layer was calculated as the product of the top layer thickness in millimeters and the mean reduced scattering coefficient of the top layer phantom material over the range of wavelengths (500 - 700 nm) used in the singular value decomposition algorithm.

It can be seen in Figure 5.4 that there is a range of optical thicknesses, from 0 to 2, for which the concentration of added absorber in the bottom layer can be determined to within 10%. Within this range of optical thicknesses, the accuracy of the retrieved concentration was comparable to the accuracy in retrieved

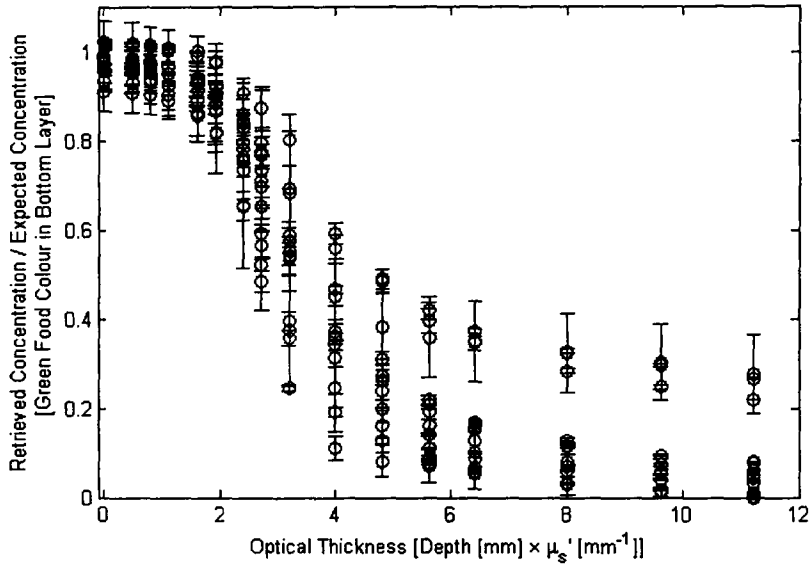

Figure 5.4: Retrieved concentration as a function of top layer optical thickness. For three independent measurement the open circles represent the mean in the fraction given by retrieved/expected concentration and the error bars represent the standard deviation in this mean.

concentration observed in the homogeneous geometry. Beyond this region the retrieved concentration was an underestimate of the expected concentration; optical thicknesses from 2 to 5 showed an underestimate in the retrieved concentration of approximately 10% to 75% respectively. For optical thicknesses greater than about 5, a further dependence on the reduced scattering coefficient was observed, appearing as a separation in the dataset. However, further investigations are required to determine a precise cause. An alternate measure of the top layer, the product of top layer thickness and the effective attenuation coefficient (μ_{eff}) was explored to optimize the response relationship, with the effective attenuation coefficient defined as $3\mu_a(\mu_a + \mu_s')^{1/2}$. Using μ_{eff} resulted in an increased separation of the data

according to optical properties and was thus considered inferior.

The top layer optical thickness relationship can be used to generate an approximate correction factor for measurements made in geometries where the optical thickness exceeds the range for which the retrieved absorber concentration can be determined accurately. The application of the approximate correction factor will be discussed in Section 5.4.1.

5.3 Deoxygenation of horse whole blood in the bottom layer

Erythema is associated with an increase of the apparent concentration of oxygenated haemoglobin within the uppermost part of the dermis. The dermis lies beneath the epidermis, the outermost layer of skin. There is a range of optical properties and physical dimensions which have been associated with the epidermis: thickness ranges from 0.05 mm to 0.13 mm and the scattering coefficient ranges from $\mu_s = 35$ mm^{-1} to $\mu_s = 80$ mm^{-1} Zhang *et al.* (2005).

Most tissue is considered to have an anisotropy parameter of g=0.9, giving the reduced scattering coefficient, for the epidermis, a value ranging from $\mu_s^{'} = 3.5$ mm^{-1} to $\mu_s^{'} = 8.0$ mm^{-1}. Using the expression for the dimensionless parameter optical thickness discussed in Section 5.2, the maximum optical thickness expected from these values for the epidermis is 1.04, a value within the range (0 to 2) for which the concentration of the absorber in the bottom layer can be determined accurately.

Having confirmed that the physiological changes associated with erythema occur

at a depth where the optical properties of the epidermis do not influence results, deoxygenation experiments were completed in a two-layer experimental geometry. Dilute solutions of 1% Intralipid® in 1% phosphate buffered saline (PBS), were used as a scattering base for both the top and bottom layers of liquid phantom material. Whole horse blood was added to the bottom layer of the phantom while being constantly stirred to ensure a homogeneous suspension of blood cells. The temperature of the bottom layer was kept at $36 \pm 2°$ C using a water bath. The temperature was monitored throughout. The oxygenation of the bottom layer was assessed using the oxygen electrode. The top layer thickness was set at 1 mm; a 1% Intralipid® solution, $\mu_s' = 1.283 \pm 0.064$ mm^{-1} at 550 nm to yield an optical thickness comparable to the maximum value expected in skin (1.28 as compared to 1.04). Due to the high rate at which oxygen is consumed by the yeast (a result of the high temperature of the phantom) measurements were made at a constant top layer thickness.

Three haemoglobin deoxygenation experiments were performed, each with a different top layer configuration. The first top layer configuration was a volume of 1% Intralipid® solution ($\mu_s' = 1.283 \pm 0.064$ mm^{-1} at 550 nm) without any added absorber. The second and third top layer configurations consisted of a 1% Intralipid® solution with ink added to simulate fair skin ($\mu_a \approx 0.025$ mm^{-1}) and darker skin ($\mu_a \approx 0.07$ mm^{-1}) (Tuchin, 2007).

Figure 5.5 is a representative example of the results of the three haemoglobin deoxygenation experiments. It shows the calculated concentrations of oxyhaemoglobin, deoxyhaemoglobin, total haemoglobin and expected total haemoglobin plotted against phantom pO_2 for a top layer simulating darker skin.

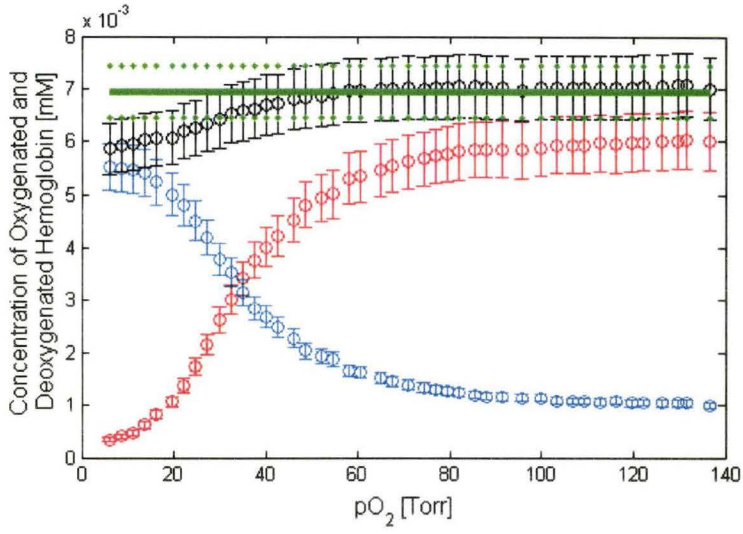

Figure 5.5: Retrieved concentration of total (black circles), oxy- (red circles), and deoxyhaemoglobin (blue circles) in the bottom layer of a two-layer phantom, at temperature = $36 \pm 2°$ C and pH ≈ 7.4. The expected total haemoglobin concentration is shown in green. The top layer consisted of 1% Intralipid® with ink added to $\mu_a \approx 0.07$ mm^{-1}.

μ_s' [mm^{-1}] (at 550 nm)	μ_a [mm^{-1}] (added ink)	rms error in [tHb]	n	p_{50} [Torr]
1.283 ± 0.064	0	11%	2.43 ± 0.21	38 ± 3
1.283 ± 0.064	0.025 ± 0.002	8%	2.27 ± 0.23	41 ± 3
1.283 ± 0.064	0.070 ± 0.005	6%	2.52 ± 0.22	38 ± 3
Mean			2.41 ± 0.13	38 ± 3

Table 5.1: Summary of results for two layer haemoglobin deoxygenation experiments.

The results of the three haemoglobin deoxygenation experiments are summarized in Table 5.1.

The mean Hill coefficient for the three phantoms was 2.41 ± 0.13 which agrees with the published values for the Hill coefficient of 2.47 ± 0.05 (Zwart *et al.*, 1984)

and 2.42 ± 0.05 (Hull *et al.*, 1998). The p_{50} value calculated from these three phantoms was 38 ± 6 Torr. This value is different than those in the literature which take values in the range of 21.8 ± 0.9 Torr (Hull *et al.*, 1998) and 25.95 ± 1.43 Torr (Zwart *et al.*, 1984). There are several sources which could have contributed to this difference. The deoxygenation experiments used a second blood sample, acquired from the same provider (Hemostat Laboratories, Davis CA), but from a different lot that could have varied oxygen carrying abilities due to physiological changes in the animal such as the increased concentration of 2,3-di-phosphoglycerate (DPG); Zwart *et al.* found that p_{50} varied with intra-erythrocytic concentration of DPG such that a 10% increase in intra-erythrocytic DPG concentration resulted in a roughly 8% increase in p_{50} (Zwart *et al.*, 1982). The possible variations in blood physiology, and the resulting changes in oxygen carrying capacity, cannot be excluded as the source for the shift in measured p_{50} value. Second, to test whether the two-layer geometry affected the measurement of p_{50} a deoxygenation experiment was repeated in the homogeneous geometry. A similar deviation ($p_{50} = 41 \pm 3$ Torr) without a significant change in the Hill coefficient (2.38 ± 0.19) was determined. This indicated that the new two-layer configuration had not contributed to the change in p_{50}. Third, the deviation in p_{50} may simply be the result of a scale shift in the pO_2 as measured by the oxygen electrode. At this time, it has not been possible to measure oxygen partial pressure with an alternate device. Last, small changes in temperature could have resulted in a right-shift of the oxygen dissociation curve, resulting in an apparent increase in p_{50}. The temperature was monitored throughout the measurements using a thermometer placed in the bottom layer. A hot plate and water bath were used to warm the liquid phantom material to $36 \pm 2°$ C. Ice

was added to the water bath if temperature drifted beyond this range. Calculating the expected values over this range results in $p_{50} = 22 \pm 2$ at 34°C and $p_{50} = 29 \pm 2$ at 38°C (Dash and Bassingthwaighte, 2004). The combined effect of changes in concentration of 2,3-di-phosphoglycerate and temperature could have contributed to a portion of the increase observed in p_{50} however, the magnitude of this variation requires further study.

The agreement between the measured estimate of total haemoglobin concentration, the value calculated from the packed cell volume provided by the supplier, and the volume of blood added to the phantom is an indication that the retrieved concentrations of oxygenated and deoxygenated haemoglobin are also accurate. The agreement of the Hill coefficient with values published in the literature also confirms these results. The deviation of the p_{50} from expected values may not be indicative of errors in the concentrations of oxygenated and deoxygenated haemoglobin because there are many other sources that could account for this shift. Therefore, from these results it can be concluded that the integrating sphere probe can determine the total haemoglobin concentration in the bottom layer of a two-layer tissue simulating phantom to within 11% in the absence of a broadband absorber in the top layer when the optical thickness of the top layer is less than 2. The accuracy of these measurements increases as the amount of absorption in the top layer increases such that for a top-layer $\mu_a \approx 0.07$ mm^{-1} the total haemoglobin concentration is retrieved to within 6%.

5.4 Discussion - Measurements in layered phantoms

5.4.1 Top layer thickness response correction

Measurements in a two-layered geometry revealed that increasing the top layer optical thickness resulted in an underestimate of the concentration of absorber in the bottom layer. A top layer thickness response relationship was obtained from a series of measurements using two-layered liquid phantoms. The relationship, shown in Figure 5.6, relates the sensitivity of measured μ_a to the concentration of an added absorber in the bottom layer, to the optical thickness of the top layer. Recall that optical thickness is a dimensionless parameter given by the product of the physical thickness and the mean reduced scattering coefficient. It was shown in Figure 5.1 that for optical thicknesses less than 2, the concentration of added absorber in the bottom layer can be determined accurately. Within this range of optical thicknesses, the accuracy of the retrieved concentration is comparable to that obtained for a homogeneous geometry. For optical thicknesses from 2 to 5, there was an underestimate in the retrieved concentration of approximately 10% to 75% respectively. Consequently, the top layer thickness response relationship can be used to generate an approximate correction factor for measurements made in geometries where the optical thickness exceeds 2.

To test the top layer response relationship, a two-layer deoxygenation experiment was performed using a 2.5% Intralipid® phantom with an average $\mu_s' = 3.04 \pm 0.15$ mm^{-1} taken between 500 nm and 600 nm. This is the wavelength range which is used in determining the concentration of haemoglobin using the singular value

decomposition algorithm. Phantom preparation and measurements were performed as described earlier.

Figure 5.6 shows the top layer thickness response relationship with a fitted sigmoidal line. For clarity, lines have been added to the figure at an optical thickness of 3 representing the two layer phantom. The top layer response relationship predicts that the retrieved concentration of haemoglobin in the bottom layer will be approximately 70% of the expected value. The total haemoglobin concentration calculated from the known volume of blood added was 0.0090 $\pm$ 0.0006 mM. The retrieved concentration was approximately 0.0063 $\pm$ 0.0004 mM (Figure 5.7) which is 70% of the expected value. However, the retrieved value appears to vary throughout the experiment, ranging from 0.0077 $\pm$ 0.0005 mM to 0.0058 $\pm$ 0.0004 mM.

The top layer thickness response relationship can be used as an approximate correction for geometries where the optical thickness of the top layer is greater than 2, however, much more testing is required. It is not necessary to use the correction for optical thickness values less than 2; the spread of the data about the fitted line indicates that there is no advantage to applying the correction to these values. For values of optical thickness greater than 5 the approximate correction must be used with caution. There appears to be an additional dependence on reduced scattering coefficient as the data separate into distinct groups. However, further investigations are required to characterize the effects observed in this region. There may be value in applying separate fits, based on the reduced scattering coefficient, to the response relationship. As μ_s' is required for integrating sphere measurements, fitting the response relationship to account for the scattering dependence at large optical thicknesses may extend the useful range of the correction and may minimize

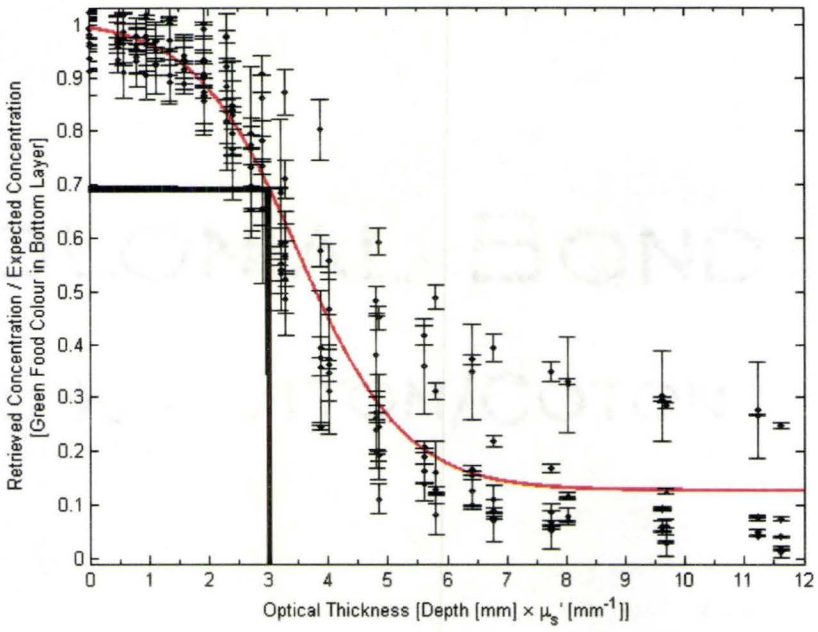

Figure 5.6: The top layer response relationship (Figure 5.4) with a fitted line. The black dots represent the mean in the fraction given by retrieved/expected concentration the error bars represent the standard deviation in this mean. The red line is a fitted line using the sigmoidal appearance of these data. Added to the figure are lines indicating the optical thickness of the two-layer phantom described and the fraction of the concentration retrieved for an absorber in the bottom layer.

the effect of the wide distribution of data about the fitted line. The approximate correction aids in assessing the estimate of absolute absorber concentration in the bottom layer of a layered geometry. However, fitting these data with a single line results in a wide distribution of data about the fitted line. Therefore this provides only an approximate correction for the effect of the top layer.

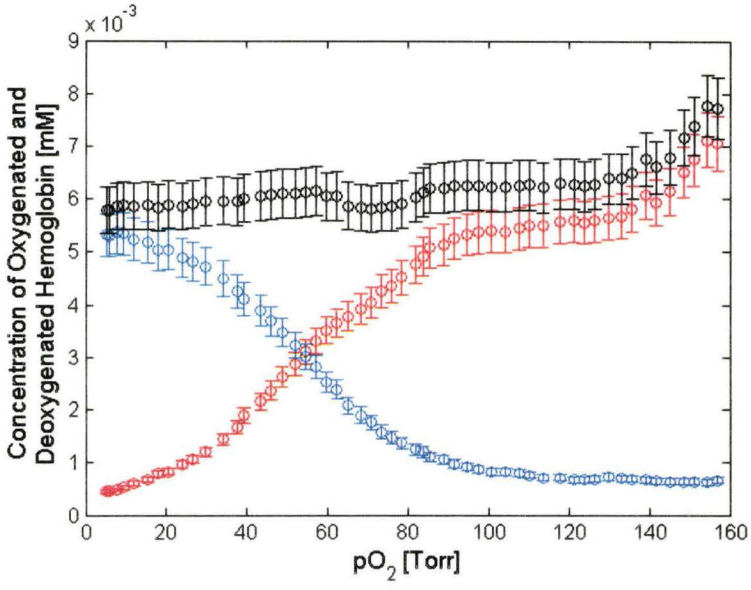

Figure 5.7: Retrieved concentration of total (black circles), oxy- (red circles), and deoxyhaemoglobin (blue circles) in the bottom layer of a two-layer phantom, at temperature = $36 \pm 1°$ C and pH ≈ 7.4. The top layer consisted of 2.5% Intralipid® with ink added to $\mu_a \approx 0.02$ mm^{-1}.

5.4.2 Effect of a third underlying layer

The geometry of tissue normally consists of more than two layers. Skin is considered to be composed of three primary layers: the epidermis, the dermis, and the subcutaneous tissue. Figure 5.8 shows a schematic representation of the layered structure of skin.

A vascular plexus located between the epidermis and the dermis has been associated with the increased blood flow to the skin observed as erythema (Nyström *et al.*, 2004). However, beyond the dermis are larger vessels that, if observable through the dermis, may contribute to the erythema measurement. It is important to assess the transparency of the dermis when making measurements using the

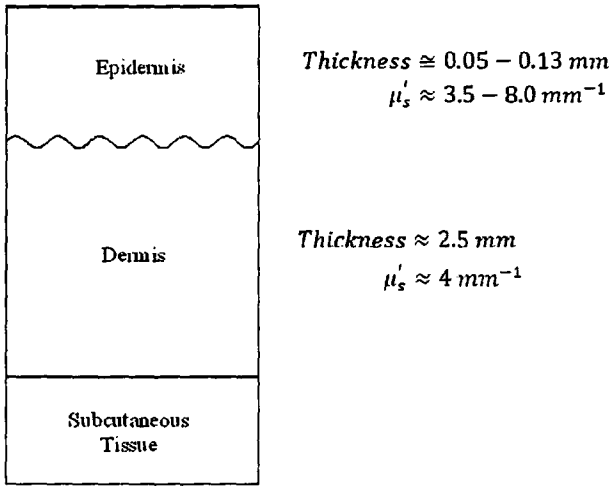

Figure 5.8: A schematic diagram of the skin.

integrating sphere.

The epidermis, with a thickness ranging from 0.05 mm to 0.13 mm, and a reduced scattering coefficient ranging from $\mu_s' = 3.5$ mm^{-1} to $\mu_s' = 8.0$ mm^{-1}, has a calculated maximum optical thickness of 1.04 (Zhang *et al.*, 2005). From the top layer thickness response relationship, the effect of this layer on the measurement of the bottom layer was shown to be negligible. To consider the effect of haemoglobin in the larger vascular network beyond the dermis, suppose that the skin can be approximated as another two-layer system composed of the dermis and the subcutaneous tissue. The dermis can be approximated by a thickness of 2.5 mm and a reduced scattering coefficient of $\mu_s' = 4$ mm^{-1} at 527 nm (Salomatina *et al.*, 2006). This yields an optical thickness of 10 which is well beyond the region of optical transparency for integrating sphere measurements. Therefore, the vascular network lying beyond the dermis should not contribute to the absorption signal as measured by the integrating sphere system.

5.5 Summary

A two-layer tissue-simulating liquid phantom was used to simulate the layered structure of skin. Measurements in a two-layered geometry revealed that increasing the top-layer optical thickness beyond a determined threshold value resulted in underestimates of the concentrations of absorbers in the bottom layer. It was shown that for optical thicknesses less than 2, the concentration of added absorber in the bottom layer was determined within experimental uncertainties. For this range of optical thicknesses, the accuracy of the retrieved concentration was comparable to the accuracy in retrieved concentration observed in a homogeneous geometry and was within 10% of the expected value using SR measurements. Beyond an optical thickness of 2 the retrieved concentration underestimated the expected concentration; optical thicknesses from 2 to 5 showed an underestimate in the retrieved concentration of approximately 10% to 75%. The top layer thickness response relationship can be used to generate an approximate correction factor for measurements made in geometries where the optical thickness exceeds 2.

Haemoglobin deoxygenation experiments in the two-layered geometry, with a top layer optical thickness simulating the epidermis, showed that the concentration of total haemoglobin in the bottom layer could be retrieved to within 11% when there was no broadband absorber in the top layer phantom material. Adding a broadband absorber to the top layer phantom material improved the results; the total haemoglobin concentration in the bottom layer was retrieved to within 6%. The accuracy of these results is comparable to that observed for measurements in the homogeneous geometry. The mean Hill coefficient for these experiments was 2.41 ± 0.13 which agrees with the published values for the Hill coefficient as

2.47 ± 0.05 (Zwart *et al.*, 1984) and 2.42 ± 0.05 (Hull *et al.*, 1998). The mean p_{50} value calculated from measurements on the three phantoms is 38 ± 3 Torr. This value does not agree with published values of 21.8 ± 0.9 Torr (Hull *et al.*, 1998) and 25.95 ± 1.43 Torr (Zwart *et al.*, 1984). However, the values for p_{50} vary for small changes in physiological conditions.

Chapter 6

In vivo measurements

6.1 Introduction

The integrating sphere system was developed with the intention of quantifying erythema resulting from external beam radiotherapy. Because erythema is associated with an increase in the apparent concentration of oxygenated haemoglobin, the haemoglobin oxygen saturation, SO_2, may be used to quantify changes in skin redness. It has been shown in the literature that the erythema index, first introduced by Dawson *et al.*, increased as the haemoglobin oxygen saturation increased from 0% to 90%. Comparing measurements of SO_2 made by the integrating sphere to the erythema index a linear relationship was observed. Therefore measurements of the apparent concentrations of oxygenated and deoxygenated haemoglobin, and therefore the assessment of apparent SO_2, may be used as a modified erythema index.

To assess the use of the integrating sphere probe in measuring SO_2 as a method

of quantifying erythema *in vivo*, a topical anesthetic cream was used to induce erythema in several regions on the abdomen (Bjerring *et al.*, 1989). Using the integrating sphere, reflectance measurements were used to determine the apparent SO_2 for each erythematic region over the course of several hours. These measurements were compared to clinical evaluations made by practicing radiation therapists and calculations of Dawson's erythema index (EI).

6.2 Typical *in vivo* measurement techniques

There are several techniques which have been used to assess erythema in a clinical setting. Diffuse reflectance techniques have been discussed throughout the thesis. Clinically, changes in the diffuse reflectance spectrum are often quantified by a defined index (e.g., erythema index, melanin index) in an attempt to assess the observed changes quantitatively. Reflectance colourimeters were described in Section 1.5, where diffuse reflectance measurements are standardized through an international colour system. Also discussed in Section 1.5 was the use of digital photography in the assessment of erythema. In this technique, digital images are analyzed to determine the contribution of red, blue, and green signals to the skin image. Laser doppler, and laser doppler imaging, have also been used to quantify erythema (Nyström *et al.*, 2004). In this technique a laser is used to measure changes in blood flow in an erythematic region. Light is incident on a region of tissue, photons interact with the moving red blood cells changing the frequency of the incident light. This frequency shift is related to tissue perfusion (Nyström *et al.*, 2004). While a variety of techniques have been applied to the assessment

of erythema, visual observation of skin redness remains the clinical standard as defined by the Radiation Therapy Oncology Group (RTOG) and the European organization for research and treatment of cancer (EORTC) (Cox *et al.*, 1995).

6.3 Definition of a modified erythema index

The erythema index was first introduced by Dawson *et al.* who defined the parameter to be proportional to the area under the log inverse reflectance curve, and above a determined baseline level (removing the contribution of broadband absorbers from the haemoglobin absorption), for wavelengths between 510 nm and 610 nm (Dawson *et al.*, 1980). Dawson *et al.* measured reflectance using a fibre optic system which delivered and detected light at a 45° angle to the skin surface and normalized each measurement to the reflectance of a glazed white tile assumed to have 100% reflectance at 570 nm. However, the EI does not explicitly describe any physiological parameter, such as apparent haemoglobin concentration or haemoglobin oxygen saturation, but is used to quantify changes which may be attributed to an increase in the blood concentration in skin. Feather *et al.* found that the erythema index increased as the haemoglobin oxygen saturation increased from 0% to 90% (Feather *et al.*, 1989). It has also been shown that, for irritant-induced erythema, the apparent concentration of oxygenated haemoglobin can be used to quantify erythema (Kollias *et al.*, 1995). Therefore, the apparent haemoglobin oxygen saturation, SO_2, can be used to quantify erythema because changes in apparent oxygenated haemoglobin concentration will increase apparent

SO_2 provided that the increase in apparent deoxygenated haemoglobin concentration is small in comparison to the increase in apparent oxygenated haemoglobin concentration. Quantifying erythema using changes in the apparent concentration of oxygenated haemoglobin, and hence the apparent SO_2, provides physiological information about the tissue which can be used to provide effective intervention when necessary. The linear relationship observed when comparing values of SO_2 with the erythema index indicates that SO_2 can be used to quantify erythema while providing additional information regarding the concentration of oxygenated and deoxygenated haemoglobin and tissue physiology.

6.3.1 Comparison of erythema index to SO_2 in two layer phantoms

For three haemoglobin deoxygenation experiments described in Chapter 5, the SO_2 was determined as described in Section 5.3, for each of the three phantoms. Additionally, the erythema index was calculated as described by Dawson *et al.* (Dawson *et al.*, 1980). The inverse of the normalized reflectance spectrum, R*, was taken and the logarithm to base 10 of the inverse reflectance spectrum calculated. The result is known as the LIR (log inverse reflectance) spectrum. The erythema index was calculated from the definition using the values of the LIR spectrum at specific wavelengths according to

$$EI = 100[r + 1.5(q + s) - 2.0(p + t)] \tag{6.1}$$

where p, q, r, s, and t are the LIR values at 510, 543, 560, 576, and 610 nm respectively giving the area under the curve above a baseline value (Dawson *et al.*, 1980). Figure 6.1 shows an example of a LIR spectrum and the points at which LIR values are used to determine the erythema index.

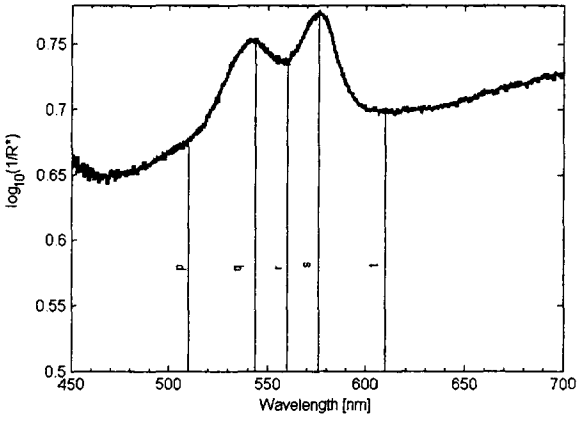

Figure 6.1: An example of the LIR spectrum used to determine the erythema index. Lines are drawn on the figure to show the values of LIR required by Equation 6.1.

The relationship between haemoglobin oxygen saturation and erythema index is shown in Figure 6.2. There appears to be a linear relationship between SO_2 and the Dawson EI. For a given data set, haemoglobin oxygen saturation increases with increasing erythema index. The variation in the erythema index between experiments is the result of differences in the magnitude of the reflectance spectrum caused by variations in the amount of ink in the top layer of the two layer phantoms and differences in the reduced scattering coefficient between phantom measurements. These variations make a direct comparison of these results difficult without a suitable normalization.

For clinical measurements, Dawson defines a relative EI as the difference between

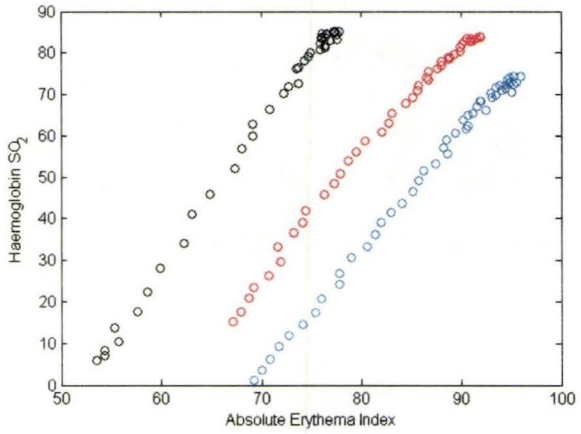

Figure 6.2: The relationship between erythema index and haemoglobin oxygen saturation determined for three deoxygenation experiments; blue circles (no ink in top layer), red circles (small quantity of ink in top layer) and black circles (larger quantity of ink in top layer).

the measured EI in a region of redness and the EI for a control region (Dawson *et al.*, 1980). Because EI is determined from values of LIR this difference is termed the relative EI. In the absence of a control region (as in the case of tissue-simulating phantoms), the minimum EI was selected as a "control" point in order to calculate the relative EI. This correction is shown in Figure 6.3. The result is that increasing SO_2 is associated with positive values of relative EI. Calculating the relative EI allowed for the direct comparison between measurements on phantoms of different optical properties but with the same expected concentration of haemoglobin further clarifying the linear relationship between EI and SO_2.

There are uncertainties associated with both the erythema index and the haemoglobin SO_2. The uncertainty in the erythema index is typically 5% as determined by the uncertainty in the magnitude of the reflectance signal. The uncertainty in SO_2 is determined from the uncertainty in the concentrations of oxygenated and

total haemoglobin and was typically 10% (Section 5.3). These results demonstrate a linear relationship between SO_2 and EI and thus that haemoglobin oxygen saturation may be used to quantify erythema as a surrogate to the erythema index described by Dawson *et al.*. This must also be shown for erythema induced *in vivo*. In normal tissues, haemoglobin within an artery is more that 95% saturated. In this work the measured concentration of oxy- and deoxyhaemoglobin is measured over the bulk of the tissue, and the calculated haemoglobin oxygen saturation is referred to as apparent SO_2.

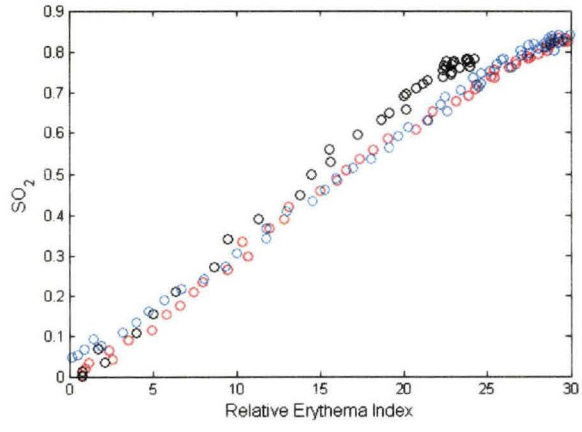

Figure 6.3: The relationship between the relative erythema index and haemoglobin oxygen saturation determined for three two-layer deoxygenation experiments, shown by uniquely coloured markers; blue circles (no ink in top layer), red circles (small quantity of ink in top layer) and black circles (larger quantity of ink in top layer).

6.4 Description of *in vivo* measurements

The integrating sphere system was developed with the intention of quantifying erythema resulting from external beam radiotherapy. To assess the use of the

apparent SO_2 as a measure of erythema *in vivo*, erythema was induced on the skin of a volunteer by the application of a topical cream. EMLA® cream (Astra Zeneca© Canada, Mississauga) is a topical anesthetic composed of 2.5% lidocaine and 2.5% prilocaine. It has been shown to induce erythema when applied to the skin for durations longer than 3 hours, as measured by an increased erythema index (Bjerring *et al.*, 1989). For application times less that 1.5 hours, a blanching response was observed and measured as negative erythema index as compared to a baseline value (Bjerring *et al.*, 1989).

Approval was obtained from the McMaster University Research Ethics Board (REB) for human studies consisting of a single volunteer. Erythema was induced on the abdomen through the application of 2.5 g of EMLA® cream for durations of 0.5, 1, 1.5, 2, 3, 4, 5, and 6 hours. The cream was applied to a 10 cm^2 area of skin and covered with Tegaderm™, a transparent dressing, to hold the cream in place. The application time was adjusted to ensure that the cream could be removed from each region at the same time. At the end of the application time the dressing and the excess cream were removed and the area was gently cleaned. Figure 6.4 shows a photograph of the cream applied to the abdomen.

Reflectance measurements were made at each site using both the integrating sphere system and the SR system immediately prior to the application, and immediately following the removal of the cream. The integrating sphere system was used to make additional measurements at thirty minute intervals thereafter. The reflectance measurements performed with the SR system were used to estimate the reduced scattering coefficient of the skin in each particular region. A mean value of $\mu_s' = 2.32 \pm 0.35$ mm^{-1} was used for each region. There were no significant

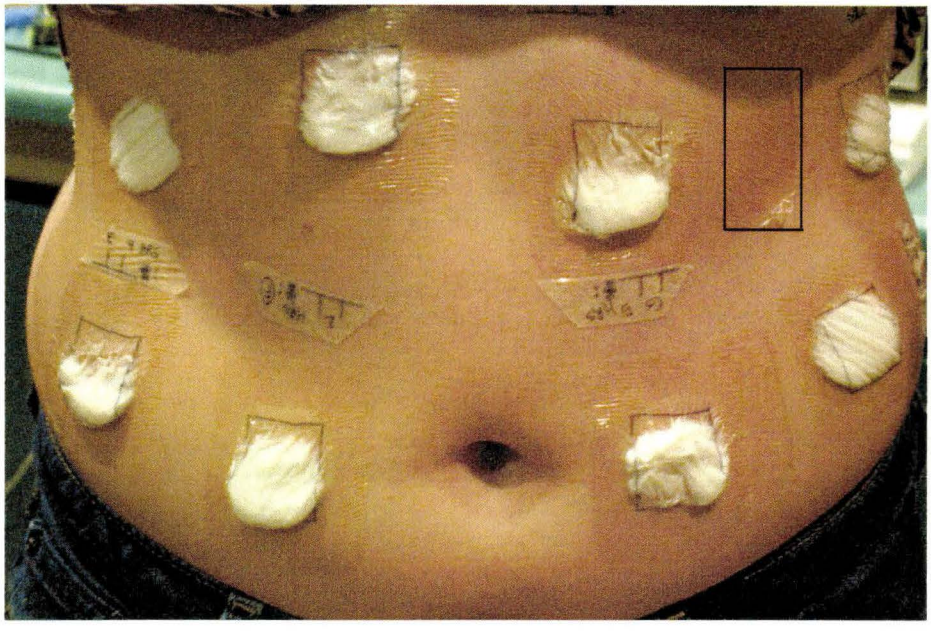

Figure 6.4: EMLA® cream applied to regions on the abdomen in a non-specific pattern. A control region where no cream was used but the dressing applied was also included and highlighted by a rectangle.

variations in reduced scattering coefficient across the regions nor were there significant variations in $\mu_s^{'}$ over time. This value of $\mu_s^{'}$ was used with the integrating sphere reflectance measurements to determine the absorption coefficient by using the empirical relationship. The singular value decomposition algorithm was modified to include the extinction coefficient for melanin (Prahl, 1998) and the retrieved absorption spectra were used to determine the apparent SO_2 for the areas under investigation. Additionally, the EI was determined for each region over time.

Clinical observations of each site were made by radiation therapists at the Juravinski Cancer Centre over a 1 hour period, 3 hours after the removal of the cream. Radiation therapists were asked to grade the erythema according to the Common Terminology Criteria for Adverse Effects v3.0 (CTCAE)(August 9 2006), where

faint erythema is given Grade 1 and Grade 2 is considered to be moderate to brisk erythema. The grading scale also includes Grade 3 (moist desquamation and/or bleeding), Grade 4 (skin necrosis or ulceration of full thickness dermis) and Grade 5 (death). A grade of 0 was not included in the CTCAE grading scale but was used by the radiation therapists to indicate the absence of erythema. The radiation therapists were also asked to rank the regions of erythema from the most severe to the least severe.

6.5 Results

Visible changes in skin colour were observed after exposure to EMLA® cream. Figure 6.5 is a photograph of the exposed skin after removal of the cream. Several regions of erythema were observed, corresponding to the areas of skin exposed to the topical anesthetic for the greatest periods of time. Additionally, several areas of blanching were observed, corresponding to areas of skin exposed for shorter times.

To correct for variation in the values of apparent SO_2 measured in each region, the apparent SO_2 was normalized to the value of apparent SO_2 measured prior to the application of the cream. For clarity, the normalized apparent SO_2 will be referred to as the relative SO_2. Figures 6.6, 6.7, and 6.8 show the relative SO_2 and the erythema index plotted over the time course of measurement where time T=0 hours is the time the cream is removed for the control region, the 3 hour exposure region, and the 6 hour exposure region. Data from the remaining regions is shown is Appendix B. Figures 6.6, 6.7, and 6.8 also show the relative erythema index as a function of the relative SO_2 (lower plot). The relative EI was calculated as the

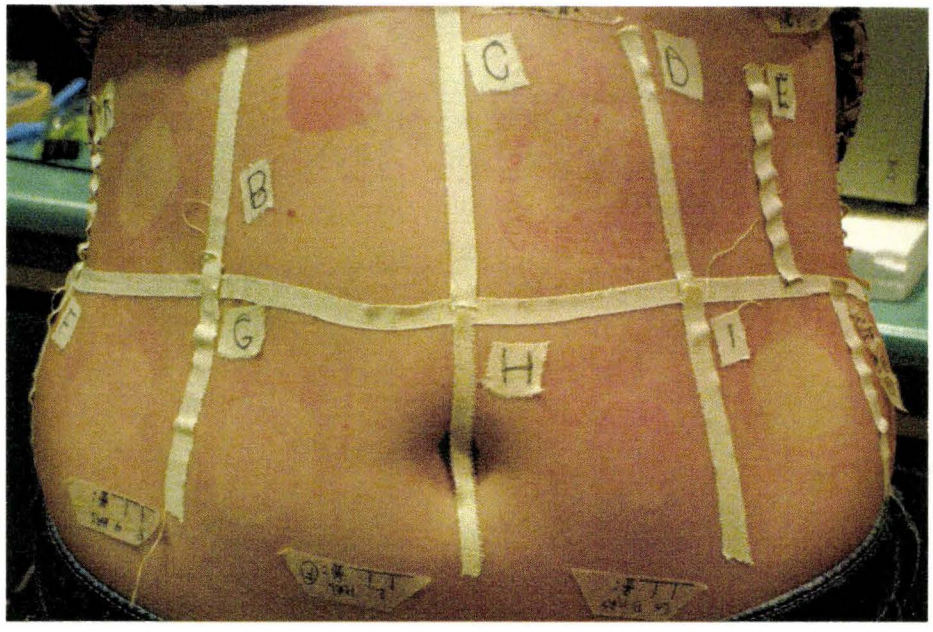

Figure 6.5: Photograph of *in vivo* results after EMLA® cream application. Note the regions of blanching (i.e. A, G, and I) and the appearance of erythema (i.e. B, D, and H). The control region is labeled as region D.

difference between the EI of the measured region and the EI determined for that region before the cream was applied (Dawson *et al.*, 1980). There appears to be a linear relationship between the relative SO_2 and the relative EI.

Tegaderm™ was used to cover a region to which no cream was applied, and this region was used as a control. Removal of the transparent dressing was found to increase the apparent SO_2 and erythema index (Figure 6.6). This reactive hyperemia was observed in a majority of the regions as removal of the Tegaderm™ caused a measurable change in apparent SO_2 measured at the 0 hour time point.

Figure 6.9 shows the relative SO_2 for the control region, the 3 hour exposure region, and the 6 hour exposure region plotted on the same axes. A region of increased SO_2 was measured for several hours after the removal of the cream for

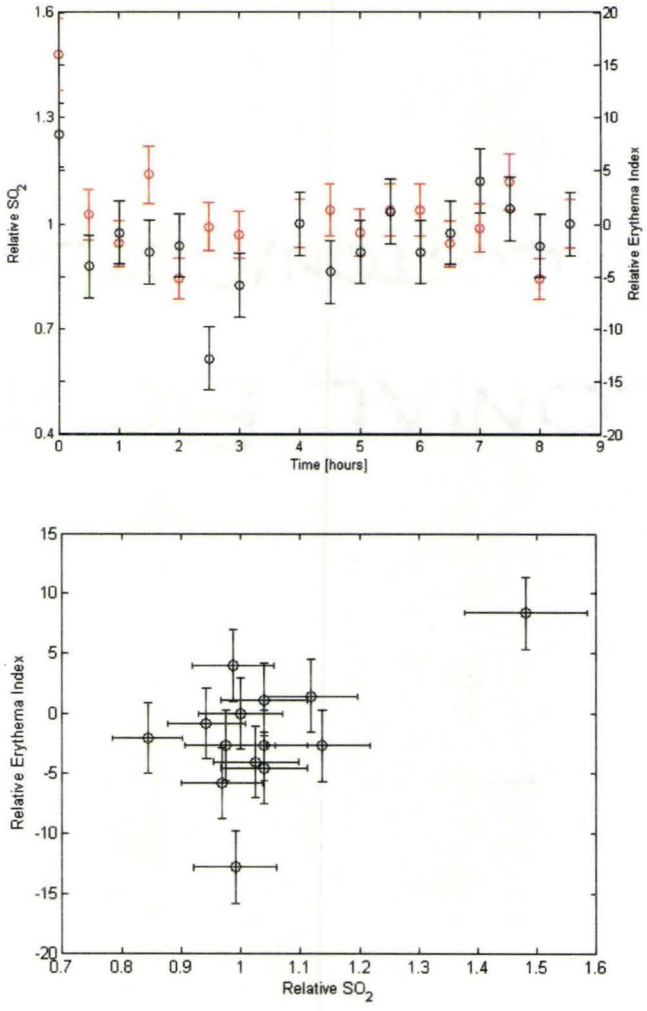

Figure 6.6: The control region for the *in vivo* experiment (Region D). The relative SO_2 is shown in red while the relative erythema index is shown in black.

the 6 hour exposure region. This corresponded to a region of brisk erythema. For the 3 hour exposure region, a decreased SO_2 was measured immediately following the removal of the cream and an increased SO_2 was measured 2 hours later. This corresponded to the observation of blanching followed by the appearance of brisk erythema. For the control region the SO_2 remained generally stable over the course

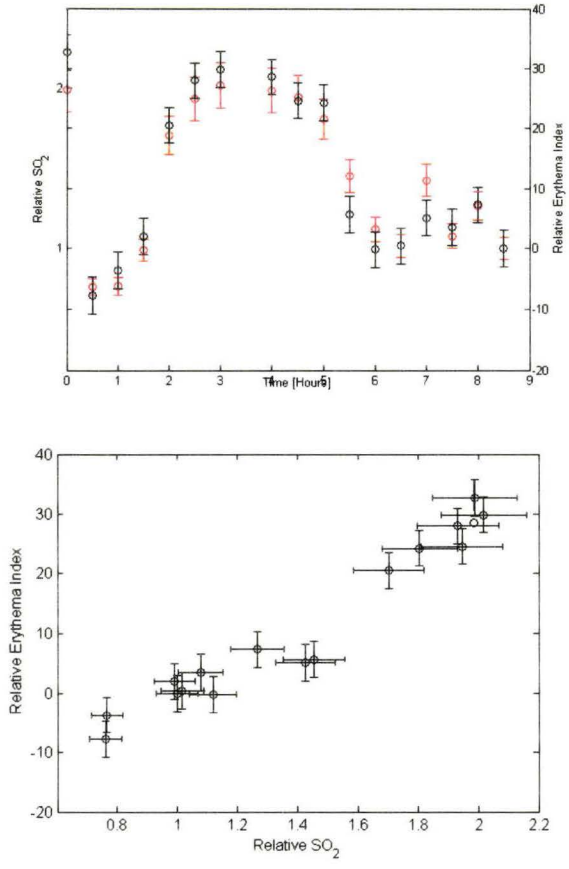

Figure 6.7: Erythema induced *in vivo* by topical anesthetic – 3 hour exposure (Region E). The relative SO_2 is shown in red while the relative erythema index is shown in black.

of measurement.

The clinical gradings assigned by the radiation therapists are summarized in Figure 6.10. For two regions (A and C) erythema was given a clinical score of 1 associated with a mild erythematic response when no change in SO_2 was measured as compared to the region before the cream was applied. This may be result of radiation therapists attempting to observe redness which is presumed to be there based on the delineation of the regions. Three regions (D, I, and G) were identified

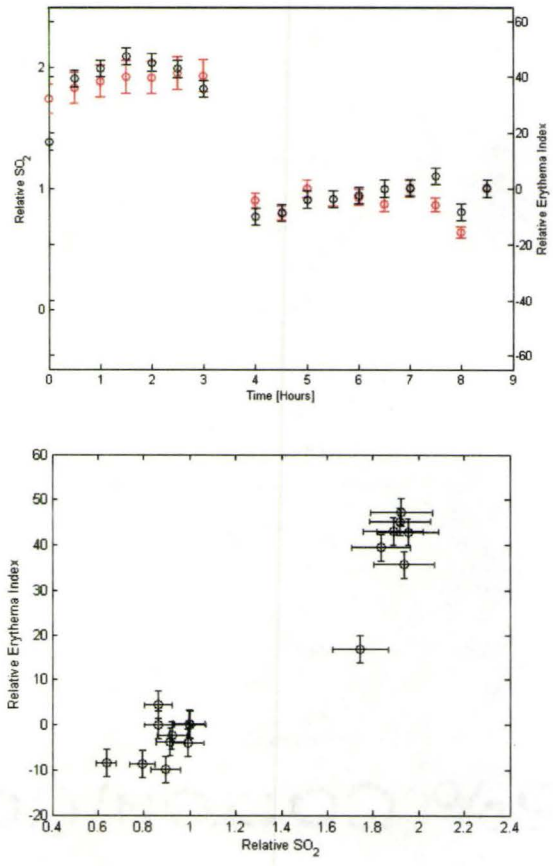

Figure 6.8: Erythema induced *in vivo* by topical anesthetic – 6 hour exposure (Region B). The relative SO_2 is shown in red while the relative erythema index is shown in black.

as having no erythema present which corresponds to no change in the measured SO_2. Three regions (F, E, and H) identified as regions of brisk erythema had a measured SO_2 more than 2 times greater as compared to the pre-application values.

Radiation therapists were also asked to rank the erythematic regions from the most severe to the least. These results are summarized in Figure 6.11 which plots the relative SO_2 as a function of the severity rank as scored by the majority of radiation therapists.

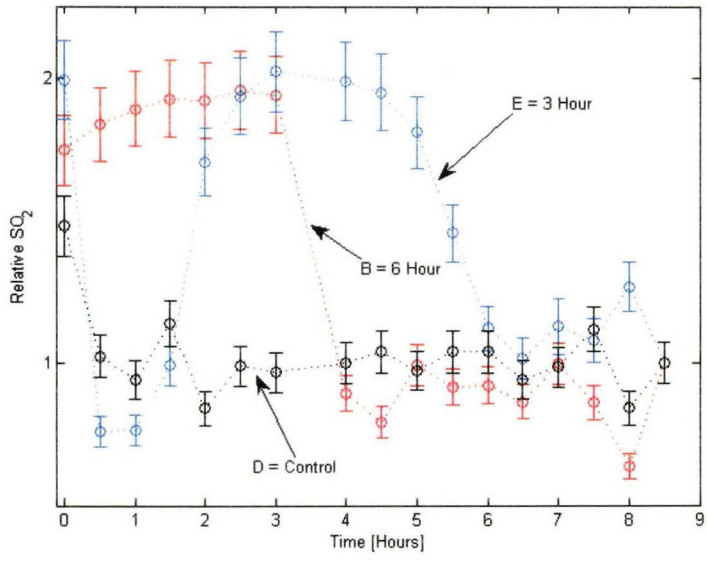

Figure 6.9: A comparison of the relative SO_2 measured for three regions: control (black), 3 hour application (blue), and 6 hour application (red).

The relative SO_2 is generally correlated with the severity rank scored by the majority of radiation therapists. However, although the severity rankings of the therapists correspond to the regions of increase in SO_2, further studies should consider that changes associated with radiation-induced erythema will be observed over time, and not as a side-by-side comparison between regions. Repeated observations over time make the visual assessment of erythema more difficult. The use of the integrating sphere system to quantify erythema based on changes in apparent SO_2 would provide an objective assessment of skin redness. This could provide physiological information which may be used to provide effective intervention to minimize dermatological toxicities thus improving patient quality of life.

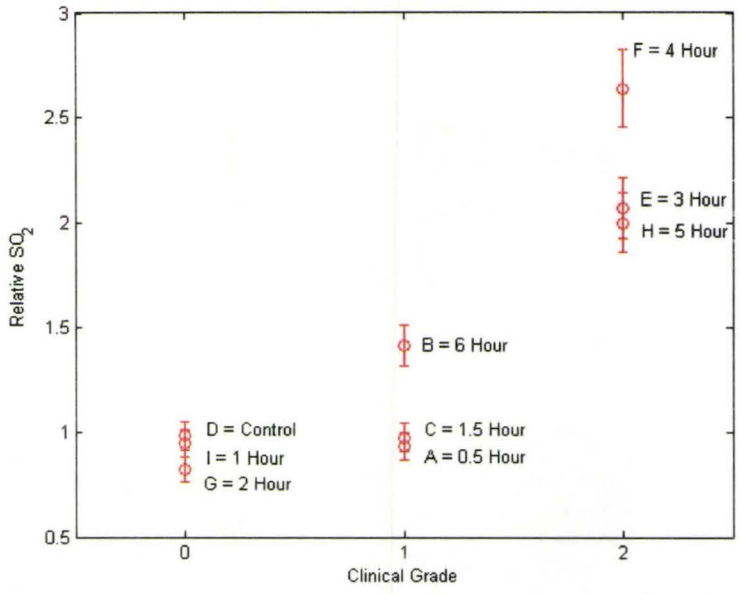

Figure 6.10: A summary of the clinical grading compared to the relative SO_2 measured for each region.

6.6 Summary

The IS system uses measurements of the apparent concentration of oxygenated and deoxygenated haemoglobin to determine the apparent SO_2 providing information about the physiological condition of the tissue. In Section 6.3.1, calculating the SO_2 for two-layer deoxygenation experiments revealed a linear relationship between the erythema index and the SO_2. These results suggested that the apparent SO_2 determined by the IS system could be used to assess erythema. The physiological information determined by the integrating sphere system cannot be retrieved from the EI.

The integrating sphere appears to provide information regarding changes in apparent blood content in the skin, and apparent SO_2 that are missed by the

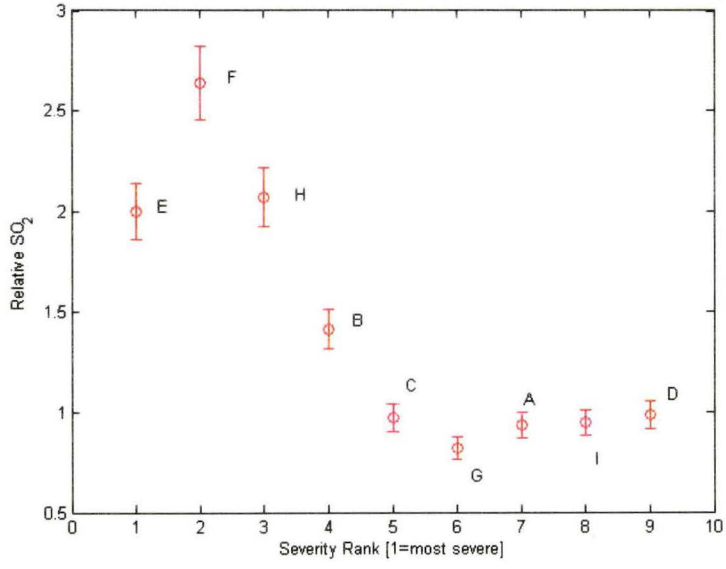

Figure 6.11: This figure shows the ranking of erythema severity compiled for the clinical observations.

clinical grading scale. This information could be used to manage adverse effects more effectively through adequate intervention. However, further *in vivo* studies must be performed to assess the performance of the probe when assessing skin of a wide range of pigmentations.

Chapter 7

Conclusions

7.1 Summary

This thesis described the characterization of an integrating sphere system for the non-invasive assessment of the optical properties of biological tissues over a broad spectral range, with the ultimate goal of quantifying erythema resulting from external beam radiotherapy. Constructed of Spectralon®, a highly reflective material, the integrating sphere served as both a diffuse illumination source and a diffuse reflectance detector; diffusely illuminating a material across the port opening and measuring the remitted light using a coupled detector. With an empirical model, the measured diffuse reflectance was used to determine the absorption coefficients of the material under investigation.

The empirical model related the normalized integrating sphere measurement R^*, to the reduced scattering coefficient μ_s', and the absorption coefficient, μ_a. Using this model and estimates of μ_s' measured using a fibre-based spatially-resolved

diffuse reflectance (SR) measurement system, values of μ_a were determined for tissue simulating phantoms doped with an added absorber. The retrieved values of μ_a were verified by measurements with the SR system. The concentration of the added chromophore was determined from the retrieved values of μ_a together with the known absorption spectrum of the chromophore. Experiments with a simple absorber in a homogeneous phantom were used to assess the validity of the empirical model. These measurements showed that the integrating sphere system could determine the concentration of an added absorber in a homogenous tissue-simulating liquid phantom to within 10%.

A region of erythema is associated with an increase in the apparent concentration of oxygenated haemoglobin as oxygen-rich blood is delivered to the areas of injury to promote healing as a result of a general inflammatory response. Measurements were thus performed in tissue simulating phantoms simulating a wide range of oxygenation. Whole horse blood was added to tissue-simulating phantoms and reflectance measurements were made while using yeast to deoxygenate the haemoglobin in the blood. The concentrations of oxygenated and deoxygenated haemoglobin were determined from the retrieved values of μ_a using a singular value decomposition algorithm and published extinction spectra.

In general, the integrating sphere probe determined the total haemoglobin concentration in homogeneous liquid phantoms to within 12% of the expected values for $\mu_s' = 1.283 \pm 0.064$ mm^{-1} at 550nm with no broadband absorber added. For optical properties more typical of those measured for human skin ($\mu_s' = 1.283 \pm 0.064$ mm^{-1} to $\mu_s' = 2.57 \pm 0.13$ mm^{-1} at 550nm, and a broadband absorption of $\mu_a = 0.025 \pm 0.002$mm^{-1} to $\mu_a = 0.15 \pm 0.01$mm^{-1} at 550 nm) the accuracy in

retrieving the concentration of total haemoglobin improved to within 7%.

The haemoglobin oxygen saturation of the phantoms was calculated from the concentration of oxygenated haemoglobin and the total haemoglobin concentration. Physiological parameters describing the oxygen dissociation curve were calculated from the haemoglobin oxygen saturation and the phantom pO_2 as measured by a Clark-type oxygen electrode. The mean Hill coefficient, n, was found to be 2.47 ± 0.22. Typical published values for the Hill coefficient are 2.46 ± 0.05 (Zwart *et al.*, 1984) and 2.42 ± 0.05 (Hull *et al.*, 1998). The p_{50} value is the pO_2 value at which 50% oxygen saturation is attained. For the temperature and pH described, assuming normal values of other parameters such as pCO_2 and intra-erythrocytic concentration of DPG, p_{50} takes values in the range of 21.8 ± 0.9 Torr (Hull *et al.*, 1998) and 25.95 ± 1.43 Torr (Zwart *et al.*, 1984); the mean value calculated from the three phantoms was 21 ± 3 Torr which is in agreement with published values.

The agreement of the Hill coefficient, n, with values published in the literature suggests that the integrating sphere accurately determines haemoglobin oxygen saturation. The agreement of p_{50} values with those published in the literature indicates that the horse blood used in the deoxygenation experiments had a normal oxygen dissociation curve. These results demonstrate the potential use of the integrating sphere probe to quantify haemoglobin concentration and tissue oxygenation.

Biological tissues are typically not simple, homogeneous media. Skin, in particular, possesses a layered structure, with various chromophores found in specific layers. Therefore, it was necessary to characterize the response of the integrating sphere system in a more complex, layered geometry. A two-layer geometry was chosen for its relative simplicity, allowing for the use of homogenous liquid phantoms

as each of the distinct layers, and for its approximation of human skin.

Measurements in a two-layered geometry revealed that increasing the top-layer optical thickness (defined as a product of the physical thickness and the μ_s' of the top layer) beyond a determined threshold value, resulted in underestimates of the concentrations of absorbers in the bottom layer. It was shown that for optical thicknesses less than 2, the concentration of an added absorber in the bottom layer was comparable to the accuracy in retrieved concentration observed in a homogeneous geometry and was within 10% of the expected value determined using SR measurements. Beyond this region the retrieved concentration underestimated the expected concentration; optical thicknesses from 2 to 5 showed an underestimate in the retrieved concentration of approximately 10% to 75%. The top layer thickness response relationship can be used to generate an approximate correction factor for measurements made in geometries where the optical thickness exceeds 2 but is less than 5.

The increase in the apparent concentration of oxygenated haemoglobin associated with erythema occurs beneath the epidermis. The optical thickness of the epidermis was found to be 1.04 which is less than 2 and thus the epidermis should not influence the measurement of changes in the apparent concentration oxygenated and deoxygenated haemoglobin in the papillary dermis.

Deoxygenation experiments were completed in a two-layer geometry. The mean Hill coefficient for these experiments was 2.41 ± 0.13 which agrees with the published values for the Hill coefficient of 2.47 ± 0.05 (Zwart *et al.*, 1984) and 2.42 ± 0.05 (Hull *et al.*, 1998). The mean p_{50} value calculated from measurements on three phantoms was 38 ± 3 Torr. This value does not agree with published values of 21.8 ± 0.9 Torr

(Hull *et al.*, 1998) and 25.95 ± 1.43 Torr (Zwart *et al.*, 1984). However, the values for p_{50} vary for small changes in physiological conditions. The combined effect of small changes in concentration of 2,3-di-phosphoglycerate and temperature could have contributed to increases observed in p_{50}. There was agreement between the estimate of total haemoglobin concentration and the value expected from the packed cell volume provided by the supplier and the volume of blood added to the phantom. This agreement is an indication that the retrieved concentrations of oxygenated and deoxygenated haemoglobin are also accurate. The agreement of the Hill coefficient with values published in the literature also confirms these results. The deviation of the p_{50} from expected values may not arise from inaccurate measurements of oxygenated and deoxygenated haemoglobin but may be due to the numerous other causes for this shift. Therefore, from these results it can be concluded that the integrating sphere probe can determine the total haemoglobin concentration in a two-layer tissue simulating phantom to within 12% when the optical thickness of the top layer is less than 2. The accuracy of these measurements increases as the amount of broadband absorption in the top layer increases such that for a top-layer simulating a darker skin type where $\mu_a \approx 0.07$ mm^{-1}, the total haemoglobin concentration is retrieved to within 6%. The addition of the broadband absorber increased the amount of absorption improving the accuracy of the empirical model when determining μ_a.

The integrating sphere system was developed with the intention of quantifying erythema resulting from external beam radiotherapy. The erythema index was first introduced by Dawson *et al.*, who quantified the change in skin colour using changes in the measured LIR spectrum of tissue. Changes in the LIR spectrum are

due to changes in the concentrations of oxygenated and deoxygenated haemoglobin. Rather than quantifying changes in the LIR spectrum, the apparent SO_2 was used as a modified erythema index where apparent SO_2 was calculated using the retrieved apparent concentrations of oxygenated haemoglobin and total haemoglobin. Calculations of SO_2, for phantom of known haemoglobin concentration, were related to the EI and it was found that these values were linearly correlated.

Preliminary *in vivo* experiments measured erythema induced on the abdomen through the application of a topical anesthetic cream. Clinical observations were made by radiation therapists at the Juravinski Cancer Centre over a 1 hour period, 3 hours after the removal of the cream. Radiation therapists used the CTCAE grading scale to assess each region. Using a coarse scale (0,1 and 2) to quantify the erythema induced with radiotherapy may miss the subtle changes in tissue physiology which were measured using the integrating sphere. Additionally, radiation therapists were asked to rank the regions of erythema in order of severity. The regions of erythema ranked as most severe by radiation therapists often correlated to the greatest increases in apparent oxygen saturation as measured by the integrating sphere. Meanwhile, the integrating sphere appeared to provide information of subtle changes in blood content in the skin, and apparent oxygen saturation. However, these *in vivo* studies are preliminary and further studies should be undertaken before the integrating sphere system can be used for clinical applications.

A method to quantify erythema in its early stages may provide an opportunity for intervention prior to its progression to more serious conditions, dramatically improving a clinician's ability to predict the integrity of the skin throughout a radiotherapy treatment (Pearse *et al.*, 1990). The integrating sphere system has

shown the potential for quantifying changes in optical absorption associated with erythema. Preliminary *in vivo* measurements show that there is an increase in apparent haemoglobin oxygen saturation for regions of increased erythema. The changes in apparent haemoglobin oxygen saturation are also correlated with the erythema index traditionally used to quantify skin redness.

There are several advantages of the integrating sphere that make it an ideal measurement system for use in a clinical setting. It is simple, easy-to-use and portable. The large area of the port opening makes measurements of diffuse reflectance less sensitive to local inhomogeneities as compared to traditional fibre-based diffuse reflectance techniques. However, it was the empirical model, together with a known reduced scattering coefficient, that defined how values of R* measured using the integrating sphere system were used to determine the absorption spectrum. Without this model, the IS system was limited to measurements of diffuse reflectance that could not provide any additional information about the concentration of chromophores present. With the empirical model the absorption spectra were retrieved from values of R*. The retrieved absorption spectra were used to determine the concentration of specific chromophores using a singular value decomposition algorithm. Characterization measurements have shown that the integrating sphere can resolve the contribution of several chromophores in a mixture, even when measured at a depth. While the knowledge of reduced scattering coefficient introduced a cost, particularly when $\mu_s^{'}$ is measured using a spatially-resolved diffuse reflectance system, information regarding the absolute chromophore concentration may be worth the added expense. However, if the relative chromophore concentration is sufficient, the need for a well-known reduced scattering coefficient is eliminated, as an

estimated value can be used to determine relative chromophore concentrations to within 10% of expected values.

7.2 Future Studies

The use of the integrating sphere system in a clinical environment requires further study. Although the preliminary *in vivo* measurements presented in this thesis show the potential of the device for clinical measurements of erythema, the participation of a single human participant limits these results. The sole participant was fair-skinned and further assessment of the effect of pigmentation on the measured quantities must be determined through the study of induced erythema in individuals of varying skin pigmentations. Additionally, erythema induced by external beam radiotherapy is often accompanied by increases in pigmentation. While the singular value decomposition algorithm can resolve these changes in the absorption spectrum according to contributing chromophores, the effect of increasing pigmentation on the measurement of haemoglobin concentration warrants further study. Other volunteer studies could explore the potential use of the integrating sphere system in assessing jaundice or edema, monitoring extremity vascular perfusion in diabetic patients or determining the age of hematomas induced by traumatic injury. Since it has been demonstrated that the concentrations of chromophores can be monitored, those chromophores involved in specific pathologies could potentially be monitored.

The integrating sphere probe design could be optimized for specific measurements; a range of sphere sizes could expand the areas available for measurement.

Smaller probes could be developed for measurements in confined spaces (e.g., oral mucosa). Computer modeling would contribute to the optimization of the probe design and could be used to generate an appropriate light transport model such that the measured R* could be compared directly to Monte Carlo simulation to determine μ_a. This may eliminate the need for characterization measurements in order to define an empirical model for integrating sphere probes in different physical configurations.

Appendix A

Optical properties of homogeneous phantoms

A.1 Phantoms used in defining the empirical relationship

% Concentration of ink	μ_a [mm^{-1}] at 650 nm
0	0
0.02	0.015 ± 0.001
0.05	0.037 ± 0.003
0.11	0.085 ± 0.006
0.21	0.155 ± 0.011
0.31	0.229 ± 0.016

Table A.1: Expected absorption coefficients (determined from the volume added and the measured extinction coefficient) for ink concentrations used in the definition of the empirical relationship.

% Concentration of Intralipid®	μ_s' [mm^{-1}] at 650 nm
1	1.08 ± 0.05
1.25	1.35 ± 0.07
1.5	1.63 ± 0.08
1.75	1.90 ± 0.09
2	2.17 ± 0.11
3	3.25 ± 0.16

Table A.2: Expected reduced scattering coefficient (as measured by the SR system) for Intralipid® concentrations used in the definition of the empirical relationship.

A.2 Phantoms used with green food colour

% Concentration of green food colour	μ_a [mm^{-1}] at 630 nm
0	0
0.01	0.010 ± 0.001
0.02	0.019 ± 0.001
0.03	0.029 ± 0.002
0.04	0.039 ± 0.003
0.05	0.049 ± 0.003
0.06	0.059 ± 0.004
0.07	0.069 ± 0.005
0.08	0.079 ± 0.005
0.09	0.088 ± 0.006
0.10	0.098 ± 0.007
0.15	0.148 ± 0.010

Table A.3: Expected absorption coefficients (determined from the volume added and the measured extinction coefficient) for greed food colour concentrations.

Appendix B

In vivo measurement data

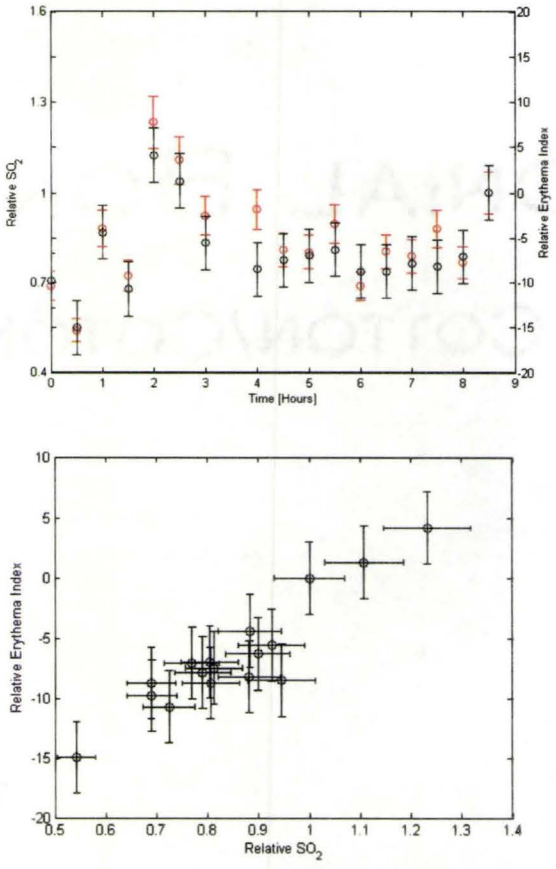

Figure B.1: Erythema induced *in vivo* by topical anesthetic – 0.5 Hour exposure (Region A). The relative SO_2 is shown in red while the relative erythema index is shown in black.

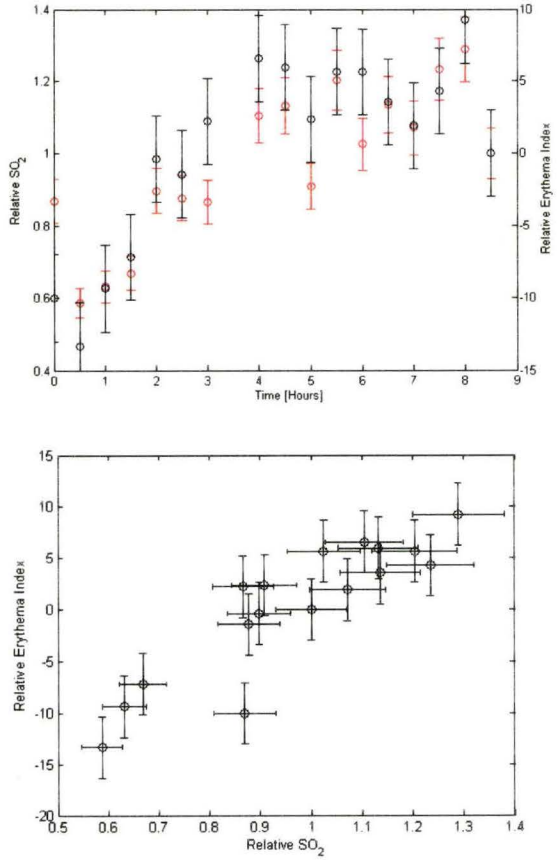

Figure B.2: Erythema induced *in vivo* by topical anesthetic – 1 Hour exposure (Region I). The relative SO_2 is shown in red while the relative erythema index is shown in black.

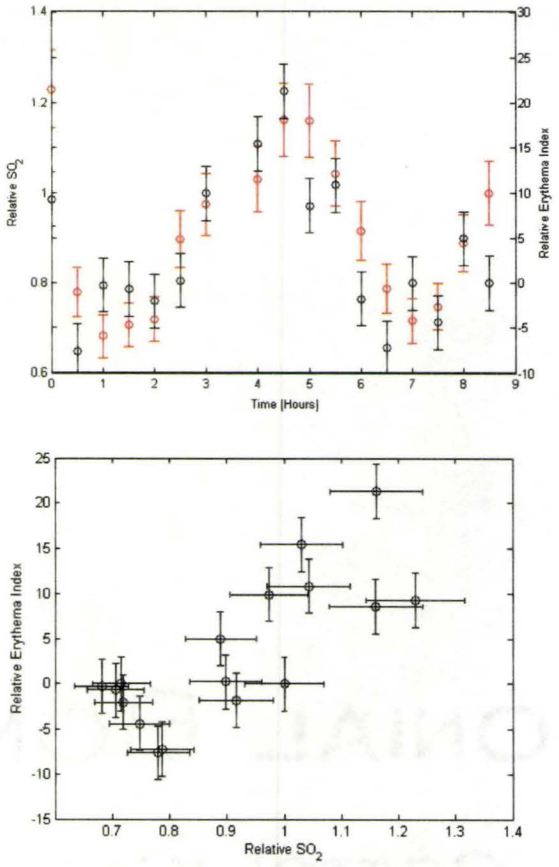

Figure B.3: Erythema induced *in vivo* by topical anesthetic – 1.5 Hour exposure (Region C). The relative SO_2 is shown in red while the relative erythema index is shown in black.

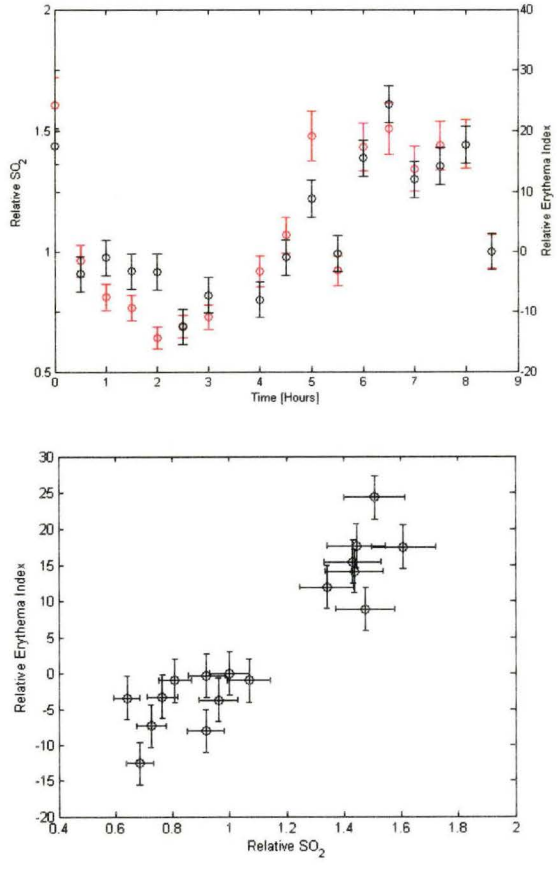

Figure B.4: Erythema induced *in vivo* by topical anesthetic – 2 Hour exposure (Region G). The relative SO_2 is shown in red while the relative erythema index is shown in black.

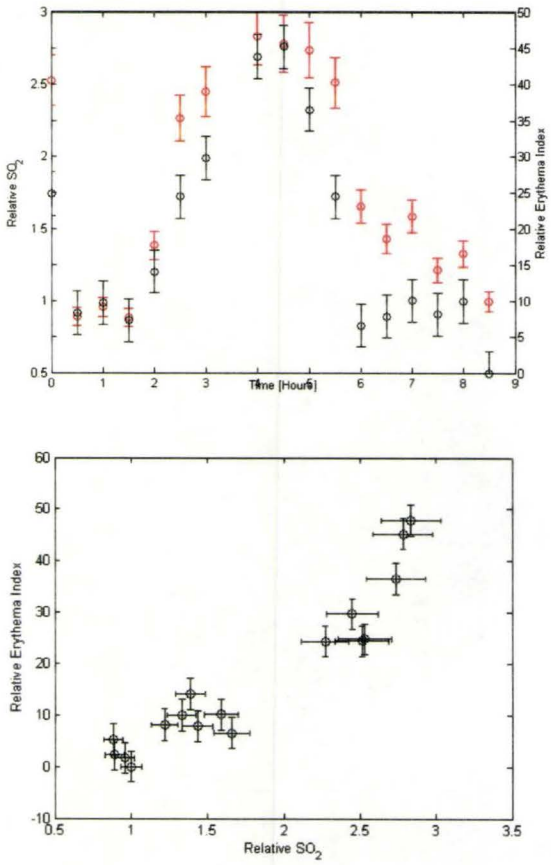

Figure B.5: Erythema induced *in vivo* by topical anesthetic – 4 Hour exposure (Region F). The relative SO_2 is shown in red while the relative erythema index is shown in black.

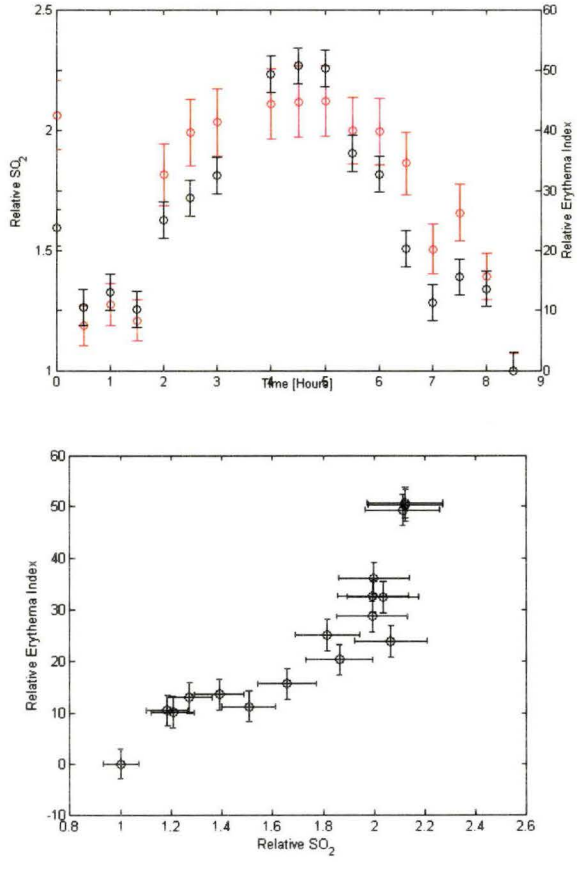

Figure B.6: Erythema induced *in vivo* by topical anesthetic – 5 Hour exposure (Region H). The relative SO_2 is shown in red while the relative erythema index is shown in black.

Bibliography

Ballard, J. L., Eke, C. C., Bunt, T., and Killeen, J. (1995). A prospective evaluation of transcutaneous oxygen measurements in the management of diabetic foot problems,. *Journal of Vascular Surgery*, **22**(4), 485–492.

Bargo, P. R., Prahl, S. A., Goodell, T. T., Sleven, R. A., Koval, G., Blair, G., and Jacques, S. L. (2005). In vivo determination of optical properties of normal and tumor tissue with white light reflectance and an empirical light transport model during endoscopy. *J. Biomed. Opt.*, **10**(3), 034018–15.

Beek, J. F., Blokland, P., Posthumus, P., Aalders, M., Pickering, J. W., Sterenborg, H. J. C. M., and van Gemert, M. J. C. (1997). In vitro double-integrating-sphere optical properties of tissues between 630 and 1064 nm. *Physics in Medicine and Biology*, (11), 2255.

Bjerring, P., Andersen, P., and Arendt-Nielsen, L. (1989). Vascular response of human skin after analgesia with EMLA cream. *Br. J. Anaesth.*, **63**(6), 655–660.

Bruulsema, J. T., Hayward, J. E., Farrell, T. J., Patterson, M. S., Heinemann, L., Berger, M., Koschinsky, T., Sandahl-Christiansen, J., Orskov, H., Essenpreis, M., Schmelzeisen-Redeker, G., and Böcker, D. (1997). Correlation between blood

glucose concentration in diabetics and noninvasively measured tissue optical scattering coefficient. *Opt. Lett.*, **22**(3), 190–192.

Bunn, H. F. and Guidotti, G. (1972). Stabilizing interactions in hemoglobin. *Journal of Biological Chemistry*, **247**(8), 2345–2350.

Chance, B., Leigh, J. S., Miyake, H., Smith, D. S., Nioka, S., Greenfeld, R., Finander, M., Kaufmann, K., Levy, W., Young, M., Cohen, P., Yoshioka, H., and Boretsky, R. (1988a). Comparison of time-resolved and -unresolved measurements of deoxyhemoglobin in brain. *Proceedings of the National Academy of Sciences of the United States of America*, **85**(14), 4971–4975.

Chance, B., Nioka, S., Kent, J., McCully, K., Fountain, M., Greenfeld, R., and Holtom, G. (1988b). Time-resolved spectroscopy of hemoglobin and myoglobin in resting and ischemic muscle. *Analytical Biochemistry*, **174**(2), 698 – 707.

Cheong, W., Prahl, S., and Welch, A. (1990). A review of the optical properties of biological tissues. *Quantum Electronics, IEEE Journal of*, **26**(12), 2166–2185.

Comsa, D. C., Farrell, T. J., and Patterson, M. S. (2006). Quantification of bioluminescence images of point source objects using diffusion theory models. *Physics in Medicine and Biology*, **51**(15), 3733–3746.

Cope, M. and Delpy, D. (1988). System for long-term measurement of cerebral blood and tissue oxygenation on newborn infants by near infra-red transillumination. *Medical and Biological Engineering and Computing*, **26**(3), 289–294.

Cox, J. D., Stetz, J., and Pajak, T. F. (1995). Toxicity criteria of the radiation therapy oncology group (rtog) and the european organization for research and

treatment of cancer (eortc). *International Journal of Radiation Oncology Biology Physics*, **31**(5), 1341–1346.

Dash, R. K. and Bassingthwaighte, J. B. (2004). Blood hbo2 and hbco2 dissociation curves at varied o2, co2, ph, 2,3-dpg and temperature levels. *Annals of Biomedical Engineering*, **32**(12), 1676–1693.

Dawson, J. B., Barker, D. J., Ellis, D. J., Cotterill, J. A., Grassam, E., Fisher, G. W., and Feather, J. W. (1980). A theoretical and experimental study of light absorption and scattering by in vivo skin. *Physics in Medicine and Biology*, **25**(4), 695–709.

Delpy, D. T., Cope, M., van der Zee, P., Arridge, S., Wray, S., and Wyatt, J. (1988). Estimation of optical pathlength through tissue from direct time of flight measurement. *Physics in Medicine and Biology*, **33**(12), 1433–1442.

Diffey, B., Oliver, R., and Farr, P. (1984). A portable instrument for quantifying erythema induced by ultraviolet radiation. *British Journal of Dermatology*, **111**(6), 663–672.

Dolotov, L., Sinichkin, Y., Tuchin, V., Utz, S., Altshuler, G., and Yaroslavsky, I. (2004). Design and evaluation of a novel portable erythema-melanin-meter. *Lasers in Surgery and Medicine*, **34**(2), 127–135.

Doornbos, R. M. P., Lang, R., Aalders, M. C., Cross, F. W., and Sterenborg, H. J. C. M. (1999). The determination of in vivo human tissue optical properties and absolute chromophore concentrations using spatially resolved steady-state diffuse reflectance spectroscopy. *Physics in Medicine and Biology*, **44**(4), 967–981.

Ducharme, A., Daniels, A., Grann, E., and Boreman, G. (1997). Design of an integrating sphere as a uniform illumination source. *Education, IEEE Transactions on*, **40**(2), 131–134.

Elsner, P. (1995). *Bioengineering of the skin: cutanous blood flow and erythema*, chapter 19, pages 247–252. CRC Press.

Farrell, T. J., Patterson, M. S., and Wilson, B. (1992). A diffusion theory model of spatially resolved, steady-state diffuse reflectance for the noninvasive determination of tissue optical properties in vivo. *Medical Physics*, **19**(4), 879–888.

Feather, J. W., Hajizadeh-Saffar, M., Leslie, G., and Dawson, J. B. (1989). A portable scanning reflectance spectrophotometer using visible wavelengths for the rapid measurement of skin pigments. *Physics in Medicine and Biology*, **34**(7), 807–820.

Flock, S., Patterson, M., Wilson, B., and Wyman, D. (1989). Monte carlo modeling of light propagation in highly scattering tissues. i. model predictions and comparison with diffusion theory. *Biomedical Engineering, IEEE Transactions on*, **36**(12), 1162–1168.

Groenhuis, R. A. J., Bosch, J. J. T., and Ferwerda, H. A. (1983). Scattering and absorption of turbid materials determined from reflection measurements. 2: Measuring method and calibration. *Appl. Opt.*, **22**(16), 2463–2467.

Haskell, R. C., Svaasand, L. O., Tsay, T.-T., Feng, T.-C., McAdams, M. S., and Tromberg, B. J. (1994). Boundary conditions for the diffusion equation in radiative transfer. *J. Opt. Soc. Am. A*, **11**(10), 2727–2741.

Hopewell, J. (1990). The skin: Its structure and response to ionizing radiation. *International Journal of Radiation Biology*, **57**(4), 751–773.

Hughes, V. K., Ellis, P. S., Burt, T., and Langlois, N. E. I. (2004). The practical application of reflectance spectrophotometry for the demonstration of haemoglobin and its degradation in bruises. *J Clin Pathol*, **57**(4), 355–359.

Hull, E. L., Nichols, M. G., and Foster, T. H. (1998). Quantitative broadband near-infrared spectroscopy of tissue-simulating phantoms containing erythrocytes. *Physics in Medicine and Biology*, **43**(11), 3381–3404.

Hunter, R. (2001). *Hemoglobin oxygenation of a two-layer tissue-simulating phantom from time-resolved reflectance.* Ph.D. thesis, McMaster University.

Jacquez, John A.and Kuppenheim, H. F. (1955). Theory of the integrating sphere. *J. Opt. Soc. Am.*, **45**(6), 460–466.

Kienle, A. and Patterson, M. S. (1996). Determination of the optical properties of turbid media from a single monte carlo simulation. *Physics in Medicine and Biology*, **41**(10), 2221–2227.

Kienle, A. and Patterson, M. S. (1997a). Determination of the optical properties of semi-infinite turbid media from frequency-domain reflectance close to the source. *Physics in Medicine and Biology*, **42**(9), 1801–1819.

Kienle, A. and Patterson, M. S. (1997b). Improved solutions of the steady-state and the time-resolved diffusion equations for reflectance from a semi-infinite turbid medium. *J. Opt. Soc. Am. A*, **14**(1), 246–254.

Kienle, A., Lilge, L., Patterson, M. S., Hibst, R., Steiner, R., and Wilson, B. C. (1996a). Spatially resolved absolute diffuse reflectance measurements for non-invasive determination of the optical scattering and absorption coefficients of biological tissue. *Appl. Opt.*, **35**(13), 2304–2314.

Kienle, A., Lilge, L., Vitkin, I. A., Patterson, M. S., Wilson, B. C., Hibst, R., and Steiner, R. (1996b). Why do veins appear blue? A new look at an old question. *Appl. Opt.*, **35**(7), 1151.

Kollias, N., Gillies, R., Muccini, J. A., Uyeyama, R. K., Phillips, S. B., and Drake, L. A. (1995). A single parameter, oxygenated hemoglobin, can be used to quantify experimental irritant-induced inflammation. *J Investig Dermatol*, **104**(3), 421–424.

Kollias N, B. A. (1988). Quantitative assessment of uv-induced pigmentation and erythema. *Photodermatology*, **5**(1), 53–60.

Labsphere® (1998). A guide to integrating sphere therory and applications. Technical report, Labsphere®.

LeFevre, M. E. (1969). Calibration of clark oxygen electrode for use in aqueous solutions. *J Appl Physiol*, **26**(6), 844–846.

Martelli, F. and Zaccanti, G. (2007). Calibration of scattering and absorption properties of a liquid diffusive medium at nir wavelengths. cw method. *Opt. Express*, **15**(2), 486–500.

Metropolis, N. and Ulam, S. (Sep., 1949). The monte carlo method. *Journal of the American Statistical Association*, **44**(247), 335–341.

Mourant, J. R., Fuselier, T., Boyer, J., Johnson, T. M., and Bigio, I. J. (1997). Predictions and measurements of scattering and absorption over broad wavelength ranges in tissue phantoms. *Appl. Opt.*, **36**(4), 949–957.

Nei, L. and Compton, R. G. (1996). An improved clark-type galvanic sensor for dissolved oxygen. *Sensors and Actuators B: Chemical*, **30**(2), 83–87.

Nichols, M. G., Hull, E. L., and Foster, T. H. (1997). Design and testing of a white-light, steady-state diffuse reflectance spectrometer for determination of optical properties of highly scattering systems. *Appl. Opt.*, **36**(1), 93–104.

Nyström, J., Geladi, P., Lindholm-Sethson, B., Rattfelt, J., Svensk, A.-C., and Franzen, L. (2004). Objective measurements of radiotherapy-induced erythema. *Skin Research and Technology*, **10**(4), 242–250.

Ocean Optics, I. (2000). *Operating Manual and User's Guide: S2000 Miniature Fibre Optic Spectrometers and Accessories.* Ocean Optics, Inc., 830 Douglas Ave. Dunedin, FL 34698 USA.

Patterson, M. S., Chance, B., and Wilson, B. C. (1989). Time resolved reflectance and transmittance for the non-invasive measurement of tissue optical properties. *Appl. Opt.*, **28**(12), 2331–2336.

Patterson, M. S., Moulton, J. D., Wilson, B. C., Berndt, K. W., and Lakowicz, J. R. (1991a). Frequency-domain reflectance for the determination of the scattering and absorption properties of tissue. *Appl. Opt.*, **30**(31), 4474–4476.

Patterson, M. S., Wilson, B. C., and Wyman, D. R. (1991b). The propagation of

optical radiation in tissue i. models of radiation transport and their application. *Lasers in Medical Science*, **6**(2), 155–168.

Pearse, A. D., Edwards, C., Hill, S., and Marks, R. (1990). Portable erythema meter and its application to use in human skin. *International Journal of Cosmetic Science*, **12**(2), 63–70.

Pickering, J. W., Moes, C. J. M., Sterenborg, H. J. C. M., Prahl, S. A., and van Gemert, M. J. C. (1992). Two integrating spheres with an intervening scattering sample. *J. Opt. Soc. Am. A*, **9**(4), 621–631.

Pickering, J. W., Prahl, S. A., van Wieringen, N., Beek, J. F., Sterenborg, H. J. C. M., and van Gemert, M. J. C. (1993). Double-integrating-sphere system for measuring the optical properties of tissue. *Appl. Opt.*, **32**(4), 399–410.

Pogue, B. W. and Patterson, M. S. (1994). Frequency-domain optical absorption spectroscopy of finite tissue volumes using diffusion theory. *Physics in Medicine and Biology*, **39**(7), 1157–1180.

Prahl, S. (1998). Tabulated molar extinction coefficient for hemoglobin in water.

Randeberg, L. L., Haugen, O. A., Haaverstad, R., and Svaasand, L. O. (2006). A novel approach to age determination of traumatic injuries by reflectance spectroscopy. *Lasers in Surgery and Medicine*, **38**(4), 277–289.

Riedinger, T. M. and Rodak, B. F. (1998). *Clinical Hematology: Principles, Procedures, Correlations*, chapter Quantitative laboratory evaluation of erythrocytes, pages 106–124. Lippincott-Raven inc.

Salomatina, E., Jiang, B., Novak, J., and Yaroslavsky., A. (2006). Optical properties of normal and cancerous human skin in the visible and near-infrared spectral range. *Journal of Biomedical Optics*, **11**(6).

Setaro, M. and Sparavigna, A. (2002). Quantification of erythema using digital camera and computer-based colour image analysis: a multicentre study. *Skin Research and Technology*, **8**(2), 84–88.

Shoemaker, W. C., Appel, P. L., and Kram, H. B. (1988). Tissue oxygen debt as a determinant of lethal and nonlethal postoperative organ failure. *Critical Care Medicine*, **16**(11), –.

Stamatas, G. N. and Kollias, N. (2007). In vivo documentation of cutaneous inflammation using spectral imaging. *J. Biomed. Opt.*, **12**(5), 051603–7.

Star, W. M., Marijnissen, J. P. A., and Gemert, M. J. C. v. (1988). Light dosimetry in optical phantoms and in tissues: I. multiple flux and transport theory. *Physics in Medicine and Biology*, **33**(4), 437–454.

Stratonnikov, A. A. and Loschenov, V. B. (2001). Evaluation of blood oxygen saturation in vivo from diffuse reflectance spectra. *Journal of Biomedical Optics*, **6**(4), 457–467.

Stryer, L. (1988). *Biochemistry*. W H Freeman & Co.

Taylor, A. H. (1920). The measurement of diffuse reflection factors and a new absolute reflectometer. *J. Opt. Soc. Am.*, **4**(1), 9–9.

Taylor, S., Westerhof, W., Im, S., and Lim, J. (2006). Noninvasive techniques for the evaluation of skin color. *Journal of the American Academy of Dermatology*, **54**(5, Supplement 2), S282–S290.

Tortora, G. J. (2000). *Principles of anatomy and physiology.* John Wiley & Sons, Inc.

Tseng, S.-H., Grant, A., and Durkin, A. J. (2008). In vivo determination of skin near-infrared optical properties using diffuse optical spectroscopy. *Journal of Biomedical Optics*, **13**(1), 014016.

Tsuneshige, A., Park, S., and Yonetani, T. (2002). Heterotropic effectors control the hemoglobin function by interacting with its t and r states–a new view on the principle of allostery. *Biophysical Chemistry*, **98**(1-2), 49–63.

Tuchin, V. (2007). *Tissue optics: light scattering methods and instruments for medical diagnosis.* SPIE, Bellingham WA, second edition edition.

Turgeon, M., editor (1999). *Clinical Hematology: Theory and Procedures.* Lippincott Williams & Wilkins.

van Staveren, H. J., Moes, C. J. M., van Marie, J., Prahl, S. A., and van Gemert, M. J. C. (1991). Light scattering in intralipid-10% in the wavelength range of 400–1100 nm. *Appl. Opt.*, **30**(31), 4507–4514.

Weersink, R. A., Hayward, J. E., Diamond, K. R., and Patterson, M. S. (1997). Accuracy of noninvasive in vivo measurements of photosensitizer uptake based on a diffusion model of reflectance spectroscopy. *Photochemistry and Photobiology*, **66**(3), 326–335.

Wilson, B. C. and Adam, G. (1983). A monte carlo model for the absorption and flux distributions of light in tissue. *Med. Phys.*, **10**(6), 824–830.

Yang, L., Egawa, M., Akimoto, M., and Miyakawa, M. (2003). An imaging colorimeter for noncontact skin color measurement. *Optical Review*, **10**(6), 554–561.

Zhang, R., Verkruysse, W., Choi, B., Viator, J. A., Jung, B., Svaasand, L. O., Aguilar, G., and Nelson, J. S. (2005). Determination of human skin optical properties from spectrophotometric measurements based on optimization by genetic algorithms. *J. Biomed. Opt.*, **10**(2), 024030–11.

Zijlstra, W., Buursma, A., Falke, H., and Catsburg, J. (1994). Spectrophotometry of hemoglobin: absorption spectra of rat oxyhemoglobin, deoxyhemoglobin, carboxyhemoglobin, and methemoglobin. *Comparative Biochemistry and Physiology - Part B: Biochemistry and Molecular Biology*, **107**(1), 161–166.

Zwart, A., Kwant, G., Oeseburg, B., and Zijlstra, W. (1982). Oxygen dissociation curves for whole blood, recorded with an instrument that continuously measures po2 and so2 independently at constant t, pco2, and ph. *Clin Chem*, **28**(6), 1287–1292.

Zwart, A., Kwant, G., Oeseburg, B., and Zijlstra, W. G. (1984). Human whole-blood oxygen affinity: effect of temperature. *J Appl Physiol*, **57**(2), 429–434.